NASA CR-144895

A STEADY AND OSCILLATORY KERNEL FUNCTION METHOD FOR INTERFERING SURFACES IN SUBSONIC, TRANSONIC AND SUPERSONIC FLOW

By
Atlee M. Cunningham, Jr.

Prepared under Contract No. NAS1-12399 by
GENERAL DYNAMICS CORPORATION
Fort Worth Division
Fort Worth, Texas

for

NATIONAL AERONAUTICS AND SPACE ADMINISTRATION

30 September 1976

A STEADY AND OSCILLATORY KERNEL FUNCTION METHOD FOR INTERFERING SURFACES IN SUBSONIC, TRANSONIC AND SUPERSONIC FLOW

By Atlee M. Cunningham, Jr.
Fort Worth Division of General Dynamics

Abstract

This report presents the theory, results and user instructions for the aerodynamic program. The theory is based on linear lifting surface theory and the method is the kernel function. The program is applicable to multiple interfering surfaces which may be coplanar or non-coplanar. Local linearization is used to treat non-uniform flow problems without shocks. For cases with imbedded shocks, the appropriate boundary conditions are added to account for the flow discontinuities. The data describing non-uniform flow fields must be input from some other source such as experiment or a finite difference solution. The results are in the form of small linear perturbations about non-linear flow fields. The method is applied to a wide variety of problems for which it is demonstrated to be significantly superior to the uniform flow method. The program user instructions are given in the last appendix for easy access.

LIST OF TABLES

LIST OF FIGURES

A STEADY AND OSCILLATORY KERNEL FUNCTION METHOD FOR INTERFERING SURFACES IN SUBSONIC, TRANSONIC AND SUPERSONIC FLOW

By Atlee M. Cunningham, Jr.
Fort Worth Division of General Dynamics

SUMMARY

This report presents the theory, results, and user instructions for a computer program to calculate steady and unsteady aerodynamics on interfering surfaces in subsonic, transonic or supersonic flow. The theory is based on linear lifting surface theory and the method is the kernel function. The program is applicable to multiple interfering surfaces which may be coplanar or non-coplanar. Local linearization is used to treat non-uniform flow problems without shocks. For cases with imbedded shocks, the appropriate boundary conditions are added to account for the flow discontinuities. The data describing non-uniform flow fields must be input from some other source such as experiment or a finite-difference solution. The results are in the form of small linear perturbations about non-linear flow fields. The method is applied to a wide variety of problems for which it is consistently demonstrated to be significantly superior to the uniform flow method.

All equations used in the method are summarized in the appendices along with detailed derivations. A set of instructions for using the program is presented in the last appendix for easy access. The instructions are included in this report so that reference to pressure function or surface types and example cases can be easily made.

In addition to the non-uniform flow capability, the program can be used to obtain uniform flow solutions with a single option change. Interference effects can be calculated for coplanar, non-coplanar and intersecting planar surfaces. The aerodynamic input geometry data format permits the input of arbitrarily arrayed surfaces which are constrained only to being streamwise.

Each surface may or may not have an image surface, hence, asymmetric configurations may be constructed.

The program has a built-in interpolation scheme for structural mode shapes. The scheme uses a surface spline fit over various structural surfaces or regions. This will permit interpolation of modes for total airplane configurations with all-movable and vertical surfaces.

Generalized forces can be calculated in unsteady flow and pressure distributions can be obtained in both steady and unsteady flow. The solutions obtained are essentially independent in computer cost of the number of modes or downwash vectors input. Once the aerodynamic matrices are computed, inverted and saved on a magnetic tape, they can be used on subsequent problems for very little cost as long as Mach number, reduced frequencies, and aerodynamic geometry remain unchanged. Thus, the method is tailored for design applications where the structural mode shapes change continually for structural changes and payload variations while aerodynamic parameters remain constant.

INTRODUCTION

In recent years, interest has grown considerably in the desire to fly efficiently in the high subsonic regime. As a result, the need has increased for better unsteady transonic aerodynamic tools so that flutter and dynamic response characteristics can be more accurately predicted in this flow regime. Presently, these characteristics are predicted only with methods which are based on linearized theory in uniform potential flow. In addition, since buffet and limit cycle flutter appear to be similar in experimental flutter and buffet testing, it is important that their distinction be better understood.

The characteristic of transonic flow which causes the greatest difficulty when attempting to apply uniform flow theory to such problems is the presence of shocks imbedded in the flow. Such a gradient in velocity as that which exists across a shock is no longer small, thus, linear theory methods (ref. 1) cannot account for this phenomenon and hence become invalid. Finite difference methods or other iterative schemes can account for such discontinuities but they are usually very expensive to use in terms of computer time required (refs. 2, 3, 4 and 5). More-

over, if they are used for flutter or dynamic response analyses where solutions must be computed for 10 or more frequencies, the computer costs quickly become astronomical.

For example, a simple cantilevered wing flutter analysis with four natural modes and 10 frequencies could require 20 or more hours of computer time on an IBM 360/65 for a single flutter solution. Thus, such an approach is not well suited for solving unsteady transonic aerodynamic problems in a practical sense.

A study was conducted to investigate the feasibility of using combined subsonic and supersonic linear theory as a means for solving unsteady transonic flow problems economically (ref. 6). In the method developed, a wing over which the flow was mixed supersonic and subsonic with imbedded shocks was treated as an array of general aerodynamic lifting surface (GALS) elements. Each element was allowed to have mutual interference with the other elements. Also, each was assigned a different Mach number, either subsonic or supersonic, and its downwash was modified accordingly. The Mach number distribution and shock geometry was obtained from either experiment or a finite difference solution, hence the method was used to predict unsteady perturbations about known steady mean flows. Once assembled, the solution proceeded in a manner identical to ordinary aerodynamic interference methods (ref. 7). The frequency sweep could be performed at about the usual cost of a standard subsonic or supersonic unsteady aerodynamic analysis which is less than one hour - usually about 10 minutes - as opposed to 20 hours or more for a finite difference solution. As a result of the feasibility study the computer procedure documented in this report was developed.

The theory, results and program utilization are given in this volume for the subsonic, transonic and supersonic aerodynamic program. The program is described in Volume II of this report. This program is applicable to steady and unsteady flow over multiple arbitrarily arrayed lifting surfaces. The Mach range is subsonic, mixed transonic with or without shocks, and supersonic. In addition to uniform flow subsonic and supersonic solutions, non-uniform Mach number distributions can be used which lead to significant improvements in solution accuracy. The method is based on a kernel function technique which uses assumed pressure functions with unknown coefficients. By matching flow tangency boundary conditions at the control points, the unknown coefficients are uniquely determined. The Mach number

and reduced frequency at the control point are used to calculate the aerodynamic influence coefficients at that point. The presence of a normal shock is simulated by a line doublet which represents the load induced by shock movement. The appropriate steady or unsteady normal shock boundary conditions, as derived in this report, are satisfied across the shock along the surface of the wing. In the application of the transonic method to several cases, the solutions are shown to be significantly superior to uniform flow theory solutions with a relatively small increase in computer costs.

SYMBOLS

a	free stream speed of sound, meters/second
$\bar{a}$	conical coordinate
AR	aspect ratio
b_{REF}	reference length, meters - usually ½ wing chord for 2-dimensional flow or ½ MAC for finite wings in 3-dimensional flow
$b(\tilde{\eta})$	wing semi-chord at span station $\tilde{\eta}$, non-dimensionalized by b_{REF}
$C_p = \frac{p-p_\infty}{q_\infty}$	pressure coefficient
$h(\tilde{x},\tilde{y})$	mode amplitude at point $\tilde{x},\tilde{y}$ non-dimensionalized by b_{REF}
$i = (-1)^{\frac{1}{2}}$	
$k = \frac{\omega b_{REF}}{U}$	reduced frequency
$m = \frac{\beta}{\tan \Lambda_{LE}}$	
$M = \frac{U}{a}$	Mach number

MAC	mean aerodynamic chord, meters
$P_q(\tilde{\xi}, \tilde{\eta})$	supersonic pressure weighting function in the plane of the qth surface, non-dimensional
p	pressure, Newtons/meter^2
$\Delta \bar{p}_q(\underline{\xi}, \underline{\eta})$	lifting pressure amplitude in the plane of the q^{th} surface, Newtons/meter^2
$q = \frac{\rho U^2}{2}$	dynamic pressure, Newtons/meter^2
$r = \left[(y-\eta)^2 + (z-\zeta)^2\right]^{\frac{1}{2}}$	non-dimensionalized by b_{REF}
s_o	wing semi-span, non-dimensionalized by b_{REF}
U	free stream velocity, meters/second
u,v,w	velocity components in the x,y,z directions, respectively, meters/second
$\bar{w}_p(\tilde{x},\tilde{y})$	amplitude of the oscillatory downwash normal to the p^{th} surface, meters/second
$\bar{W}_p(\tilde{x},\tilde{y}) =$	$\bar{w}_p(\tilde{x},\tilde{y})/U$
x,y,z	cartesian coordinate location of the downwash point in the kernel function (x is in the direction of U), non-dimensionalized by b_{REF}
$\tilde{x},\tilde{y},\tilde{z}$	coordinates in the plane of the p^{th} surface with $\tilde{z}$ perpendicular (see fig. 3.)
x_o, y_o, z_o	distance from an influence point to the downwash point, $(x-\xi)$, $(y-\eta)$, $(z-\zeta)$, non-dimensional
ΔC_p	lifting pressure coefficient
α	angle of attack, degrees
$\beta = \sqrt{\lvert 1-M^2 \rvert}$	
$\beta^2 = 1-M^2$	

Λ_{LE}, Λ_{TE} leading and trailing edge sweep angles, degrees

ξ, η, ζ location of an influence (or integration) point in the kernel function, non-dimensionalized by b_{REF}

$\tilde{\xi}$, $\tilde{\eta}$, $\tilde{\zeta}$ coordinates in the plane of the q^{th} surface with $\tilde{\zeta}$ perpendicular (see fig. 3.)

$\xi_m(\tilde{\eta})$ location of the mid-chord at span station $\tilde{\eta}$, non-dimensionalized by b_{REF}

$$\underline{\xi}, \underline{\eta}, \underline{\zeta} = \frac{\tilde{\xi} - \tilde{\xi}_m(\tilde{\eta})}{b(\tilde{\eta})}, \frac{\tilde{\eta}}{s_o}, \frac{\tilde{\zeta}}{s_o}$$

$\tilde{\eta}_a$, $\tilde{\eta}_b$ limits of the spanwise integration as determined by geometry and the Mach hyperbola

δ chordwise variable of integration, non-dimensional

ω rotational frequency, radians/second

Subscripts:

L local value

LE leading edge

MC Mach cone (or hyperbola) boundary

p downwash surface

q integration surface

TE trailing edge

xy local value at point x,y

∞ free stream conditions

TRANSONIC FLUTTER AND DYNAMIC RESPONSE ANALYSIS

Before proceeding with describing the transonic method, it is appropriate that a brief discussion be given concerning the problems associated with transonic flutter and dynamic response analysis.

In conventional dynamic analysis, the points to be considered are defined over a Mach number-altitude envelope. Since the analysis methods use linear theory aerodynamics, there is no coupling between the unsteady and steady flow fields, and altitude is accounted for only through the variation of air density. In transonic flow this is no longer true.

The prediction of unsteady pressure distributions induced by a surface oscillating in a mixed transonic flow is complicated by the strong coupling between the steady and unsteady flow fields. The steady flow fields are in turn drastically modified by Mach number, altitude, thickness, camber, twist, angle of attack, planform geometry, interference, and static aeroelastic and boundary layer effects. For a given Mach-altitude point and a fixed configuration, however, the only additional variable is the angle of attack, α. Thus, transonic flutter and dynamic response analysis must be performed over a three-dimensional envelope as specified by Mach-altitude-α conditions.

Transonic analysis is further complicated by the need to compute unsteady pressures on the entire configuration, that is both upper and lower surfaces, in most cases. Through changes in the static aeroelastic deformation and boundary layer, altitude effects in the shock structure and flow fields are as significant as those due to Mach number and α. Thus, a new mean flow field is needed for each Mach-altitude-α condition.

The use of finite difference or other iterative schemes such as those given in references 2, 3, 4 or 5 would pose an obvious solution to this problem. Assuming that an unsteady verision could be developed for finite wings, it might be assumed that about 30 to 60 minutes on an IBM 360/65 would be required for a single aerodynamic solution (ref. 4). A single solution would, however, refer to one Mach-altitude-α-frequency-mode condition. Thus for a single 10 frequency, 4 mode flutter solution for a simple cantilever wing, 20 to 40 hours of computer time would be

required. Expanding this to two Mach numbers, two altitudes, and two α's, the total cost would be 160 to 320 hours of computer time. This cost is on the order of magnitude of a flutter model test program and the same cost would be encountered for redesign evaluations. Since one of the primary objectives for using theoretical flutter methods is to reduce costs by minimizing the requirement of flutter model tests, then the use of the finite difference approach would defeat its intended purpose.

Although linear theory methods cannot solve the highly nonlinear mean flow problem, they can solve the small perturbation problem about the mean flow. Thus, a more realistic and yet economical approach would be to use the elaborate schemes to predict the mean flow fields and linear "transonic" theory to perform the flutter analysis at each Mach-altitude-α point. The cost of using linear theory methods is primarily a function of the number of frequencies and is practically independent of the number of modes. Also, once the aerodynamic matrices are calculated, they may be used repeatedly to evaluate design changes at very little cost.

Returning to the cantilevered wing, for a linear theory solution of about 1 minute per frequency, the cost for flutter analysis would be 10 minutes per Mach-altitude-α point. For the total, 4 to 8 hours would be required for the steady mean flow calculations and 1.33 hours for flutter analyses. Comparing 5.33 to 9.33 hours against 160 to 320 hours, it is clear that the hybrid approach would be economically very attractive. The results in this report will also demonstrate that the use of linear theory would not degrade the accuracy.

THE TRANSONIC KERNEL FUNCTION METHOD

The fundamental problem to be treated in this report is the development of a technique to solve the integral equation that relates the normal velocity imposed by boundary conditions with the load distribution on an arbitrary array of planar lifting surfaces in a subsonic, supersonic or mixed transonic flow. The equation may be written as

$$\frac{\bar{w}_p(x,y,z)}{U} = \frac{1}{4\pi\rho U^2} \sum_{q=1}^{Q} \int_{Sq} \Delta p_q(\xi,\eta,\zeta) K(x-\xi, y-\eta, z-\zeta, k, M) ds \qquad (1)$$

for Q total surfaces. The downwash $\bar{w}_p(x,y,z)$ is the velocity normal to the p^{th} lifting surface at control point (x,y,z). The function $\Delta\bar{p}_q(\xi,\eta,\zeta)$ is the normal lift distribution on the q^{th} lifting surface at load (or integration) point (ξ,η,ζ). The kernel function K( ) is the influence function which is actually the velocity field due to an elemental normal load at point (ξ,η,ζ) on the q^{th} surface. The unknown quantity is $\Delta\bar{p}(\xi,\eta,\zeta)$ and $\bar{w}_p(x,y,z)$ is prescribed by the boundary conditions on the lifting surface due to surface slope and motion.

The method used to solve equation (1) in this report is based on a collocation technique. The unknown pressure function is assumed to be composed of a series of polynomials weighted by a user selected weighting function that is characteristic of each lifting surface. The non-planar kernel function is used for which the Mach number and reduced frequency are determined by those values at the downwash control point, x,y,z. The necessary equations for evaluating equation (1) are given in the Appendix.

The algorithm for linking subsonic and supersonic linear theory solutions together is based on the following two assumptions:

1. The appropriate Mach number for computing downwash at a point is the Mach number of that point.

2. The reduced frequency, $k_\infty = \frac{\omega b_{REF}}{U}$, is modified according to the local velocity such that ω is held constant. This is approximated as

$$k_L = k_\infty \frac{U}{U_L} \approx k_\infty \frac{M}{M_L}$$

The first assumption is justified by the fact that, for any given pressure distribution, the integrated kernel function-pressure function product rapidly becomes independent of Mach number as distance increases either upstream or downstream from a loaded region. The second assumption is mandatory since the physical frequency, ω, must be held constant. The use of the Mach number ratio rather than velocity ratio will result in a small overestimate (typically about 3% to 4%) of the effect of velocity change.

With the two basic assumptions, the computational algorithm becomes a simple problem of testing the Mach number of the downwash point. If the downwash point is supersonic, then the self-induced downwash as well as all interference effects at that point are computed with the supersonic kernel function regardless of the interfering surface's Mach number. Likewise, if the downwash point is subsonic, the subsonic kernel function at that Mach number is used. The value of k in the kernel function is also determined by the local Mach number since the downwash surface sees the same value of ω regardless of what surface the disturbance is emitted from.

The correct form of the downwash-pressure function integral equation which embodies the above assumptions can be derived from the nonlinear partial differential equation that governs the flow potential. The equation in vector form is

$$\frac{1}{a^2}\frac{\partial^2\tilde{\phi}}{\partial t^2} + \frac{2}{a^2}\vec{q}\cdot\frac{\partial\vec{q}}{\partial t} = \tilde{\nabla}^2\tilde{\phi} - \frac{1}{a^2}\vec{q}\cdot\left[(\vec{q}\cdot\tilde{\nabla})\vec{q}\right]$$

where

$$a^2 = a_o^2 - \frac{\gamma-1}{2}q^2 \quad , \qquad a_o = \text{stagnation speed of sound}$$

$$\vec{q} = \nabla\tilde{\phi}$$

$$\tilde{\nabla} = \vec{j}_x\frac{\partial}{\partial\tilde{x}} + \vec{j}_y\frac{\partial}{\partial\tilde{y}} + \vec{j}_z\frac{\partial}{\partial\tilde{z}}$$

Let

$$\tilde{\phi} = \phi_1 + \tilde{\phi}\,, \quad \tilde{\phi} \ll \phi_1$$

and

$$M_1 = \frac{\tilde{\phi}_{1_x}}{a_1} = \frac{U_{xy}}{a_{xy}} = M_{xy}$$

$$k_1 = \frac{\omega b_{REF}}{\tilde{\phi}_{1_x}} = \frac{\omega b_{REF}}{U_{xy}} = k_{xy}$$

Defined at the downwash point

where U_{xy} is the mean flow field velocity parallel to the lifting surface at the downwash point location, (x,y). The first of the two basic assumptions imples that the derivatives of the mean flow field velocity components are small relative to velocity component ϕ_{1x}, i.e.

$$(\phi_{1_{xx}},\ \phi_{1_{xy}},\ \phi_{1_{xz}}) \sim (\phi_{1_{yx}},\ \phi_{1_{yy}},\ \phi_{1_{yz}})$$
$$\sim(\phi_{1_{zx}},\ \phi_{1_{zy}},\ \phi_{1_{zz}}) \sim \tilde{\phi}_x \ll \phi_{1_x} \tag{2}$$

Employing equation (2), it is possible to reduce the nonlinear equation to the following first order nondimensional form for ϕ

$$\nabla^2\phi - M_1^2\,\phi_{xx} + k_1^2\,M_1^2\phi - 2ik_1M_1^2\,\phi_x = 0$$

where

$$\phi = \frac{\tilde{\phi}}{\phi_{1x}\, b_{REF}}$$

$$\nabla = b_{REF}\,\tilde{\nabla}$$

$$\phi_x = \frac{\tilde{\phi}_x}{\phi_{1_x}}$$

It should be noted that all equations have been defined at the downwash point.

Next, the acceleration potential equations are developed also at the downwash point with one exception. The acceleration potential for harmonic motion is defined as

$$\tilde{\psi} = i\omega\tilde{\phi} + \phi_{1_x}\tilde{\phi}_x$$

It is desired to non-dimensionalize $\tilde{\psi}$ with a flow field variable at the integration point since it is directly related to the pressure difference. Hence,

$$\psi = \frac{\tilde{\psi}}{\phi_{1_\xi}^2} = \left(\frac{\phi_{1_x}}{\phi_{1_\xi}}\right)\left(ik_1\phi + \phi_x\right)$$

where ϕ_{1_ξ} is the mean flow velocity component at the integration point. The governing differential equation for ψ can thus be written as

$$\nabla^2\psi - M_1{}^2\psi_{xx} + k_1^2 M_1^2\psi - 2ik_1M_1{}^2\psi_x = 0 \qquad (4)$$

for which the well known solution is

$$\psi = \frac{A}{4\pi}\frac{\partial}{\partial z}\frac{1}{R_1'}\,\mathrm{EXP}\left\{ ik_1 \frac{M_1}{\beta_1^2}\left[M_1\,(x-\xi) - R_1' \right] \right\}$$

where

$$\beta_1^2 = 1 - M_1{}^2$$

$$R_1'^2 = \left\{ (x-\xi) + \beta_1{}^2 \left[(y-\eta)^2 + (z-\zeta)^2 \right] \right\}^{\frac{1}{2}}$$

The strength factor A is determined from the relationship

$$\tilde{\psi} = \frac{\Delta p}{\rho_\xi} \quad \Rightarrow \quad \psi = \frac{\Delta p}{2\,\frac{\rho_\xi \phi_{1\xi}}{2}} = \frac{\Delta C_{p_\xi}}{2}$$

Since flow can be assumed as nearly two dimensional in the vicinity of the downwash point, the relation

$$\frac{q_\infty}{q_\xi} = \frac{\phi_{1\infty}}{\phi_{1\xi}} \quad \Rightarrow \quad \psi = \frac{\phi_{1\infty}}{2\phi_{1\xi}}\,\Delta C_{p_\infty}$$

is approximately valid where q_∞ and q_ξ are the dynamic pressures at infinity and the integration point, and ΔC_{p_∞} is the integration point lift amplitude divided by q_∞. As a result, the solution to equation (3) is

$$\phi = \frac{1}{8\pi}\frac{\phi_{1\infty}}{\phi_{1x}}\, e^{-ik_1(x-\xi)} \int_{-\infty}^{x-\xi} \frac{\phi_{1\xi}}{\phi_{1x}}\, \Delta C_{p_\infty}\,(\xi,\eta,\zeta)$$

$$\cdot \frac{\partial}{\partial z}\left[\frac{1}{R_1}\,\mathrm{EXP}\left\{ ik_1 \frac{M_1}{\beta_1 2}\left[M_1\lambda - R_1 \right] \right\} \right] e^{-ik_1\lambda}\, d\lambda$$

where $\Delta C_{p_\infty}(\xi,\eta,\zeta)$ is the lifting coefficient at the integration point. Defining the downwash as

$$w = \frac{1}{\phi_{1x}} \frac{\partial \tilde{\phi}}{\partial \tilde{z}} = \frac{\partial \phi}{\partial z} = \phi_z = -\left(\frac{\partial z}{\partial x} + ikz\right)$$

The downwash-pressure integral equation becomes

$$-\frac{\phi_{1x}}{\phi_{1\infty}} \left(\frac{\partial z}{\partial x} + ik_1 z\right) = \frac{1}{8\pi} \iint \frac{\phi_{1\xi}}{\phi_{1x}} \Delta C_{p_\infty}(\xi, \eta, \zeta)$$

$$\cdot K\,(x-\xi,\ y-\eta,\ z-\zeta,\ k_1,\ M_1)\ d\xi\, d\eta$$

where the kernel function is defined as

$$K\,(x-\xi,\ y-\eta,\ z-\zeta,\ k_1,\ M_1)$$

$$= e^{-ik_1(x-\xi)} \frac{\partial^2}{\partial z^2} \int_{-\infty}^{x-\xi} \frac{1}{R_1}\ \mathrm{EXP}\left\{ ik_1 \frac{M_1}{\beta_1^2} \left[M_1\lambda - R_1 \right] \right\} e^{-ik_1\lambda}\, d\lambda$$

The only difference between the above formulation of the kernel function and the classical form is that the k_1 and M_1 vary with downwash point location. They are constant over the region of integration, however, for any given downwash point. These definitions are consistent with the two basic assumptions.

The presence of the term $(\phi_{1\xi}/\phi_{1x})$ in the integral in equation (5) violates the first assumption that the downwash point Mach number dominates the influence functions. Likewise as the integration points approached the downwash point, this term would approach unity, therefore its influence could be negligible. For the purposes of the study summarized in this report, it has been set equal to unity. The effect could be significant, however, for integration points in a supersonic region nearly upstream of a subsonic downwash point. The use of $(\phi_{1\xi}/\phi_{1x}) \neq 1.0$ should be investigated in future studies to determine its importance. Also, rather than use $(\phi_{1x}/\phi_{1\infty})$ in equation (5),

$$\phi_{1x}/\phi_{1\infty} \approx M_{xy}/M$$

is used which will introduce a small error as previously discussed.

As a result of the above discussion, the integral equation that is actually solved by the transonic algorithm is

$$-\left(\frac{\partial z}{\partial x} + ik_{xy}z\right)\frac{M_{xy}}{M} = \frac{1}{8\pi}\iint \Delta C_{p_\infty}(\xi,\eta) \cdot K(x-\xi,\ y-\eta,\ z-\zeta,\ k_{xy},\ M_{xy})\,d\xi\,d\eta \tag{6}$$

where $\Delta C_{p_\infty}(\xi, \eta)$ is the pressure difference at (ξ, η) divided by q_∞. Since the algorithm permits M_{xy} and k_{xy} to be used in computing the kernel function, thereby permitting the kernel function to change at each downwash point, it is possible to account for leading edge regions where the flow is continuously accelerated from subsonic to supersonic.

Shown in figure 1 is a flow diagram of the current transonic flow algorithm for unsteady flow. The same logic is applicable to steady flow. The key ingredient is the common set of surface types and pressure function types for both subsonic and supersonic flow as shown in figure 2. The integration schemes are also compatible with two exceptions. The difference in the chordwise integration is that in supersonic flow, the limits are from Mach cone to leading edge whereas in subsonic flow they are from trailing edge to leading edge. In the spanwise integration, both techniques are identical.

The pressure functions are given as a set of chordwise and spanwise varying polynomials with a weighting function which is constructed according to the pressure type shown in figure 2. The form is

$$\Delta p_q(\xi,\underline{\eta}) = \frac{4\rho U^2}{b_q(\underline{\eta})}\, s_{o_q}\, h(\underline{\xi})\ell(\underline{\eta})\left[g_{o_q}(\underline{\eta})f_o(\underline{\xi}) + g_{1_q}(\underline{\eta})f_1(\underline{\xi}) + \ldots\right] \tag{7}$$

where all items are defined in the "Symbols" section except for $g_{mq}(\underline{\eta})$, $f_n(\underline{\xi})$, $h(\underline{\xi})$ and $\ell(\underline{\eta})$. The coordinates, $\underline{\xi}$, $\underline{\eta}$, are

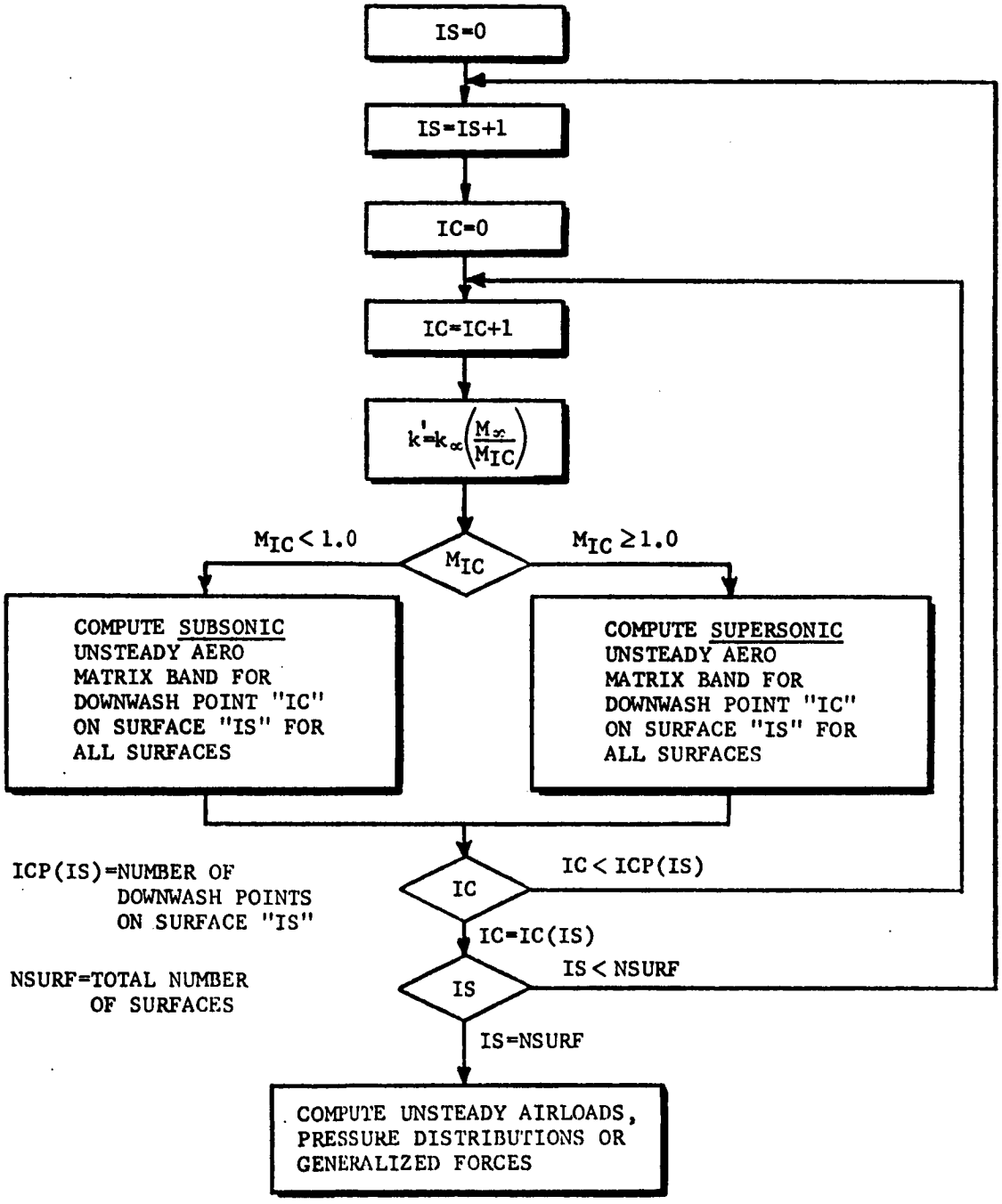

Figure 1. - Flow Diagram For Computing Unsteady Aerodynamics in Mixed Transonic Flow

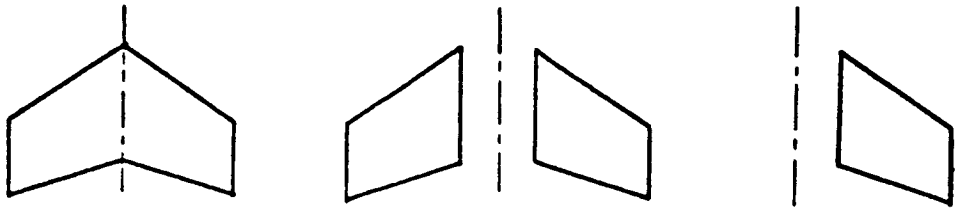

SURFACE TYPES

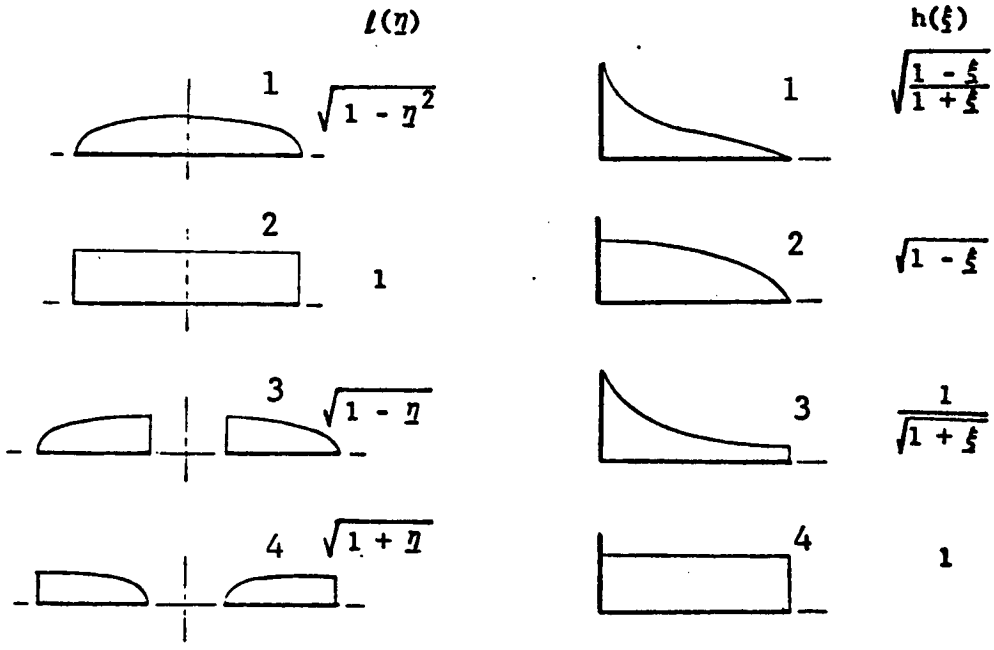

SPANWISE LOADINGS CHORDWISE LOADINGS

Figure 2. - Surface and Loading Types for the General Aerodynamic Lifting Surface Element

defined in the transformed plane of the surfaces shown in figure 3. The chordwise functions, $h(\underline{\xi})$, are defined as

$$\left.\begin{aligned} h(\underline{\xi}) &= \sqrt{\frac{1 - \underline{\xi}}{1 + \underline{\xi}}} && \text{, Type 1} \\ h(\underline{\xi}) &= \sqrt{1 - \underline{\xi}} && \text{, Type 2} \\ h(\underline{\xi}) &= \sqrt{\frac{1}{1 + \underline{\xi}}} && \text{, Type 3} \\ h(\underline{\xi}) &= 1 && \text{, Type 4} \end{aligned}\right\} \quad (8)$$

in relation to figure 2. The spanwise functions, $\ell(\underline{\eta})$, are defined as

$$\left.\begin{aligned} \ell(\underline{\eta}) &= \sqrt{1 - \underline{\eta}^2} && \text{, Type 1, surface 1 only} \\ \ell(\underline{\eta}) &= 1 && \text{, Type 2, surfaces 1, 2, 3} \\ \ell(\underline{\eta}) &= \sqrt{1 - \underline{\eta}} && \text{, Type 3, surfaces 2, 3} \\ \ell(\underline{\eta}) &= \sqrt{1 + \underline{\eta}} && \text{, Type 4, surfaces 2, 3} \end{aligned}\right\} \quad (9)$$

The chordwise functions, $f_n(\underline{\xi})$, are simply

$$\begin{aligned} f_0(\underline{\xi}) &= U_0(\underline{\xi}) = 1 \\ f_1(\underline{\xi}) &= U_1(\underline{\xi}) + U_0(\underline{\xi}) = 2\underline{\xi} + 1 \\ &\vdots \\ f_n(\underline{\xi}) &= U_n(\underline{\xi}) + U_{n-1}(\underline{\xi}) \end{aligned} \quad (10)$$

There are $\overline{m}_q$ total chordwise functions corresponding to $\overline{m}$ total downwash points in the chordwise direction for the q^{th} surface.

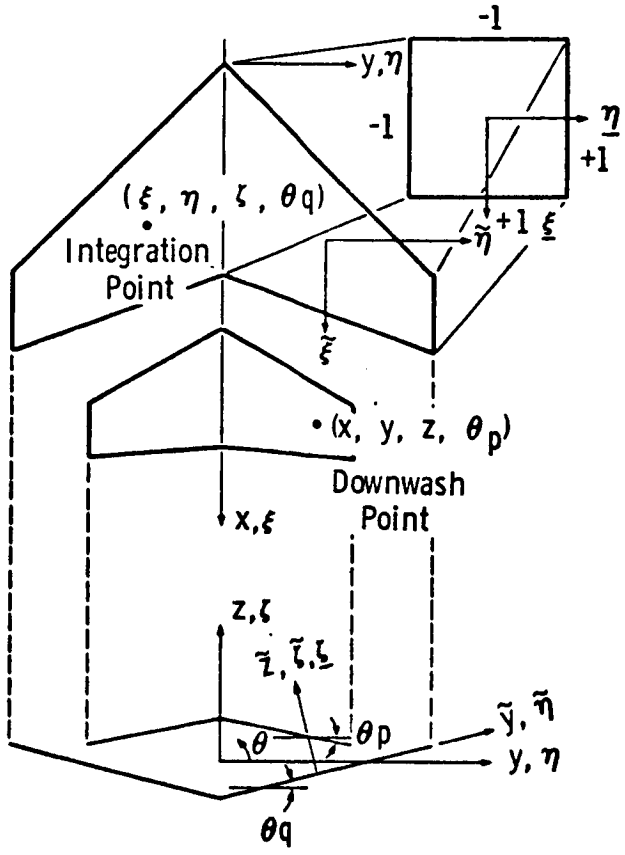

Figure 3. - Basic Geometry and Coordinate Systems for Interfering Surfaces

The spanwise functions, $g_{mq}(\underline{\eta})$, contain the unknown coefficients in the form

$$g_{mq}(\underline{\eta}) = \left[a_{moq} U_o(\underline{\eta}) + a_{m1q} U_1(\underline{\eta}) + \ldots \right] \tag{11}$$

where $U_n(\underline{\eta})$ are the Tschebychev polynomials of the second kind,

$$U_o(\underline{\eta}) = 1$$
$$U_1(\underline{\eta}) = 2\underline{\eta}$$
$$\vdots$$
$$U_n(\underline{\eta}) = U_{n-1}(\underline{\eta}) - 2\,\underline{\eta}\, U_{n-2}(\underline{\eta})$$

There are $\overline{n}_q$ total spanwise functions corresponding to $\overline{n}_q$ total downwash chords.

These pressure functions are used regardless of Mach number for subsonic or transonic solutions. For supersonic flow, these functions may be used or the supersonic weighting function may be used instead.

If the supersonic weighting function is used, the form is

$$\Delta p_q(\underline{\xi},\underline{\eta}) = 4\rho U^2 P(\tilde{\xi},\tilde{\eta}) \left[g_{oq}(\underline{\eta})\, f_o\,(\underline{\xi}) + g_{1g}(\underline{\eta})\, f_1\,(\underline{\xi}) + \ldots \right] \tag{12}$$

where $P(\tilde{\xi},\tilde{\eta})$ is the weighting function. The $g_{nq}(\underline{\eta})$ and $f_n(\underline{\xi})$ are identical to those given for the regular function in equation (7).

The supersonic weighting function is based on conical flow theory solutions to the lift distributions on flat swept wings (ref. 8). Some liberty has been taken to simplify the expressions and yet maintain the basic characteristics. The function has been developed only for simple trapezoidal wings in this program. The following derivations provide the equations necessary for wings with or without clipped tips and with subsonic or supersonic leading and trailing edges. No secondary reflections of the Mach lines are accounted for since they tend to be of second order effect and can be adequately accounted for in the collocation solution.

The basic equation for leading edge and root characteristics is the delta wing distribution. For a subsonic leading edge,

$$m = \frac{\beta}{\tan \Lambda_{LE}} \leq 1$$

we have

$$P(\tilde{\xi},\tilde{\eta}) = \frac{1}{\beta\sqrt{1-(\frac{\bar{a}}{m})^2}} \tag{13}$$

where

$$\bar{a} = \frac{\beta(\tilde{\eta}-\tilde{y}_1)}{\tilde{\xi}-\tilde{x}_1}, \qquad \tilde{x}_1,\tilde{y}_1 = \text{Location of leading edge vertex}$$

thus

$$\frac{\bar{a}}{m} = \frac{(\tilde{\eta}-\tilde{y}_1)\tan \Lambda_{LE}}{\tilde{\xi}-\tilde{x}_1}$$

For a supersonic leading edge, $m > 1.0$,

$$P(\tilde{\xi},\tilde{\eta}) = 1 - \bar{u}(\bar{a})L(m)\sqrt{1-\bar{a}^2} \tag{14}$$

where $\bar{u}(\bar{a}) = 1, \ \bar{a} < 1$

$= 0, \ \bar{a} \geq 1$

$$L(m) = 1 - \frac{\sqrt{m^2-1}}{4m}\left[\frac{7.0}{1.75+1/m}\right]$$

The term $\left(\frac{7.0}{1.75 + \frac{1}{m}}\right)$ which appears in the expression for L(m) is the approximation used for the exact function

$$\Delta p_{ROOT} = \frac{4m\alpha q}{\beta E'(m)} \approx \frac{7\alpha q}{(1.75+1/m)}$$

where E'(m) is the complete elliptic integral of the second kind of modulus $(1-m^2)^{\frac{1}{2}}$.

A tip correction is included for clipped tips. For a subsonic leading edge, $m \leq 1.0$, the lift distribution behind the tip Mach line is constant in the streamwise direction. The amplitude, a function of span only, is given as

$$P(\tilde{\xi},\tilde{\eta}) = \frac{1}{\beta\sqrt{1-(\frac{\bar{a}'}{m})^2}} \left\{ 1 - \left[\frac{(1+\bar{a}')(m+\bar{a}')}{2m(1+m)} \right]^{\frac{1}{2}} \right\} \tag{15}$$

where

$$\bar{a}' = \frac{\beta\tilde{\eta}}{\tilde{x}_{TIP} - (\tilde{y}_{TIP} - \tilde{\eta})\beta} = \text{value of "a" along the tip Mach line at span station}$$

For a supersonic leading edge, $m > 1.0$, the lift distribution behind the tip Mach line is given as

$$P(\tilde{\xi},\tilde{\eta}) = P(\tilde{\xi},\tilde{\eta})_{DELTA} \left[\frac{2}{\pi} \sin^{-1}\sqrt{\bar{a}''} \right] \tag{16}$$

where

$P(\tilde{\xi},\tilde{\eta})_{DELTA}$ = Delta wing distribution given by equation (14).

$$\bar{a}'' = \beta\left(\frac{\tilde{y}_{TIP} - \tilde{\eta}}{\tilde{x}_{TIP} - \tilde{\xi}}\right) = \text{value of "ā" relative to forward wing tip.}$$

The functions given above in equations (15) and (16) are exact shapes as required by conical flow theory.

A final correction to the delta wing distribution is the subsonic trailing edge term. This term is approximated as a multiplicative function applied to the delta plus tip term. The function is

$$P(\tilde{\xi},\tilde{\eta}) = P(\tilde{\xi},\tilde{\eta})_{DELTA+TIP} \left[\frac{2}{\pi} \sin^{-1}\sqrt{\bar{a}'''} \right] \tag{17}$$

for $0.0 \leq \bar{a}''' \leq 1.0$ where

$$\bar{a}''' = \frac{\tilde{\xi} - \tilde{x}_{TE}}{(\tilde{x}_{TEV} + \beta\tilde{\eta}) - \tilde{x}_{TEV}}$$

$\tilde{x}_{TE} = \underline{\eta}(\tan \Lambda_{TE}) + x_{TEV} = \tilde{x}$ position of trailing edge

$\tilde{x}_{TEV} = \tilde{x}$ position of the trailing edge vertex

thus

$$\bar{a}''' = \frac{\tilde{\eta} - (\tilde{\xi} - \tilde{x}_{TEV})\frac{m'}{\beta}}{\tilde{\eta}(1-m')}$$

$$m' = \frac{\beta}{\tan \Lambda_{TE}} < 1$$

The form of this approximation is not exactly correct, however, it seems to be close enough for practical purposes as experience has shown.

Three examples are shown in figures 4, 5 and 6 for the supersonic weighting function. The magnitude of the weighting function is adjusted uniformly in each case so that the shapes can be compared with other theories or experiment. The first example in figure 4 is for a rectangular wing, AR=2.0, in steady flow at M=1.2 and α=1.0 rad. The solid line is the weighting function evaluated at the span stations $\underline{\eta}$=0.1, 0.5 and 0.9 with the equations given in this section. The Mach lines are shown for clarity. The symbols are values computed by the AFFDL Mach box program for wing-tail configurations (ref. 9). The second example in figure 5 is a swept tapered wing of the standard AGARD wing-tail configuration (the true planform is shown). The conditions are steady flow, M=1.2 and α=1.0 rad. The solid line is again the weighting function. The symbols are results from the Woodward finite element method (ref. 10). The disagreement at the Mach line discontinuities is due to the inability of the finite element representation to conform to such characteristics with a reasonable number of elements. The third example shown in figure 6 is a trapezoidal wing with a supersonic leading edge. In this case, the leading edge vertex Mach cone intersects the tip cone. Comparison with the Woodward method and experiment clearly illustrates the validity of the function.

M_∞ = 1.2
α = 1.0 RAD
AR = 2.0

o AFFDL MACH BOX METHOD (REF. 9)
____ SUPERSONIC WEIGHTING FUNCTION

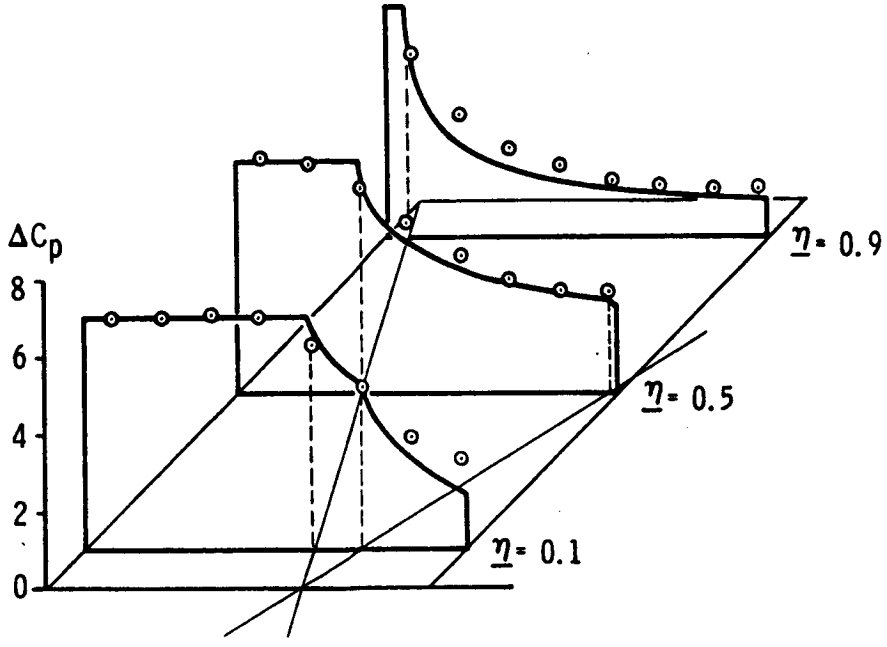

Figure 4. - Supersonic Weighting Function for a Rectangular Wing

o WOODWARD METHOD (REF. 10)
——— SUPERSONIC WEIGHTING FUNCTION

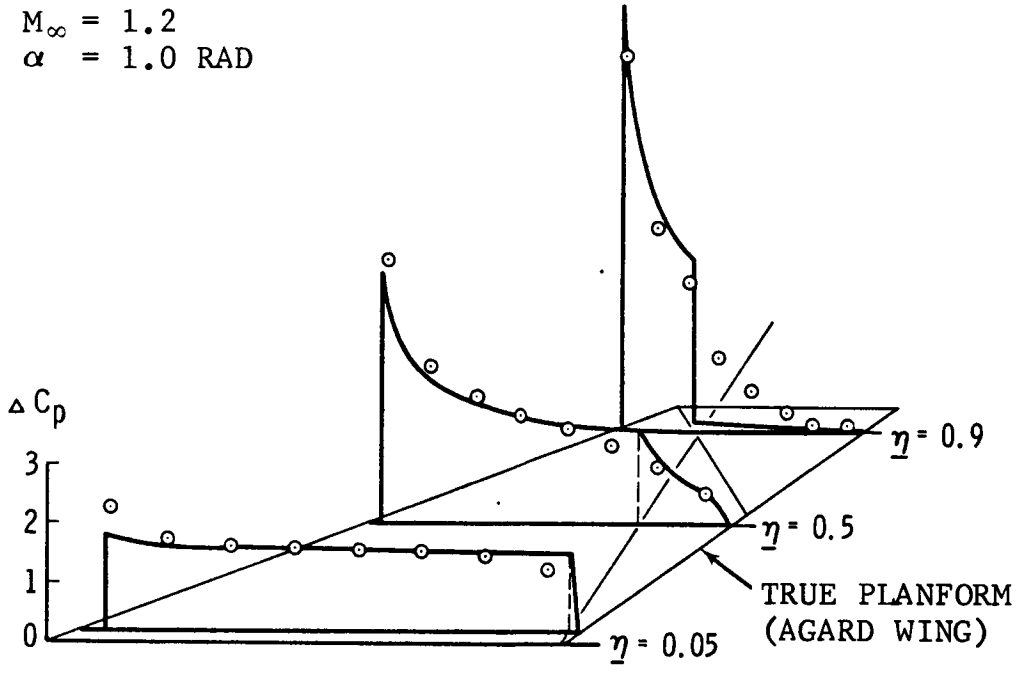

Figure 5. - Supersonic Weighting Function for a Trapezoidal Wing with Subsonic Leading and Trailing Edges

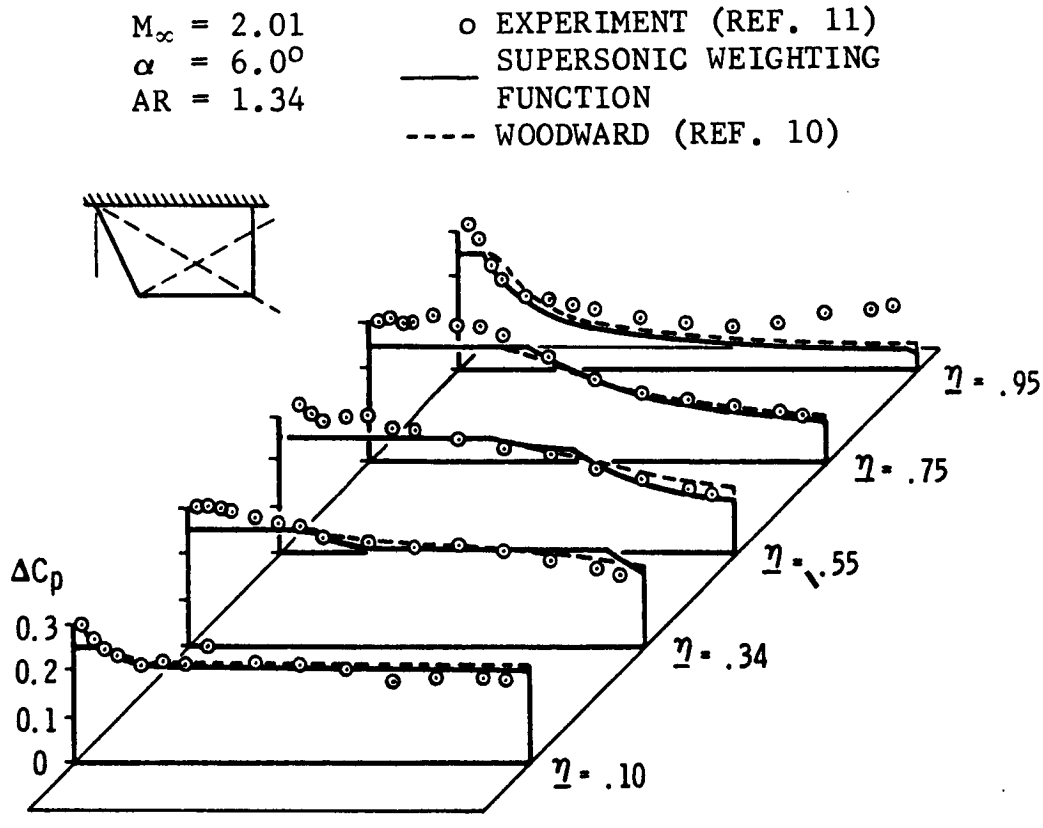

Figure 6. - Supersonic Weighting Function for a Trapezoidal Wing with Supersonic Leading and Trailing Edges

METHODOLOGY FOR INCLUSION OF IMBEDDED SHOCKS

This section summarizes how the presence of normal shocks in the flow is accounted for in the linearized model. The mean flow field may be non-linear but the perturbations must be small enough such that their non-linearities are second order effects.

Normal Shock Boundary Conditions and the Shock Model

In the calculation of unsteady aerodynamic pressures induced by surface motion in mixed transonic flows, the influence of imbedded shocks must be accounted for by satisfying the proper boundary conditions across the shocks on the flow perturbation potential. The boundary conditions are the Rankine-Hugoniot relation and the equality of total potential in front of and behind the shock. The constraint is that the shock movement necessary to satisfy Rankine-Hugoniot is equal to that necessary to maintain equality of potential. The resulting boundary condition in steady flow as derived in Appendix D is

$$\phi_x^+ - K\phi^+ = -\mu\phi_x^- - K\phi^- \tag{18}$$

where

$$K = \frac{\phi_{1xx}^+ + \phi_{1xx}^-}{\phi_{1x}^+ - \phi_{1x}^-}$$

$$\mu = \frac{\gamma-1}{\gamma+1} + \frac{2}{M^2(\gamma+1)}$$

ϕ = Perturbation potential

ϕ_1 = Mean flow potential with shock

$\phi_x = \frac{\partial\phi}{\partial x}$, etc.

The superscripts, + and -, refer to conditions just downstream or upstream of the shock, respectively, as shown in figure 7. Since the right hand side of equation (18) is determined only by upstream perturbations and mean flow conditions, the equation serves simply as an additional constraint on the downstream perturbations.

Considering equation (18) for a case of downstream excitation only, such as a control surface deflection, it can be shown that the existing lifting surface representation must be changed. For such a case, $\phi^- = \phi_x^- = 0$, and since the downstream region is subsonic, $\phi^+ = 0$. Thus, in order to satisfy equation (18), ϕ_x^+ must be zero; however, this is not the case as shown by experiment. In order for $\phi_x^+ \neq 0$, then $\phi^+ \neq 0$, thus another potential must be added to the multiple surface model for mixed transonic flow with shocks.

The finite potential ϕ^+ can be achieved by placing a lifting line (or line doublet) between the upstream and downstream surfaces along the shock location. In reality, this lifting line represents the lift due to shock movement which is otherwise not accounted for in the multiple surface model. Without the "shock doublet", the solution yields a peak in pressures at the leading edge of the subsonic surface by satisfying the flow tangency conditions. This peak, however, violates the shock boundary conditions since $\phi^+ = 0$, or else it requires that $K = 0$ in equation (18). If $\phi^+ = 0$, the shock movement, λ, (shown in Appendix D, equation (D11)) becomes

$$\lambda = - \frac{\phi^+ - \phi^-}{\phi_{1x}^+ - \phi_{1x}^-} = 0$$

since $\phi^- = 0$. Thus, for the case of downstream excitation, the shock does not move which is contrary to experimental observations. Also, for K=0, it is implied that

$$\phi_{1xx}^+ + \mu \phi_{1xx}^- = 0$$

which is inadmissible since the shock movement would be infinite as given by

$$\lambda = - \frac{\phi_x^+ + \mu \phi_x^-}{\phi_{1xx}^+ + \mu \phi_{1xx}^-} = - \frac{\phi_x^+ + \mu \phi_x^-}{0} = \infty$$

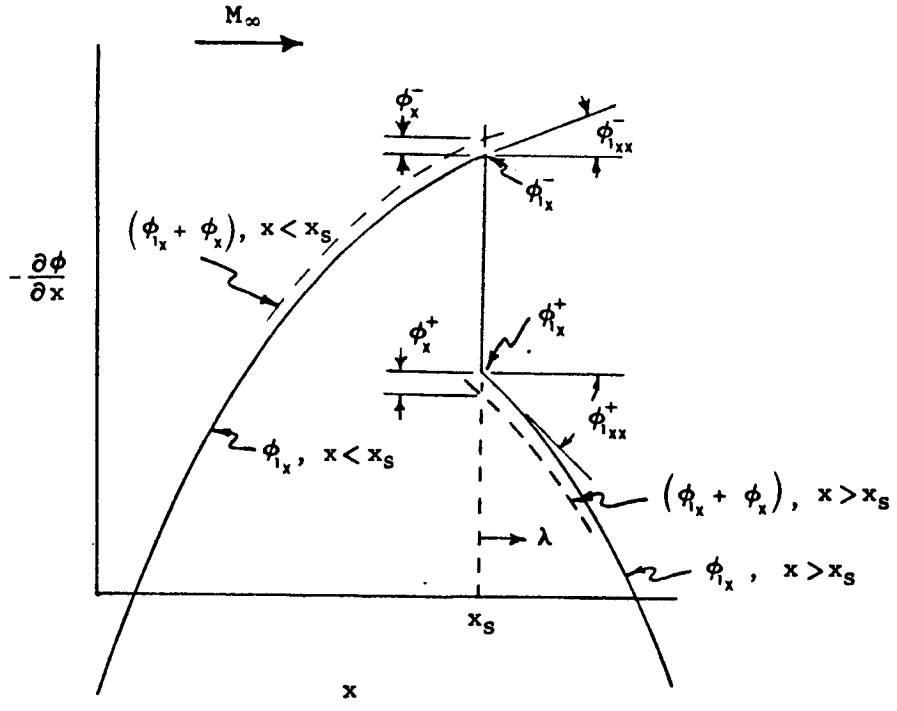

Figure 7. - Mean and Perturbation Flow Potentials About an Idealized Normal Shock

(shown in Appendix D, equation (D13)). The final conclusion is that if the constraint

$$K\phi^{+} = 0$$

is imposed, satisfaction of the shock boundary conditions becomes an indeterminant problem. Thus, for the case of mixed flow with imbedded shocks, these boundary conditions must be satisfied in order to properly represent the flow fields. They can be satisfied only by inclusion of the shock doublet.

The normal shock boundary conditions for oscillatory flow perturbations are similar to those given in equation (18) for steady flow. They are also derived in Appendix D and are expressed as

$$\phi_x^{+} - K^{*}\phi^{+} = -\mu\phi_x^{-} - K^{*}\phi^{-} - i\nu\phi^{-} \tag{19}$$

where

$$\nu = \frac{2k(\gamma-1)}{\gamma+1}$$

$$K^{*} = K + i\nu\left[\frac{\phi_{1x}^{-} - \frac{2}{\gamma-1}}{\phi_{1x}^{+} - \phi_{1x}^{-}}\right]$$

It can be seen that as k or υ goes to zero, the oscillatory condition reduces to the steady flow condition. This property is not present in Landahl's boundary condition (equation 10.11, ref. 12); however, for

$$\phi_{1xx}^{+} + \phi_{1xx}^{-} \sim \phi_{1x}^{-} \ll \frac{2}{\gamma-1}$$

and

$$k \sim 1.0$$

the above reduces to Landahl's equation. These conditions are rather restrictive and are not suitable for cases which involve flutter or dynamic response analysis.

The shock doublet is used in the unsteady case in the same manner as is used in the steady case. The same rationale for its inclusion is applicable to unsteady flow.

The form of the shock doublet strength is similar to that of a lifting line. In order to be compatible with the pressure functions, it is expressed as

$$\Delta l_{SH_q}(\eta) = \frac{4pU^2}{b_{AVG_q}} So_q \ell(\eta) \left[b_{o_q} U_o(\eta) + b_{1_q} U_1(\eta) + \ldots \right] \tag{20}$$

where $\ell(\eta)$ is the spanwise weighting function given in equation (9). The unknown coefficients, b_n, are real for steady flow and complex for unsteady flow.

Solution Process with Imbedded Shocks

For the solution to be rigorous, the upper and lower surface solutions for mixed transonic flow should be coupled together along the edge boundaries of the wing. Such an undertaking was felt to be too ambitious for the current study, hence, the assumption of decoupled upper and lower surface solutions was retained. This assumption was justified through examination of experimental data which indicated that the trailing edge pressure coefficient does approach zero for small perturbations and it is not too large for large perturbations. Thus, the trailing edge and tip pressure coefficients were set to zero as is usually done in lifting surface methods. The leading edge was left alone which resulted in some problems in the prediction of large perturbations in steady flow. The adequacy of the decoupled assumption will be discussed further in the next section on application of the method.

The potentials, ϕ^+ and ϕ^- in equations (18) or (19), are calculated as shown in Appendix E for both the lifting surface distributions and the shock doublets. Since the change across the shock of potential due to interfering surfaces is small, its effect is neglected. Hence, ϕ^+ and ϕ^- are calculated only from the two surfaces adjacent (upstream and downstream) to the shock. The potential derivatives are calculated with the pressure coefficient. As shown in Appendix E, the boundary conditions are satisfied in steady flow according to the expression

$$C_p^+(x_s,y) - \frac{K}{2} G_D(y,y) + \mu C_p^-(x_s,y) = 0$$

and in unsteady flow with

$$C_p^+(x_s,y) - \frac{K^*}{2} G_D(y,y) + \mu C_p^-(x_s,y) + \frac{i\nu}{2} G^-(y,y) = 0$$

The $C_p^+(x_s,y)$ and $C_p^-(x_s,y)$ are the pressure coefficient values just aft of and forward of the shock. The $G^-(x,y)$ and $G_D(y,y)$ are the chordwise integrals of the supersonic and shock doublet products with the kernel function along the downwash chord at span station, y. These are the same integrals given in Appendix B.

The downwash induced by the shock doublets is calculated in the same manner as is done for surface lift distributions. The equations given in Appendices B and C are directly applicable where the chordwise integration is simplified to a one-point evaluation along the shock doublet. The spanwise integrals are identical.

The physical problem for a wing in mixed transonic flow is represented with a "transonic pair" of lifting surfaces as shown in figure 8. The upstream surface may have all supersonic flow or a subsonic leading edge with accelerating flow to supersonic at the trailing edge just forward of the shock. The downstream surface must have a leading edge Mach number of less than 1.0 as well as the remainder of the surface. The shock doublet is located between the upstream and downstream surfaces. The potential ϕ^+ is calculated only from the shock doublet since the potential at the leading edge of the subsonic surface is always zero for linear theory.

The aerodynamic matrix construction for a "transonic pair" is shown in figure 9. The downwash submatrices A_{11}, A_{12}, A_{21} and A_{22} are calculated in the manner discussed in Appendices B and C. The matrix A_{1D} is the downwash induced on the supersonic surface by the shock doublet and is all zeros as is the matrix A_{12}. The A_{2D} matrix is finite and is the downwash induced on the subsonic surface by the shock doublet. This matrix is calculated as discussed above. The B_{S1} and B_{S2} matrices are the contributions due to the supersonic and subsonic surfaces, respectively, to the shock boundary conditions. The B_{SD} matrix is the $-K\phi^+$ term in the boundary conditions due to the shock doublet. The a_1

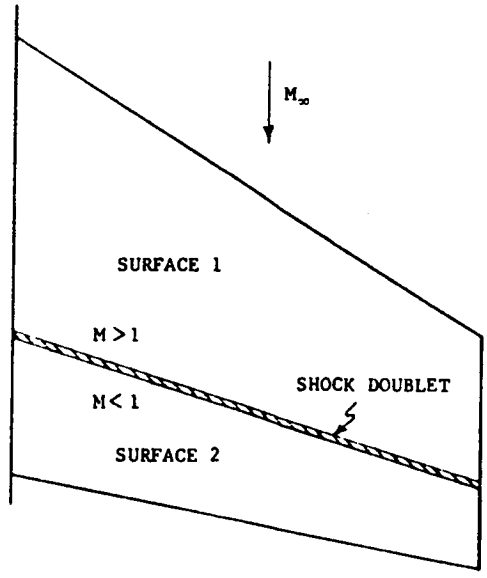

Figure 8. - Geometric Arrangement for a "Transonic Pair" of Lifting Surfaces

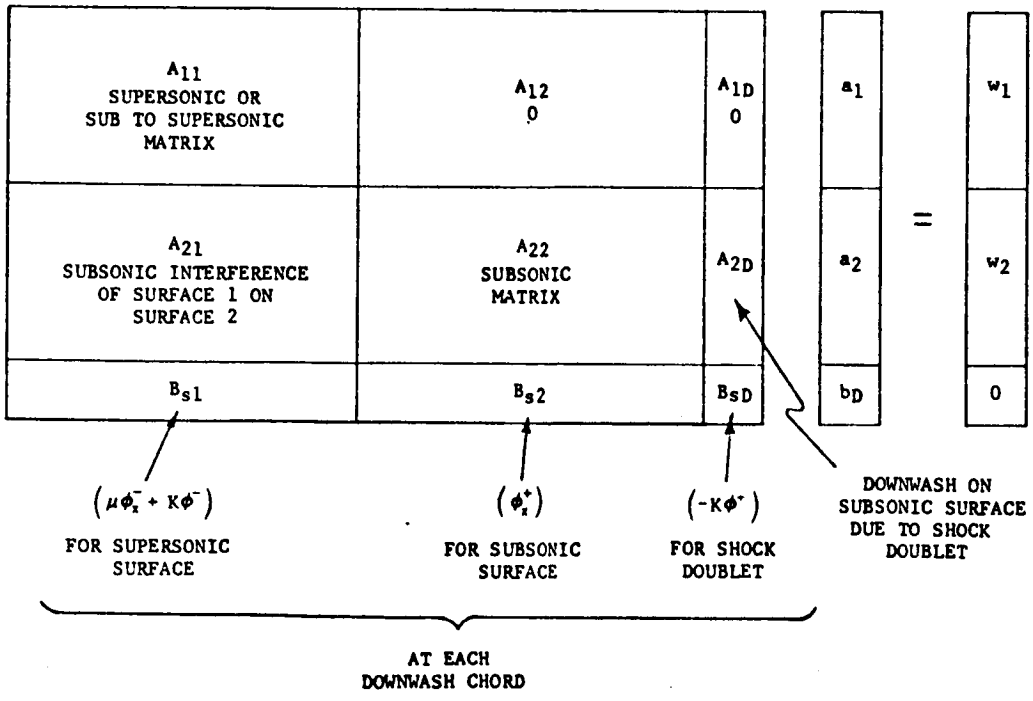

Figure 9. - Matrix Construction for a "Transonic Pair" of Lifting Surfaces

and a_2 vectors are the usual pressure series coefficients for both surfaces which are unknown. The b_D vector is the shock doublet strength series coefficients. The W_1 and W_2 vectors are the known downwash boundary conditions on the two surfaces. The matrix equation as shown in the figure is solved to obtain the full vector of unknown coefficients, a_1, a_2 and b_D. If surfaces 1 and 2 are not a transonic pair, then the shock doublet and boundary conditions are removed which leaves the usual interference matrix form

$$\begin{bmatrix} A_{11} & A_{12} \\ A_{21} & A_{22} \end{bmatrix} \begin{Bmatrix} a_1 \\ a_2 \end{Bmatrix} = \begin{Bmatrix} W_1 \\ W_2 \end{Bmatrix}$$

The effect of using the two different solutions on the same problem will be discussed in the next section on application of the method.

APPLICATION TO TRANSONIC PROBLEMS

The computer program was applied to a variety of problems involving mixed transonic flow over stationary and oscillating lifting surfaces. The steady flow application demonstrated the capability of the method for predicting incremental changes to the steady mean flow lift distribution. The unsteady flow applications included rectangular and swept trapezoidal planforms oscillating in both elastic and rigid body motions. The frequency variation ranged from near steady flow to moderately unsteady flow. Comparisons were made between theory and experiment for uniform flow, transonic flow without shocks and transonic flow with shocks. In addition, a case was considered in which theoretical wall interference effects were accounted for which led to an improvement in agreement with experiment. Where shocks were used in the solution, shock movement was shown as 2% of the local chord in order to illustrate the resulting lift increment.

Rectangular Wing in Steady Flow

The transonic method was applied to a case for an aspect ratio 3.0 rectangular wing in steady flow at $M_\infty = 1.0$ (ref. 13). The lift change was predicted for an increment in angle of attack, $\Delta\alpha = \alpha_2 - \alpha_1$ where $\alpha_2 = 5^\circ$ and $\alpha_1 = 0^\circ$. Predictions were compared with the sum of the change in lift on the upper and lower surfaces obtained from experiment as

$$\Delta C_{p_{\Delta\alpha}} = \Delta C^{L}_{p_{\Delta\alpha}} - \Delta C^{U}_{p_{\Delta\alpha}}$$

where

$$\left.\begin{aligned} \Delta C^{U}_{p_\Delta} &= C^{U}_{p_{\alpha_2}} - C^{U}_{p_{\alpha_1}} \\ \Delta C^{L}_{p_\Delta} &= C^{L}_{p_{\alpha_2}} - C^{L}_{p_{\alpha_1}} \end{aligned}\right\} \Delta\alpha = \alpha_2 - \alpha_1$$

Such a definition of incremental lift eliminated error due to non zero lift at $\alpha=0$ and was consistent with a piecewise linear representation of transonic flow problems.

Comparison of prediction and experiment is shown in figure 10. The first solution shown (solid line) is obtained by using the average of the predicted pressure changes due to $\Delta\alpha=5^\circ$ for the local Mach number distributions, M_L, at both $\alpha=0^\circ$ and $\alpha=5^\circ$. For $\alpha=0^\circ$, the incremental pressures were the same on the upper and lower surfaces since M_L was about the same on each (symmetric biconvex airfoil). At $\alpha=5^\circ$, separate solutions were run on the upper and lower surfaces. The need for three solutions stemmed from the large variation in M_L at $\alpha=0^\circ$ and at $\alpha=5^\circ$. At $\alpha=0^\circ$, M_L varied at midspan from about 0.85 at the leading edge to 1.38 at the trailing edge. At $\alpha=5^\circ$, the variation was from about 1.28 to 1.39 on the upper surface and from about 0.68 to 1.30 on the lower surface. In all cases, the control points used were 4 chordwise and 6 spanwise. The problem run time was about 12 seconds of CPU time on the CDC 6600 or a total cost of 36 seconds.

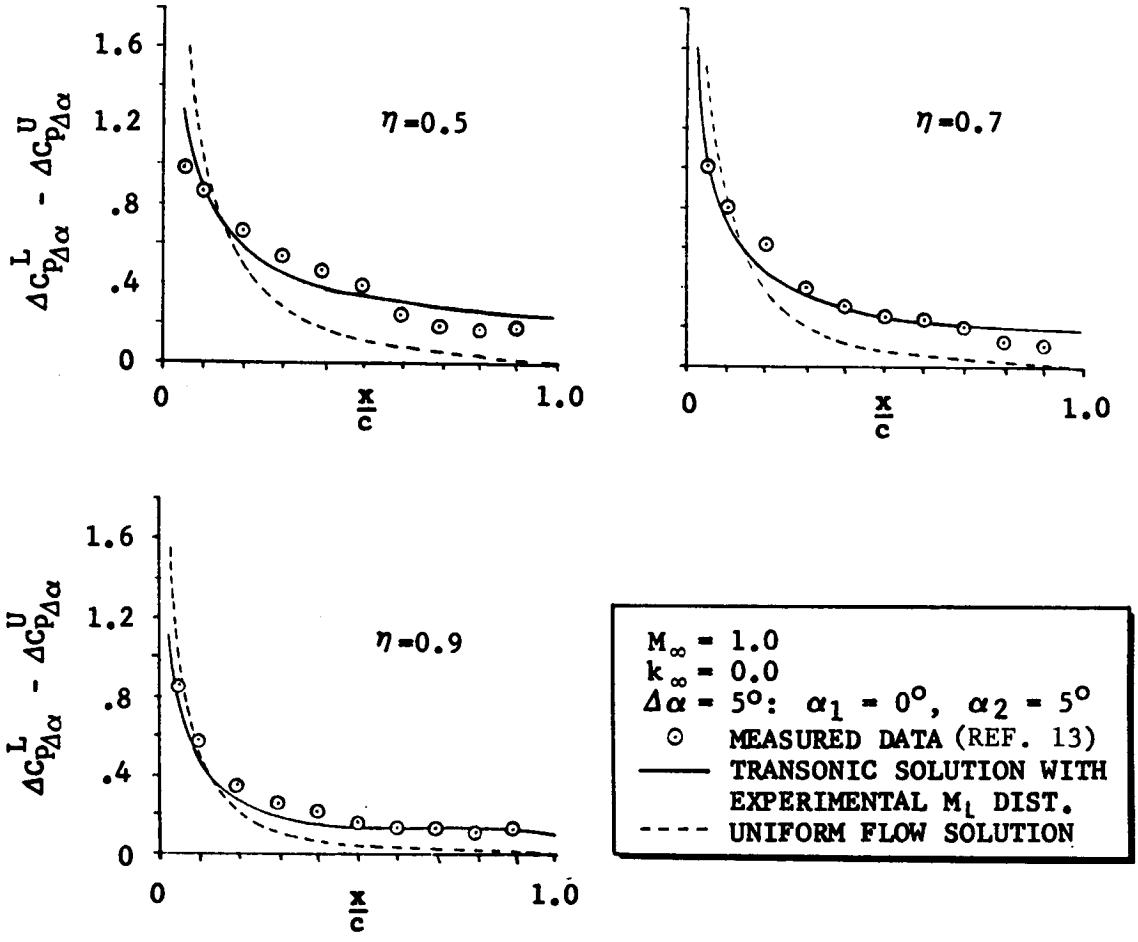

Figure 10. - Results for an AR 3.0 Rectangular Wing in Steady Flow at M_∞ = 1.0

A second solution is shown (dashed line) obtained with the same computer program for a uniform M_L=0.98 distribution. Comparison of the two solutions with experiment clearly demonstrates the superiority of the transonic solution.

Shown in figure 11 is a comparison of prediction and experiment for the same configuration as considered in figure 10 but for M_∞ =0.9. In this case a shock existed at about 70% chord on the upper and lower surfaces at α=0°. Again, three solutions were run for the transonic case in the same manner described previously. The control points used were 4 chordwise and 6 spanwise in the supersonic regionand 3 chordwise and 6 spanwise in the subsonic region. The total number of unknowns was 42 surface pressure function coefficients and 6 shock doublet function coefficients. The CPU was 20 seconds on the CDC 6600 or a total of 60 seconds for the three solutions.

Again, the transonic solution is clearly superior to the uniform flow solution. Not only that, but the results agree remarkably well with experiment.

Rectangular Wing Oscillating in Bending

The aspect ratio 3 rectangular wing was treated in the same manner as in reference 6 with only a change in the aerodynamic method. The Mach number distribution and control point arrays are shown in figure 12 along with the results for the (ref. 13) case of α=0°, M_∞=0.9, and k_∞ =0.13 (based on semi-chord). The solutions shown are for the transonic method with and without a shock and a uniform flow solution. The Mach number distribution as shown was assumed to be constant in the spanwise direction. In this case, the presence of the shock oscillation is clearly evident in the real part of the solution. Comparison with the transonic solution in reference 6 shows a significant improvement in the real part forward of the shock and in the imaginary part aft of the shock. The use of shock boundary conditions and downwash point Mach number in the kernel function resulted in correcting the discrepancies noted in reference 6.

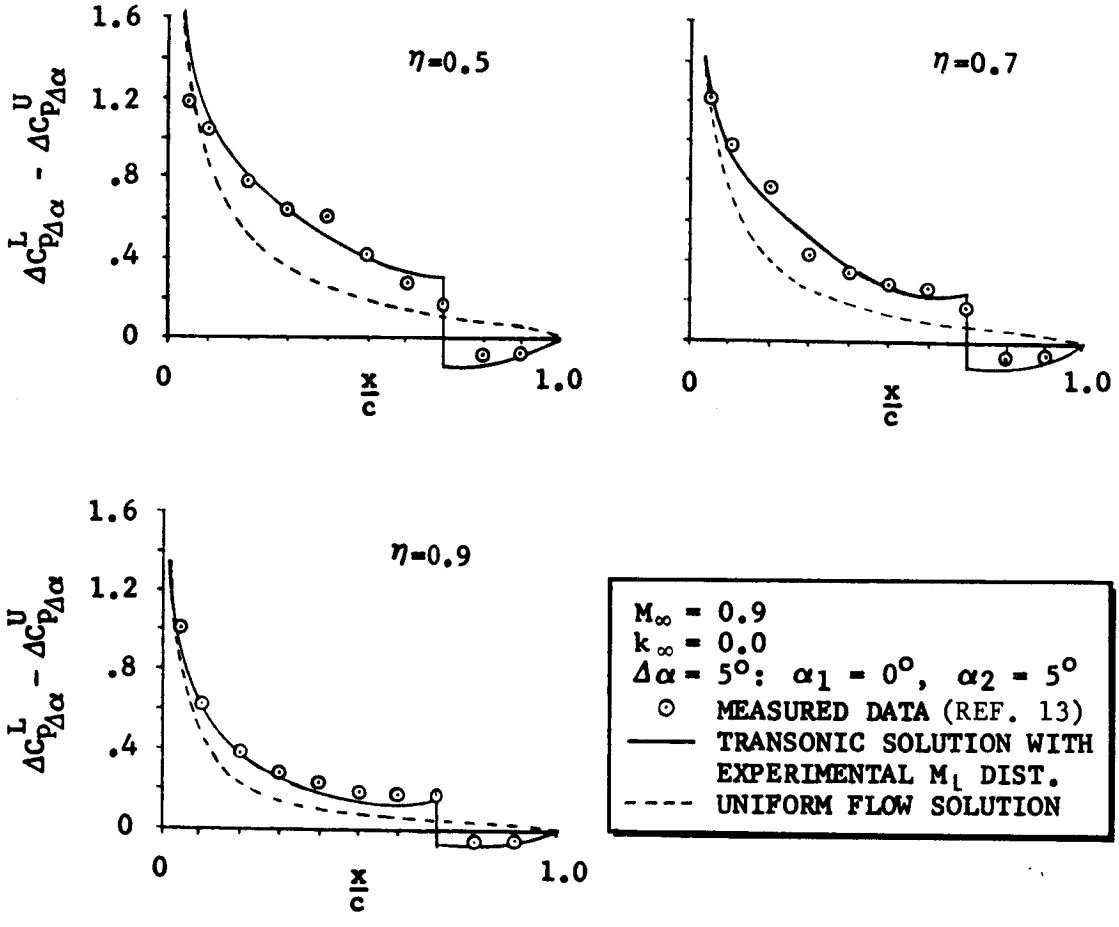

Figure 11. - Results for an AR 3.0 Rectangular Wing in Steady Flow at M_∞ = 0.90

	NC	NS
SUPERSONIC REGION	4	6
SUBSONIC REGION	3	6

CONTROL POINT ARRAYS

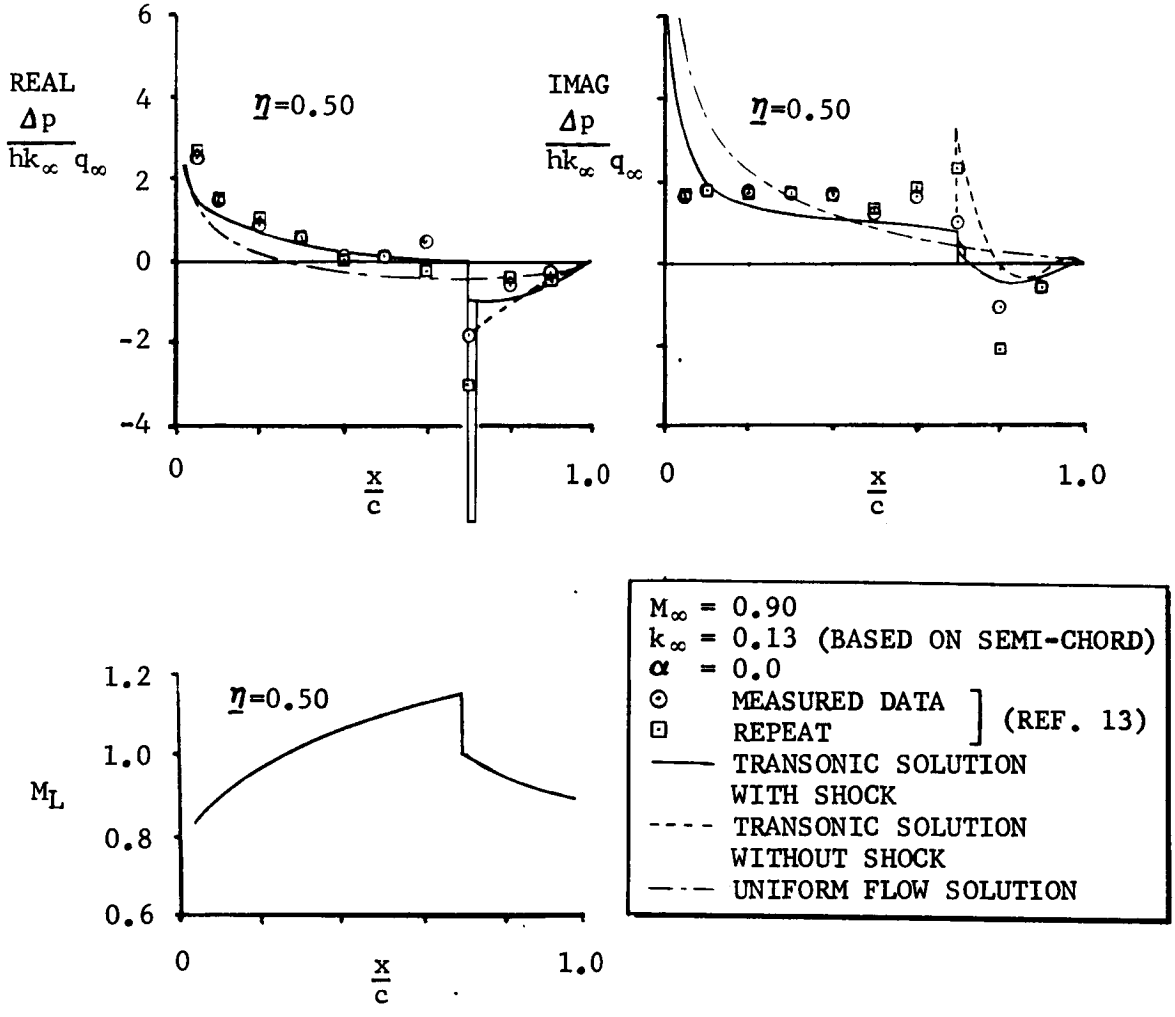

M_L DISTRIBUTION USED

Figure 12. - Results for an AR 3.0 Rectangular Wing Oscillating in M_∞ = 0.90 Flow

Swept Trapezoidal Wing With Roll Excitation

This case consisted of a swept trapezoidal wing oscillating in a roll mode at 100 Hz in an experimental study conducted by Becker (ref. 14). The actual mode included some bending and twisting motion which was somewhat difficult to determine from the data available in reference 14. This problem was discussed in reference 6 due to the fact that the mode shape used would not produce a uniform flow solution that would agree with a solution given by Becker. As a result, a study was made to determine the mode that would produce a solution that would show satisfactory agreement with Becker's data at $M_\infty = 0.8$. These results are shown in figure 13 with a tabulation of the mode used. The slopes were all assumed constant in the chordwise direction which probably has some influence on the results to be given.

The first transonic case for $M_\infty = 0.937$ and $k_\infty = 0.61$ (based on semi-span) was solved with the downwash point array and shock geometry shown in figure 14. The results are shown in figure 15 where the solid line is the transonic solution with a shock and a dashed line is the uniform flow solution. The solution given in reference 6 agreed better with experiment aft of the shock for both real and imaginary parts; however, those results were obtained with the questionable mode shape as was illustrated by a gross overprediction of the imaginary part forward of the shock. As was discussed in reference 6, the experimental data were felt to be strongly affected by wind tunnel wall interference. These effects would be stronger aft of the shock and weaker forward of the shock. Thus, the improved agreement forward of the shock indicates that the mode shown in figure 13 is more correct. If the Mach number increases so as to move the shock further aft and increase its strength, the interference effects should decrease.

The next case for $M_\infty = 0.997$ and $k_\infty = 0.58$ was solved with the downwash point array and shock geometry shown in figure 14. The results in figure 16 show a significant improvement over those of reference 6 which supports the suspicion that wall interference effects are present in the data. These results also exhibit a reasonable progression for the change in Mach number from 0.8 to 0.937 to 0.997.

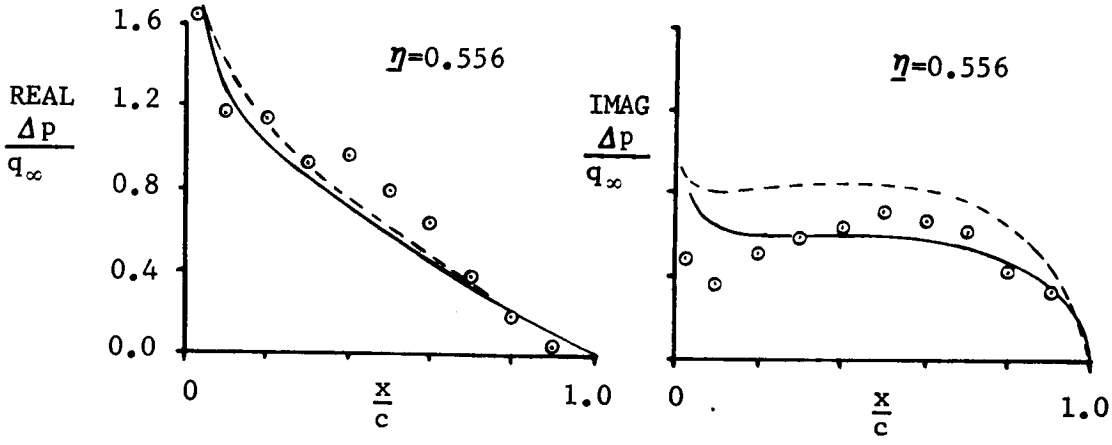

EMPIRICALLY DETERMINED MODE

η	$\tilde{z}_{LE}$	$\tilde{z}_{TE}$	$\frac{\partial \tilde{z}}{\partial \tilde{x}}$
.095	.075	.075	.008
.345	.122	.160	.086
.654	.255	.306	.336
.905	.382	.517	.625

M_∞ = 0.80
k_∞ = 0.71 (BASED ON SEMI-SPAN)
α = 0
⊙ MEASURED, (REF. 14)
—— UNIFORM FLOW SOLUTION WITH NEW MODE SHAPE
---- SOLUTION FROM (REF. 14)

Figure 13. - Uniform Flow Solution and Mode Shape for a Trapezoidal Wing Oscillating in M_∞ =0.8 Flow

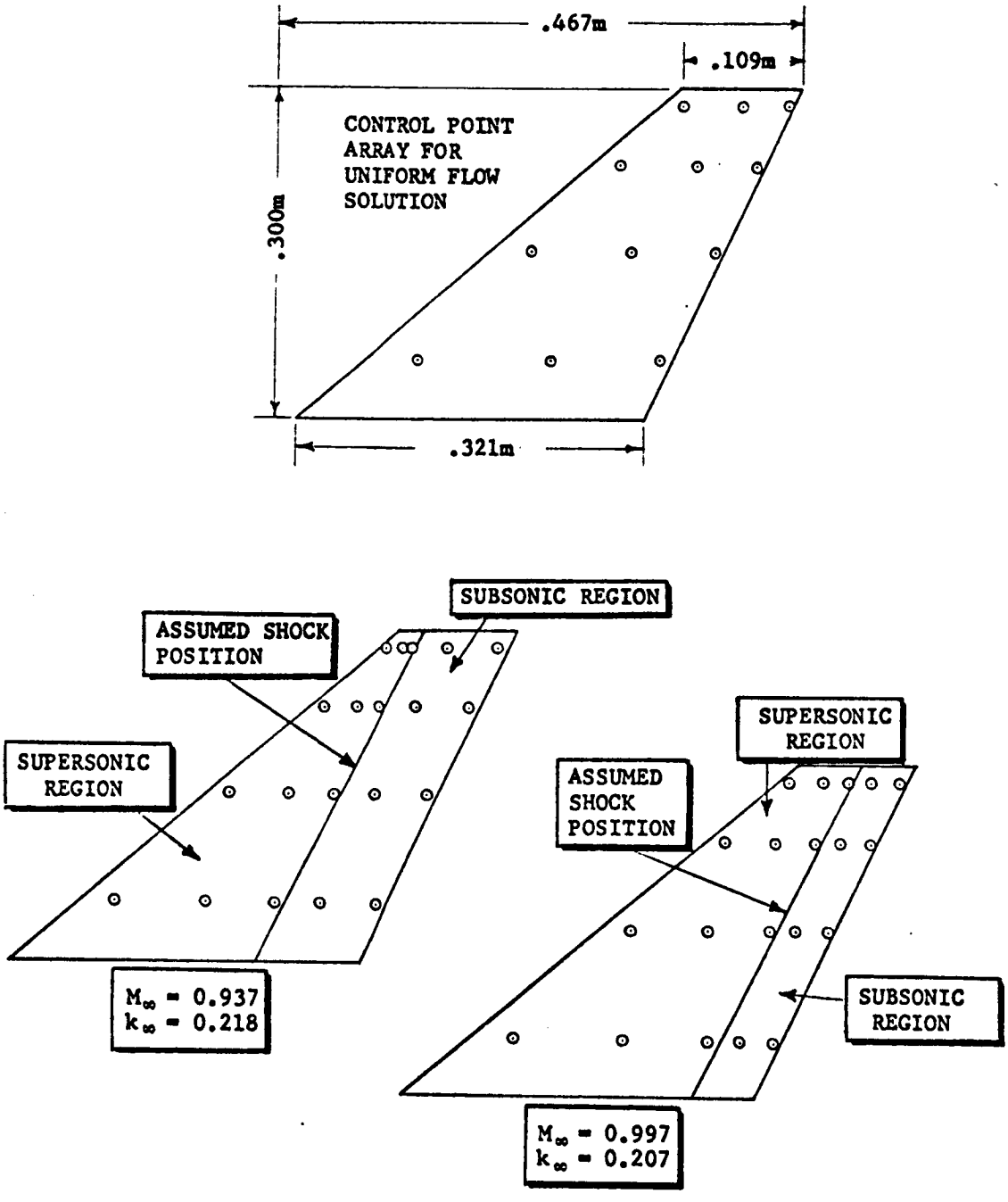

Figure 14. - Shock and Planform Geometry for the Trapezoidal Wing

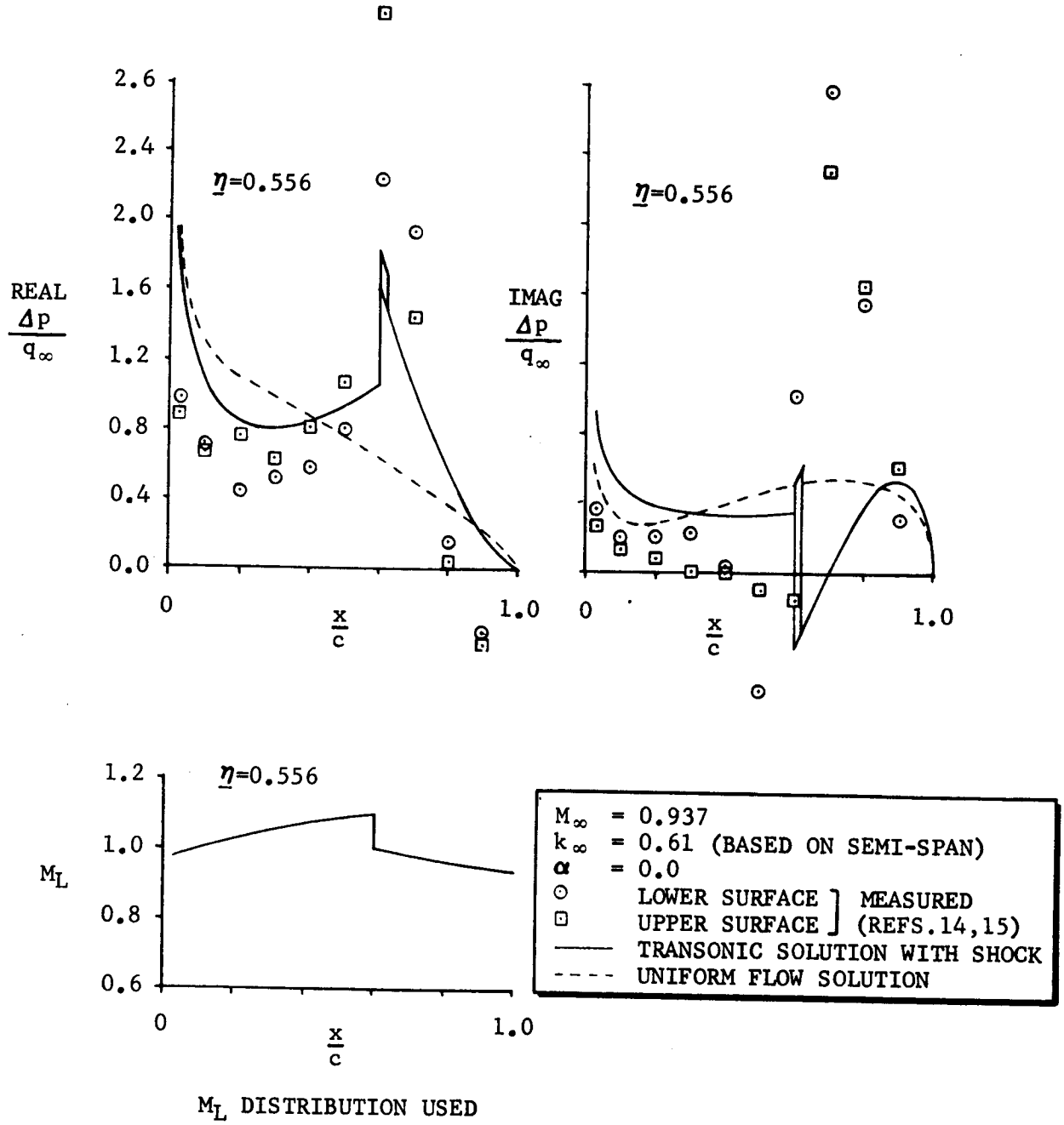

M_L DISTRIBUTION USED

Figure 15. - Results for the Oscillating Trapezoidal Wing at M_∞ = 0.937

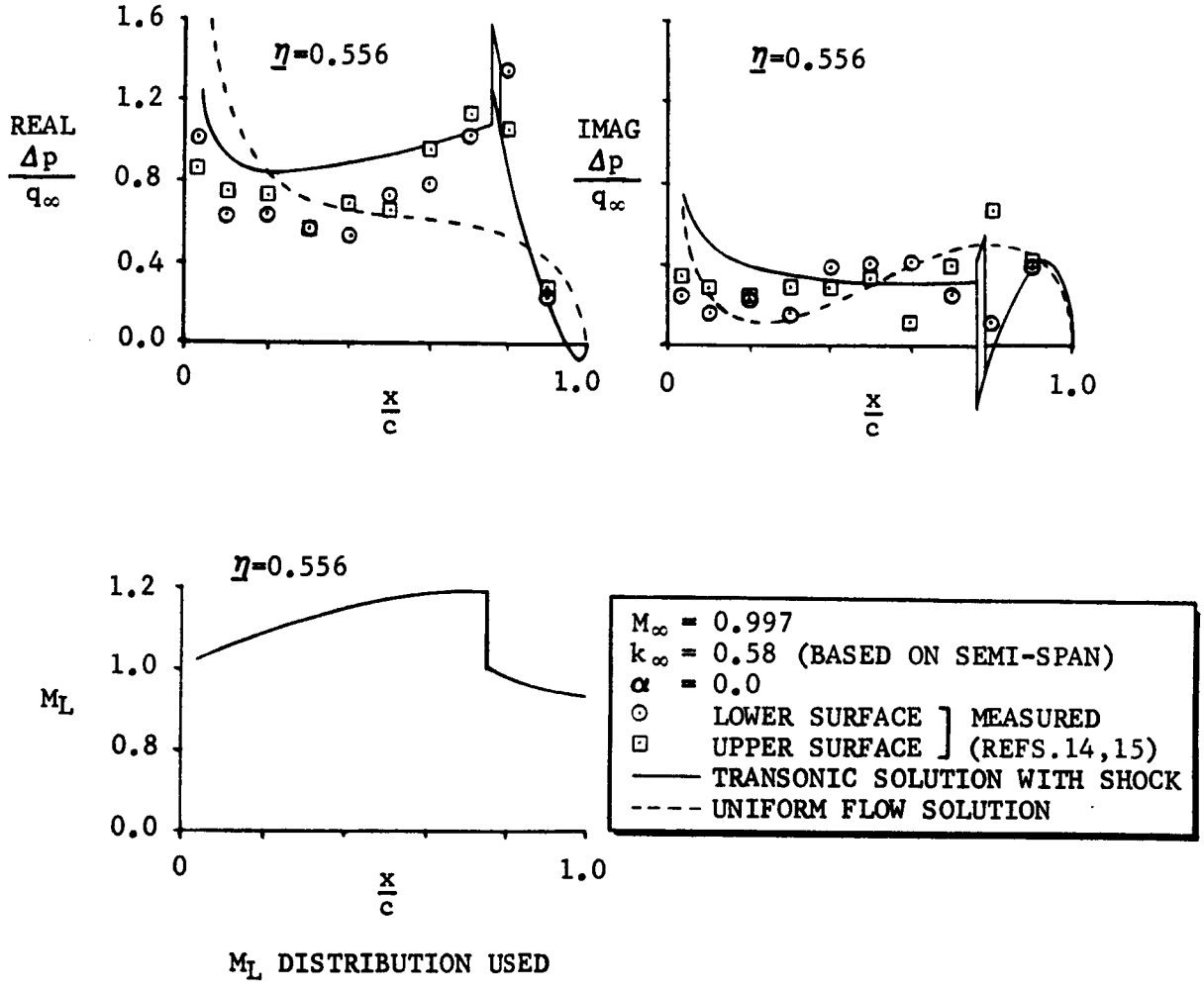

Figure 16. - Results for the Oscillating Trapezoidal Wing at $M_\infty = 0.997$

Swept Trapezoidal Wing With an Oscillating Aileron

A low aspect ratio swept trapezoidal wing with an oscillating inboard aileron in mixed flow was considered as the next case in reference 6. The conditions were M_∞ =0.942 and k_∞ =0.591 (based on semi-span) and the experimental data was obtained by Bergh, Tijdeman, and Zwaan (refs. 14 and 15). The configuration and control point arrays are shown in figure 17. In this case, it was felt that wall interference effects would not be so significant.

The solutions shown in figure 18 include those obtained from the transonic method with and without shocks and uniform flow theory. The uniform flow solution agrees quite well with experiment for points on the aileron. Over the remainder of the wing, however, both transonic solutions are far superior. The most notable point is the large negative value in the imaginary part of the measured data at η=0.55 which is predicted by the theory. Comparison with the results of reference 6 shows that the improved method is more realistic at all span stations. Inclusion of the shock boundary conditions has the greatest effect outboard of the aileron.

Wall Interference Effects in Oscillatory Flow

The aspect ratio 3 rectangular wing of reference 13 for M_∞ =1.0 and k_∞ =0.12 was chosen to determine if the transonic theory could be used to predict wall interference effects. These results are shown in figure 19 at mid-span. The first set of solutions shows comparison with the AFFDL sonic box method (ref. 1), the uniform flow kernel function solution at M_∞ =0.98, and experiment. With exception of the real part near the leading edge, the solutions essentially agree. The next set shows how the theory changes when non-uniform flow is accounted for. (The Mach number varies from 0.80 at the leading edge to 1.39 at the trailing edge.) The last set shows the effect of including the first reflection images above and below the wing for non-uniform flow (assuming 100% reflection).

The solution is most improved over the aft two-thirds when non-uniform flow effects are included and over the forward third when wall intereference effects are added. Since the forward third corresponds roughly to the subsonic region, it is expected

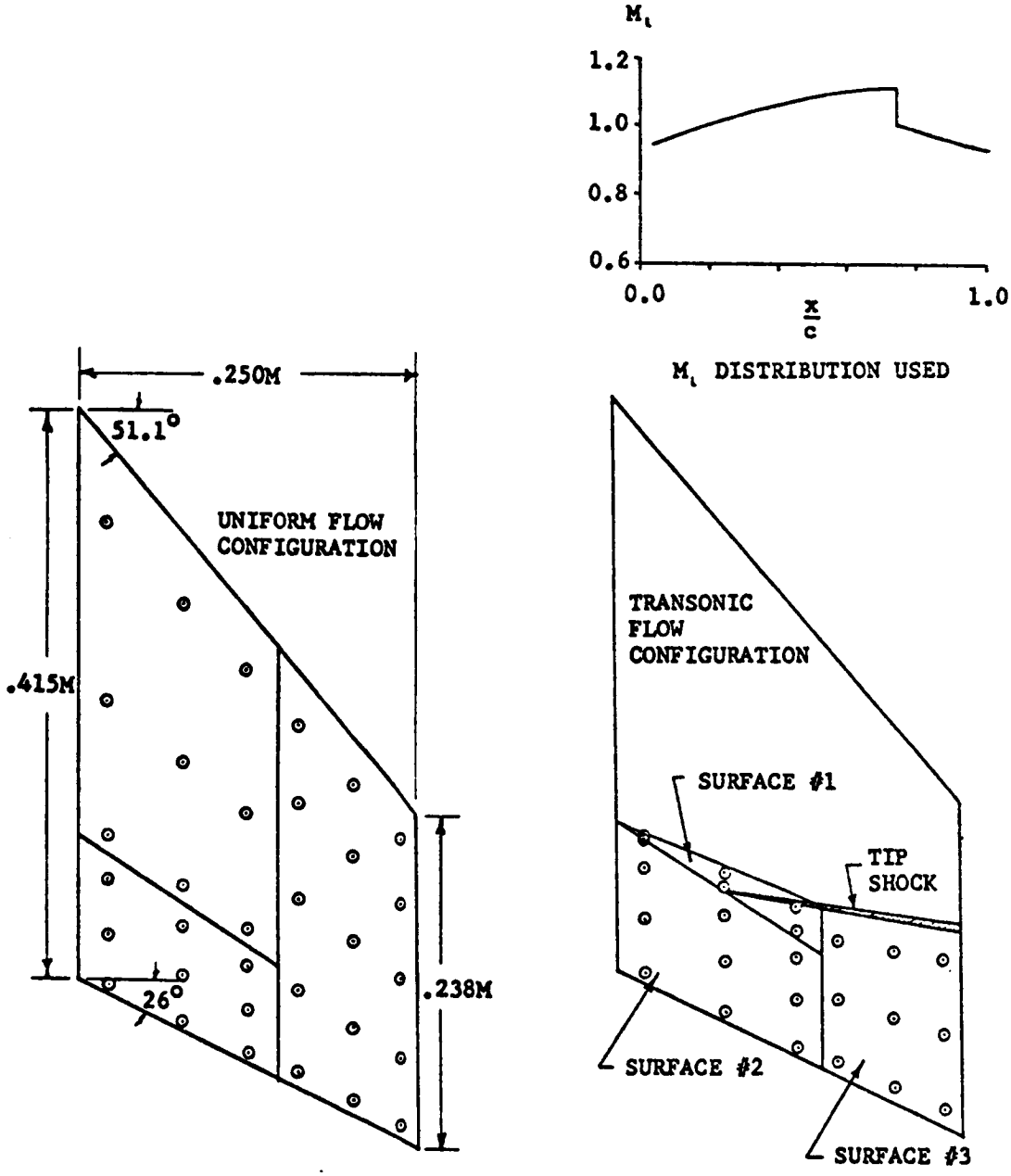

Figure 17. - Shock and Planform Geometry
For a Trapezoidal Wing With an Aileron

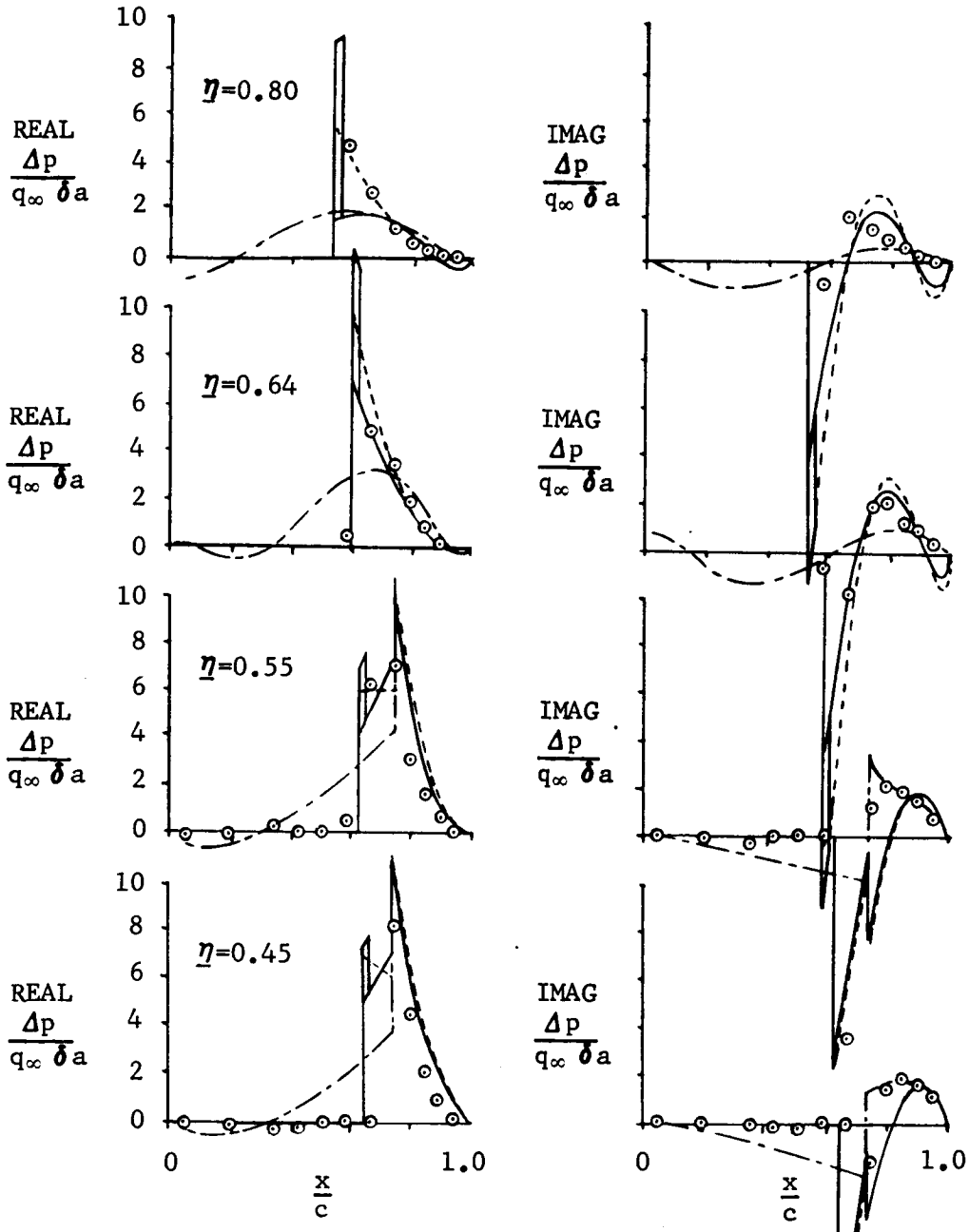

Figure 18. - Results for a Trapezoidal Wing With an Oscillating Aileron in M_∞= 0.942 Flow

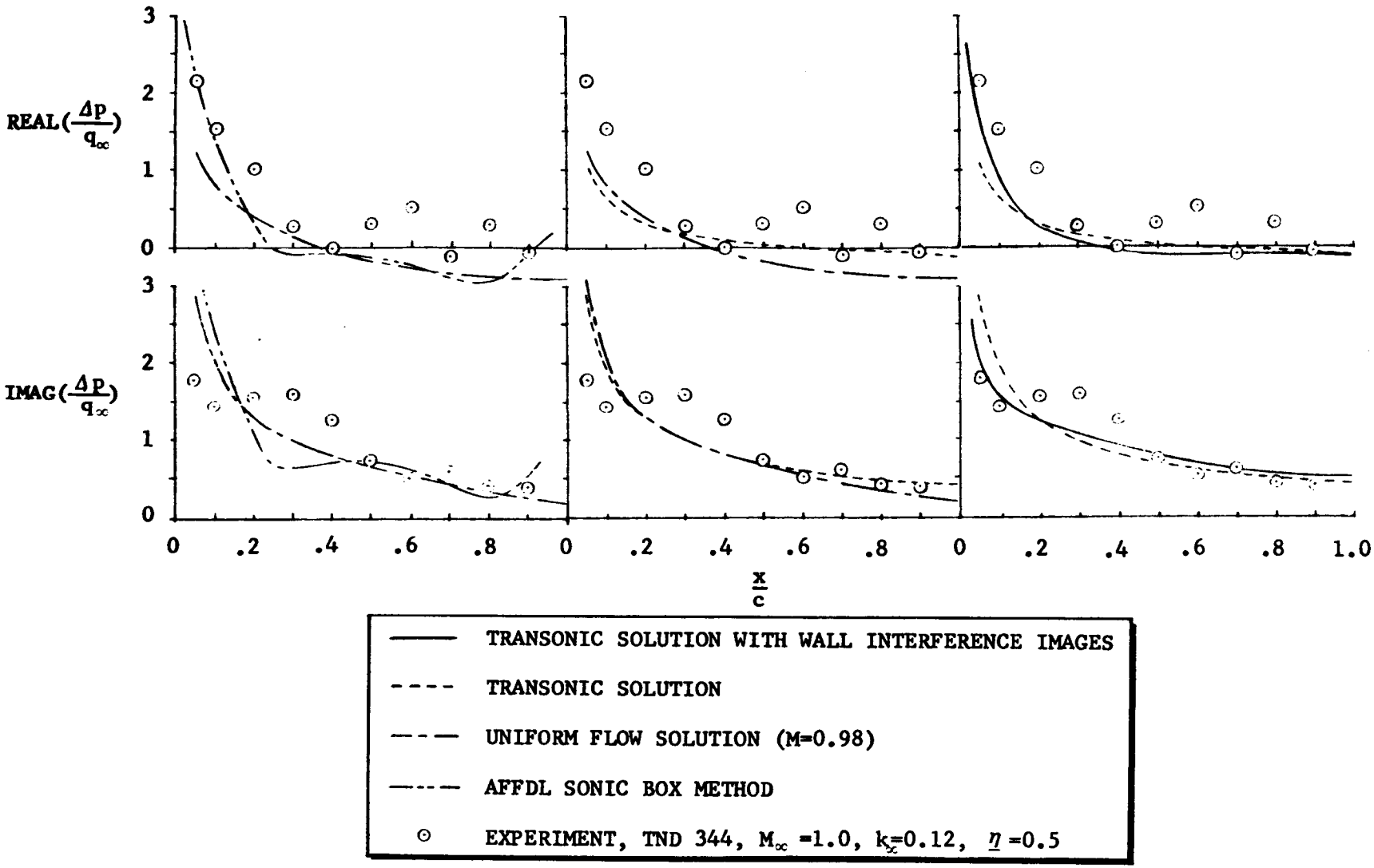

Figure 19. - Results for an AR 3.0 Rectangular Wing Oscillating in M_∞ = 1.0 Flow with Theoretical Wall Interference Effects

that in cases where shocks are present, the subsonic region aft of the shock would be greatly influenced by interference. This is felt to be the case for the experimental data given in figure 15. It also appears that the transonic results in figure 12 would be improved by including wall interference.

CONCLUSION

An improved kernel function method has been presented in this report that is applicable to multiple lifting surface problems in subsonic, transonic and supersonic flow. The method yields solutions for steady and oscillatory perturbations about linear or non-linear steady mean flows. Results have shown that the use of the local Mach number to calculate the kernel function leads to significantly improved solutions. The oscillatory normal shock boundary conditions as derived have shown the correct limiting properties as the frequency approaches zero or infinity. For cases with shocks imbedded in the flow, inclusion of the shock boundary conditions also led to improved solutions. Inclusion of an image to approximate wind tunnel wall interference was found to improve the agreement with experiment for a case involving a rectangular wing oscillating in $M_\infty = 1.0$ flow. The comparison of transonic solutions with linear theory results and experiment indicated that the effect of using transonic aerodynamics in flutter and dynamic response analyses could be significant.

General Dynamics Corporation
P. O. Box 748
Fort Worth, Texas 76101, September 30, 1976

APPENDIX A

THE NONPLANAR KERNEL FUNCTION

The nonplanar kernel function is expressed as

$$K(x_o,y_o,z_o,k,M) = -\frac{e^{-ikx_o}}{r^2}\left[K_1T_1 + \frac{K_2T_2}{r^2}\right], \quad R^2 \geq 0 \tag{A1a}$$

$$, \quad R^2 < 0 \tag{A1b}$$

where (see figure 3 for definitions of θ_p and θ_q)

$$x_o = x-\xi$$

$$y_o = y-\eta$$

$$z_o = z-\zeta$$

$$r^2 = y_o^2 + z_o^2$$

$$R^2 = x_o^2 + \beta^2 r^2$$

$$\beta^2 = 1 - M^2$$

$$T_1 = \cos(\theta_p-\theta_q)$$

$$T_2 = (z_o\cos\theta_p - y_o\sin\theta_p)(z_o\cos\theta_q - y_o\sin\theta_q)$$

which is valid for either subsonic or supersonic flow. The k and M values are those at the downwash point. The distinction between subsonic and supersonic flow is embodied in the K_1 and K_2 terms.

For supersonic flow (or supersonic downwash points), the K_1 term is defined as

$$K_1 = K_{11} + K_{12} \tag{A2}$$

where

$$K_{11} = \left(\frac{x_o}{R} + 1\right) e^{-ikru_1} - I_{11} \tag{A2a}$$

$$K_{12} = \left(\frac{x_o}{R} - 1\right) e^{-ikru_2} + I_{12} \tag{A2b}$$

$$R = (x_o^2 + \beta^2 r^2)^{\frac{1}{2}}$$

$$u_1 = -\frac{x_o - MR}{\beta^2 r}$$

$$u_2 = -\frac{x_o + MR}{\beta^2 r}$$

For $u_1 \geq 0$,

$$I_{11} = ikre^{-ikru_1} \sum_{n=1}^{11} \frac{a_n E_1^n}{nc+ikr} \tag{A3a}$$

or for $u_1 < 0$,

$$I_{11} = ikre^{-ikru_1} \sum_{n=1}^{11} \frac{a_n E_1^n}{nc-ikr} + 2\left[e^{-ikru_1} - 1 + (kr)^2 \sum_{n=1}^{11} \frac{a_n}{(nc)^2+(kr)^2}\right] \tag{A3b}$$

and

$$I_{12} = ikre^{-ikru_2} \sum_{n=1}^{11} \frac{a_n E_2^n}{nc+ikr} \tag{A3c}$$

where

$$\left.\begin{aligned} E_1 &= e^{-c|u_1|} \\ E_2 &= e^{-cu_2} \end{aligned}\right\} \quad c = 0.372$$

For the K_2 term, the following expressions are used for supersonic flow:

$$K_2 = K_{21} + K_{22} \tag{A4}$$

where

$$K_{21} = 3I_{11} - I_{21} - \left\{ 2\left(\frac{x_o}{R} + 1\right) + \frac{r^2}{R^2}\left[\frac{\beta^2 x_o}{R} + \frac{ikrM^2}{(1+u_1^2)^{\frac{1}{2}}} \right] \right\} e^{-ikru_1} \tag{A4a}$$

$$K_{22} = -3I_{12} - I_{22} - \left\{ 2\left(\frac{x_o}{R} - 1\right) + \frac{r^2}{R^2}\left[\frac{\beta^2 x_o}{R} - \frac{ikrM^2}{(1+u_2^2)^{\frac{1}{2}}} \right] \right\} e^{-ikru_2} \tag{A4b}$$

For $u_1 \geq 0$,

$$I_{21} = ikre^{-ikru_1} \sum_{n=1}^{11} \frac{b_n E_1^{2n}}{2nc+ikr} \tag{A5a}$$

or for $u_1 < 0$,

$$I_{21} = ikre^{-ikru_1} \sum_{n=1}^{11} \frac{b_n E_1^{2n}}{2nc-ikr}$$

$$+ 2\left[e^{-ikru_1} - 1 + (kr)^2 \sum_{n=1}^{11} \frac{b_n}{(2nc)^2+(kr)^2} \right] \tag{A5b}$$

and

$$I_{22} = ikre^{-ikru_2} \sum_{n=1}^{11} \frac{b_n E_2^{2n}}{2nc+ikr} \tag{A5c}$$

The a_n and b_n coefficients in the series summations in equations (A3) and (A5) are given in table A1. The a_n set are those given originally by Laschka (ref. 17) for the approximation

$$\frac{u}{(1+u^2)^{\frac{1}{2}}} - 1 \approx \sum_{n=1}^{11} a_n e^{-ncu}$$

The b_n set are those given by Cunningham (ref. 6) for the approximation

$$\frac{u}{(1+u^2)^{3/2}} - 1 \approx \sum_{n=1}^{11} b_n e^{-2ncu}$$

The expressions for K_1 and K_2 in subsonic flow (or at subsonic downwash points) are similar to but simpler than those for supersonic flow. The terms are

$$K_1 = K_{11} \tag{A6}$$

and

$$K_2 = K_{21} \tag{A7}$$

where K_{11} and K_{21} are defined for supersonic flow in equations (A2a) and (A4a), respectively.

TABLE A1. APPROXIMATION COEFFICIENTS USED IN THE KERNEL FUNCTION INTEGRALS K_1 AND K_2

n	a_n	b_n
1	0.24186198	3.509407
2	-2.7968027	-57.17120
3	24.991079	624.7548
4	-111.59196	-3830.151
5	271.43549	14538.51
6	-305.75288	-35718.32
7	-41.183630	57824.14
8	545.98537	-61303.92
9	-644.78155	40969.58
10	328.72755	-15660.04
11	-64.279511	2610.093

APPENDIX B

CALCULATION OF SELF INDUCED DOWNWASH

Evaluation of the integral given by equation (1) is performed in two steps. First the chordwise integration is performed in a manner which varies according to whether the Mach number is subsonic or supersonic. The spanwise integration is then performed independently of whether the flow is subsonic or supersonic. This appendix summarizes the manner in which these integrations are accomplished for equation (1) for q=p, the case of self induced downwash. A special treatment is given to chordwise integration in the vicinity of the downwash point.

Chordwise Integration

For steady supersonic flow, the integral equation may be cast in the form

$$\bar{w}(x,y) = -2 \oint_{\eta_a}^{\eta_b} \int_{-1}^{\xi_{mc}} \Delta\bar{C}_p(\xi,\eta) \frac{x_o}{R} \frac{b(\eta)\,d\xi\,d\eta}{s_o(y-\eta)^2} \tag{B1}$$

where

$$\bar{w}(x,y) = \frac{8\pi\bar{w}(x,y)}{U}$$

$$R^2 = x_o^2 + \beta^2 r^2$$

ξ_{mc} = Mach cone boundary in the transformed coordinate system

Since the kernel function is singular along the Mach cone boundary, $\xi = \xi_{mc}$, as $(E)^{-\frac{1}{2}}$ for $E \to 0$, a new chordwise variable of integration, δ, will be defined as

$$\delta = \frac{1-\xi_{mc}+2\xi}{1+\xi_{mc}}$$

and

$$d\delta = \frac{2d\xi}{1+\xi_{mc}}$$

where

$\xi_{mc} = \beta r$, Mach cone boundary in the physical coordinate system.

Substituting δ for ξ and multiplying and dividing the integrand by $(1-\delta^2)^{\frac{1}{2}}$, equation (B1) becomes

$$\bar{w}(x,y) = -\frac{2}{S_o} \oint_{\eta_a}^{\eta_b} \left\{ \frac{(1+\xi_{mc})}{2} \int_{-1}^{1} (1-\delta^2)^{-\frac{1}{2}} \left[(1-\delta^2)^{\frac{1}{2}} \Delta\bar{C}_p(\xi,\eta) \right] \frac{x_o d\delta}{R} \right\} \cdot \frac{b(\eta)d\eta}{(y-\eta)^2} \quad , \quad \xi_{mc} < 1 \tag{B2a}$$

and

$$\bar{w}(x,y) = -\frac{2}{S_o} \oint_{\eta_a}^{\eta_b} \left\{ \int_{-1}^{1} (1-\xi^2)^{-\frac{1}{2}} \left[(1-\xi^2)^{\frac{1}{2}} \Delta\bar{C}_p(\xi,\eta) \right] \frac{x_o d\xi}{R} \right\} \cdot \frac{b(\eta)d\eta}{(y-\eta)^2} \quad , \quad \xi_{mc} \geq 1 \tag{B2b}$$

It should be noted that regardless of whether the Mach cone is forward ($\xi_{mc} < 1$) or aft ($\xi_{mc} \geq 1$) of the trailing edge, the chordwise weighting function, $(1-\delta^2)^{-\frac{1}{2}}$ or $(1-\xi^2)^{-\frac{1}{2}}$, is the same. As a result, the same chordwise integration scheme can be applied.

The Tschebychev-Gaussian quadrature integration formula, which is applicable to the chordwise integral in equations (B2) is

$$\int_{-1}^{1} (1-\xi^2)^{-\frac{1}{2}} f(\xi)d\xi = \frac{\pi}{J} \sum_{j=1}^{J} f(\xi_j)$$

where

$$\xi_j = -\cos\left(\frac{2j-1}{2J}\pi\right) \quad , \quad j=1,2,\ldots J$$

and $f(\xi)$ is expressible as a polynomial of (2J-1) degree or less.

Now, the chordwise integrals in equations (B2) may be evaluated in steady or unsteady flow as

$$G(y,\underline{\eta}) = \frac{b(\underline{\eta})}{2S_o}(1+\xi_{mc})\frac{\pi}{J}\sum_{j=1}^{J}(1-\delta_j^2)^{\frac{1}{2}}\Delta\overline{C}_p(\underline{\xi}_j,\underline{\eta})\cdot$$

$$(y-\eta)^2 K(x-\xi_j, y-\eta, 0, k, M), \quad -1 < \xi_{mc} < 1$$

$$= 0 \qquad , \quad \xi_{mc} \le -1 \qquad \text{(B3a)}$$

where

$$\underline{\delta}_j = -\cos\left(\frac{2j-1}{2J}\pi\right), \quad j=1,2,\ldots J$$

$$\underline{\xi}_j = \tfrac{1}{2}\left|(1+\xi_{mc})\underline{\delta}_j + (\xi_{mc}-1)\right|$$

$$\xi_j = \underline{\xi}_j b(\underline{\eta}) + \xi_m(\underline{\eta})$$

and as

$$G(y,\underline{\eta}) = \frac{b(\underline{\eta})}{S_o}\frac{\pi}{J}\sum_{j=1}^{J}(1-\underline{\xi}_j^2)^{\frac{1}{2}}\Delta\overline{C}_p(\xi_j,\underline{\eta})\cdot$$

$$(y-\eta)^2 K(x-\xi_j, y-\eta, 0, k, M), \quad \xi_{mc} \ge 1 \qquad \text{(B3b)}$$

where

$$\underline{\xi}_j = -\cos\left(\frac{2j-1}{2J}\pi\right), \quad j=1,2,\ldots J$$

The value for J varies according to the downwash point location as follows:

$$J = 4+i, \quad i = 1,2,\ldots\bar{m}_q$$

where i is the chordwise downwash point number starting with i=1 at the leading edge and $i=\bar{m}_q$ at the trailing edge. Thus, as an example for $\bar{m}_q=5$, J varies as

$$J = 4+1 = 5 \quad \text{(leading edge downwash point)}$$
$$J = 4+\bar{m}_q = 9 \quad \text{(trailing edge downwash point)}$$

The same value of J is used in equations (B3) at all integration chords with exception of those near the downwash point for any given downwash point. When the Mach cone falls forward of the leading edge, the value of $G(\underline{y}, \underline{\eta})$ is set to zero as shown in equation (B3a).

The chordwise integration for subsonic flow is similar to that presented above. The integral is of the form

$$\bar{w}(x,y) = -\oint_{-1}^{1}\int_{-1}^{1} \Delta\bar{C}_p(\underline{\xi},\underline{\eta})\left[1+\frac{x_o}{R}\right]\frac{b(\underline{\eta})d\underline{\xi}d\underline{\eta}}{S_o(\underline{y}-\underline{\eta})^2} \qquad \text{(B4)}$$

The most notable difference between equations (B1) and (B4) is the limits of integration. The chordwise integration formula is also changed to

$$\int_{-1}^{1}\sqrt{\frac{1-\underline{\xi}}{1+\underline{\xi}}}\, f(\underline{\xi})d\underline{\xi} = \frac{2\pi}{2J+1}\sum_{j=1}^{J}(1-\underline{\xi}_j)f(\underline{\xi}_j) \qquad \text{(B5)}$$

where

$$\underline{\xi}_j = -\cos\left(\frac{2j-1}{2J+1}\pi\right), \quad j=1,2,\ldots J$$

The integration is performed by multiplying and dividing by $(1-\underline{\xi})^{\frac{1}{2}}/(1+\underline{\xi})^{\frac{1}{2}}$ and using equation (B5). The result for steady or unsteady flow is

$$G(\underline{y},\underline{\eta}) = \frac{b(\eta)}{S_o}\frac{2\pi}{2J+1}\sum_{j=1}^{J}(1-\xi_j^2)^{\frac{1}{2}}\Delta\overline{C}_p(\xi_j,\underline{\eta})\cdot$$

$$(y-\eta)^2K(x-\xi_j,y-\eta,0,k,M) \tag{B6}$$

The value of J is constant at

$$J=\overline{m}_q$$

for all integration chords except those near the downwash point.

Spanwise Integration

In supersonic flow, the spanwise integral is of the form

$$I(\underline{y}) = \oint_{\underline{\eta}_a}^{\underline{\eta}_b} \frac{G(\underline{y},\underline{\eta})}{(\underline{y}-\underline{\eta})^2}\,d\underline{\eta} \tag{B7}$$

where the limits of integration, $\underline{\eta}_a$ and $\underline{\eta}_b$, are the locations of the intersection of the Mach fore cone with the wing leading edge. Except for a weighting function, $(1-\underline{\eta}^2)^{\frac{1}{2}}$, and the limits $\underline{\eta}_a$ and $\underline{\eta}_b$, equation (B7) is identical to the equation for subsonic flow developed in reference 7. Since equation (B7) is more general, it is the form used in this report for subsonic as well as supersonic flow.

Let

$$G(\underline{y},\underline{\eta}) = G(\underline{y},\underline{y}) + (\underline{\eta}-\underline{y})G'(\underline{y},\underline{y}) + (\underline{\eta}-\underline{y})^2G''(\underline{y},\underline{y}) + \ldots \tag{B8}$$

Adding and subtracting equation (B8) from (B7) yields

$$I(\underline{y}) = \int_{\underline{\eta}_a}^{\underline{\eta}_b} \left\{ G(\underline{y},\underline{\eta}) - \left[G(\underline{y},\underline{y}) + (\underline{\eta}-\underline{y})G'(\underline{y},\underline{y}) + (\underline{\eta}-\underline{y})^2 G''(\underline{y},\underline{y}) + \ldots \right] \right\} \frac{d\underline{\eta}}{(\underline{y}-\underline{\eta})^2}$$

$$+ \oint_{\underline{\eta}_a}^{\underline{\eta}_b} \left[G(\underline{y},\underline{y}) + (\underline{\eta}-\underline{y})G'(\underline{y},\underline{y}) + (\underline{\eta}-\underline{y})^2 G''(\underline{y},\underline{y}) + \ldots \right] \frac{d\underline{\eta}}{(\underline{y}-\underline{\eta})^2} \qquad \text{(B9)}$$

where the first integral may be evaluated with numerical quadrature integration techniques and the second integral evaluated analytically.

The quadrature integration is performed with a formula derived from the equations for function approximation with Tschebychev polynomials of the first kind. The approximation to a function $g(\underline{\eta}')$ over the interval $(-1 \leq \underline{\eta}' \leq 1)$ is

$$g(\underline{\eta}') = \frac{C_o}{2} + \sum_{k=1}^{S'-1} C_k \, T_k(\underline{\eta}') \qquad \text{(B10)}$$

where

$$C_k = \frac{2}{S'} \sum_{s=1}^{S'} f(\underline{\eta}'_s) \, T_k(\underline{\eta}'_s) \qquad \text{(B11)}$$

$$\underline{\eta}'_s = -\cos\left(\frac{2s-1}{2S'}\pi\right), \quad s=1,2,\ldots S'$$

S' = total integration chords in the range $-1 \leq \eta \leq 1$

If $g(\underline{\eta}')$ is expressible as a polynomial of degree (S'-1) or less over the interval $(-1 \leq \underline{\eta}' \leq 1)$, the approximation is exact. The quadrature integration formula is derived by integrating equation (B10) from $\underline{\eta}' = -1$ to $\underline{\eta}' = +1$ and inserting equation (B11). The result is

$$\int_{-1}^{1} g(\underline{\eta}')d\underline{\eta}' = \frac{\pi}{S'} \sum_{s=1}^{S'} g(\underline{\eta}'_s)\ h\ (\underline{\eta}'_s) \tag{B12}$$

where

$$h(\underline{\eta}'_s) = \frac{2}{\pi} \sum_{k=0}^{S'-1} T_k(\underline{\eta}'_s)\, \mathcal{T}_k$$

and

$$\mathcal{T}_o = 1.0$$

$$\mathcal{T}_k = 0\ ,\ k=1,3,5,\ldots$$

$$\mathcal{T}_k = \int_{-1}^{1} T_k(\underline{\eta}')d\underline{\eta}' = \frac{-2}{(k-1)(k+1)}\ ,\ k=2,4,\ldots$$

The only difference in the quadrature integration formula above and that used in the subsonic spanwise integral of reference 6 is the definition of $h(\underline{\eta}'_s)$.

In order to achieve a more optimum distribution of spanwise integration points, a coordinate transformation is made such that the greatest density of integration points is next to the downwash chord. This step is particularly necessary for downwash points near the leading edge in supersonic flow. The transformation is

$$\underline{\eta}_s = \underline{y}_r + (\underline{\eta}'_s+1),\quad \underline{\eta}'_s < -\underline{y}_r$$

$$\underline{\eta}_s = \underline{y}_r + (\underline{\eta}'_s-1),\quad \underline{\eta}'_s > -\underline{y}_r$$

where

$$\underline{y}_r = \cos\left(\frac{nr\pi}{S'}\right)\ ,\ r=1,2,\ldots\bar{n}\ ,\ n=1,3,5,\ldots \tag{B13}$$

and

$$S = S' = n(2\bar{n}+1) \qquad \text{type 1 wing in figure 2} \qquad \text{(B14a)}$$

$$S = 2S' = 2n(\bar{n}+1) \qquad \text{type 2 wing in figure 2} \qquad \text{(B14b)}$$

$$S = S' = n(\bar{n}+1) \qquad \text{type 3 wing in figure 2} \qquad \text{(B14c)}$$

The y_r defined in equation (B13) are the same as used in subsonic flow and are interdigitated with the η_s points by the relationship between $\bar{n}$ and S in equations (B14).

Returning to equation (B9), the integral is evaluated with equation (B12) as

$$I(y_r) = \frac{\pi}{S} \sum_{s=1}^{S} \frac{G(y_r,\eta_s)}{(y_r-\eta_s)^2} h(\eta_s') + Q(y_r) \qquad \text{(B15)}$$

where

$$Q(y_r) = G(y_r,y_r)\, E_o(y_r) + G'(y_r,y_r)\, E_1(y_r) + G''(y_r,y_r)\, E_2(y_r) \qquad \text{(B16)}$$

The $E_n(y_r)$ terms are the differences between the quadrature and analytic integral evaluations

$$E_o(y_r) = \left[\frac{1}{(\eta_a-y_r)} - \frac{1}{(\eta_b-y_r)}\right] - \frac{\pi}{S} \sum_{s=1}^{S} \frac{h(\eta_s')d(\eta_s)}{(\eta_s-y_r)^2} \qquad \text{(B17a)}$$

$$E_1(y_r) = \ell_n \left|\frac{\eta_b-y_r}{\eta_a-y_r}\right| - \frac{\pi}{S} \sum_{s=1}^{S} \frac{h(\eta_s')d(\eta_s)}{(\eta_s-y_r)} \qquad \text{(B17b)}$$

$$E_2(y_r) = (\eta_b-\eta_a) - \frac{\pi}{S} \sum_{s=1}^{S} h(\eta_s')d(\eta_s) \qquad \text{(B17c)}$$

for

$$d(\eta_s) = 1 \ , \ \underline{\eta}_a \leq \underline{\eta}_s \leq \underline{\eta}_b$$

$$= 0 \ , \ \underline{\eta}_s < \underline{\eta}_a \text{ or } \underline{\eta}_s > \underline{\eta}_b \qquad \text{(B17d)}$$

where in the E_o term the Mangler formula was used (ref. 18). No terms higher than E2 ($\underline{y}_r$) have been found necessary, hence, the series was truncated at that point.

The same equations are used in subsonic flow by simply setting the limits at

$$\underline{\eta}_a = -1$$
$$\underline{\eta}_b = +1$$

which maintains continuity from subsonic flow to supersonic flow.

Shown in figure B1 are examples of the relationships between $\underline{y}_r$, $\underline{\eta}_s$, $\underline{\eta}_a$ and $\underline{\eta}_b$. Also shown are hypothetical distributions of $G(\underline{y}_r, \underline{\eta}_s)/(\underline{y}_r - \underline{\eta}_s)^2$ which are being integrated. The two examples illustrate the differences between the treatment of type 1, type 2 and type 3 planforms shown in figure B2. The differences are embodied in the definition of the spanwise functions and $\underline{\eta}$:

$$\eta = \underline{\eta} s_o \qquad \text{type 1 surface} \qquad \text{(B18a)}$$

$$\eta = \frac{s_o}{2} (1+\underline{\eta}) \qquad \text{type 2 and 3 surfaces} \qquad \text{(B18b)}$$

$$\eta = -\frac{s_o}{2} (1+\underline{\eta}) \qquad \text{type 2 surface} \qquad \text{(B18c)}$$

For equation (B18a), there are S' total integration chords on the wing and $\overline{n} = (S'/n-1)/2$ downwash chords on the right hand wing. For equations (B18b) and (B18c), there are 2S' and S' total integration chords for type 2 and 3 surfaces, respectively, and $\overline{n} = (S'/n-1)$ downwash chords on the right hand wing.

The G, G' and G'' terms are simply calculated as the coefficients of a quadratic curve fit of the chordwise integrals at $G(\underline{y}_r, \underline{\eta}_{S'})$, $G(\underline{y}_r, \underline{y}_r)$, and $G(\underline{y}_r, \underline{\eta}_1)$. The relationship between these integrals is also shown in figure B1. In unsteady flow, these terms will have real and imaginary parts.

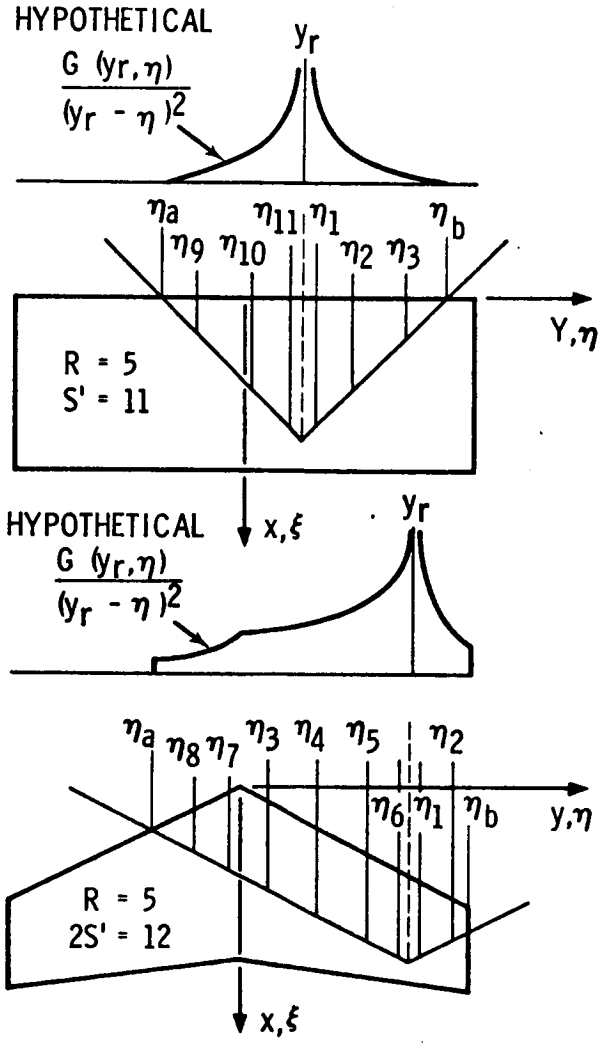

Figure B1. - Geometric Relationships in the Spanwise Integration Scheme

Chordwise Integration Near and Including the Downwash Chord

Because of the close spacing of the adjacent integration chords with the downwash chord in the spanwise integration scheme, the chordwise integrations must be extremely accurate in this region. Thus, all chordwise integrations within a small spanwise distance of the downwash chord, $\underline{y}_r$, are evaluated more precisely than for those chords outside of this distance. The distance is taken as $\pm(1-\underline{y}_1)$ where $\underline{y}_1$ is defined by equation (B13). Thus, for all $\underline{\eta}_s$ defined as

$$(\underline{y}_r-\Delta) < \underline{\eta}_s < (\underline{y}_r+\Delta)$$

where

$$\Delta = 1-\underline{y}_1$$

the number of chordwise integration points, J, are defined as

$J' = 3J+1$	subsonic integration
$J' = 3J$	supersonic integration

The terms $G(\underline{y}_r, \underline{\eta}_s)$, $G(\underline{y}_r,\underline{y}_r)$ and $G(\underline{y}_r, \underline{\eta}_1)$ are always included within this region which results in very accurate estimates of the G, G' and G'' terms required for equation (B16) for subsonic flow. For supersonic flow some additional manipulation is needed.

Because the chordwise integrand is singular at $\underline{\xi} = \underline{\xi}_{mc}$ for $\underline{\eta} \neq \underline{y}_r$, and is non-singular for $\underline{\eta} = \underline{y}_r$, a difficulty arises in the calculation of a value for $G(\underline{y}_r,\underline{y}_r)$ that is continuous with $G(\underline{y}_r, \underline{\eta})$ as $\underline{\eta} \rightarrow \underline{y}_r$. As a result, a simple but devious means for calculating $G(\underline{y}_r,\underline{y}_r)$ as a function of $G(\underline{y}_r, \underline{\eta})$ was developed as follows. For simplicity, let

$$G_S = G(\underline{y}_r, \underline{\eta}_S) \qquad G_1 = G(\underline{y}_r, \underline{\eta}_1)$$

$$G_r = G(\underline{y}_r, \underline{y}_r)$$

As a first approximation, G_{r_o}, to the value of G_r without actually calculating the integral, an average value is used

$$G_{r_o} = \frac{G_S+G_1}{2} \tag{B19}$$

Since the streamwise variation of the kernel function becomes rapidly independent of ξ for $\eta \approx y_r$, the Gr_o approximation actually represents a chordwise integral of the form

$$Gr_o = \frac{2b(\eta)}{s_o} \int_{\xi_{LE_r}}^{\xi_{\Delta'}} \Delta\bar{C}_p(\xi, y_r)(x-\xi)\left[(x-\xi)^2 + (1-M^2)(\Delta')^2\right]^{-\frac{1}{2}} d\xi \qquad (B20)$$

where

$$\xi_{\Delta'} = x-\beta\Delta'$$

$$\Delta' = y_r-\eta_S = \eta_1-y_r$$

and ξ_{LEr} is the leading edge location at y_r.

The exact value required for Gr is

$$Gr = \frac{2b(\eta)}{s_o} \int_{\xi_{LE}}^{x} \Delta\bar{C}_p(\xi, y_r)d\xi$$

Thus, a correction must be made to Gr_o. The first correction is made by removing the singularity portion at ξ_{mc} without disturbing the leading edge sweep effect as given by ξ_{LE}. Since the error in equation (B20) is near the aft limit, $\xi_{\Delta'}$, the next level of approximation, Gr_1, is

$$Gr_1 = Gr_o + \frac{2b(\eta)}{s_o}\Delta\bar{C}_p(\xi_{\Delta'}, y_r)\left\{\int_{\xi_{LE_r}}^{\xi_{\Delta'}} d\xi - \int_{\xi_{LE_S}}^{\xi_{\Delta'}} (x-\xi)\left[(x-\xi)^2 + (1-M^2)(\Delta')^2\right]^{-\frac{1}{2}}\frac{d\xi}{2} - \int_{\xi_{LE_1}}^{\xi_{\Delta'}} (x-\xi)\left[(x-\xi)^2 + (1-M^2)(\Delta')^2\right]^{-\frac{1}{2}}\frac{d\xi}{2}\right\}$$

which becomes

$$Gr_1 = Gr_o + \frac{2b(\eta)}{s_o}\Delta\bar{C}_p(\xi_{\Delta'}, y_r)\left\{(\xi_{\Delta'}-\xi_{LE_r}) - \frac{1}{2}\left[(x-\xi_{LE_S})^2 + (1-M^2)(\Delta')^2\right]^{\frac{1}{2}} - \frac{1}{2}\left[(x-\xi_{LE_1})^2 + (1-M^2)(\Delta')^2\right]^{\frac{1}{2}}\right\}$$

Now, Gr_1 is approximately

$$Gr_1 = \frac{2b(\eta)}{s_o} \int_{\xi_{LE}}^{\xi_{\Delta'}} \Delta\bar{C}_p(\xi, y_r)\, d\xi$$

Completing the integral from $\xi_{\Delta'}$ to x yields the final approximation to Gr

$$Gr \quad \frac{G_S+G_1}{2} + \frac{2b(\eta)}{s_o}\Delta\bar{C}_p(\xi_{\Delta'}, y_r) \left\{ (\xi_{\Delta'} - \xi_{LE_r}) \right.$$

$$\left. - \frac{1}{2}\left[(x-\xi_{LE_S})^2 + (1-M^2)(\Delta')^2\right]^{\frac{1}{2}} - \frac{1}{2}\left[(x-\xi_{LE_1})^2 + (1-M^2)(\Delta')^2\right]^{\frac{1}{2}} \right\}$$

$$+ \frac{b(\eta)\beta\Delta'}{s_o}\left[\Delta\bar{C}_p(\xi_{\Delta'}, y_r) + \Delta\bar{C}_p(x, y_r)\right] \qquad \text{(B21)}$$

The use of equation (B21) in place of (B3a) to obtain Gr in supersonic flow results in the desired continuity in the chordwise integrals used in the spanwise correction terms.

APPENDIX C

CALCULATION OF INTERFERENCE EFFECTS

The equations presented in Appendix B are used to evaluate the self-induced downwash in equation (1) when q=p. This Appendix summarizes the equations for calculating interference downwash in equation (1) when q≠p for which the procedure is essentially the same as given in Appendix B. The chordwise integration is performed first which for supersonic flow requires a special treatment for a 3/2 power singularity in the integrand along the Mach hyperbola. The spanwise integral follows which requires treament of the non-planar kernel function such that the integral converges to the coplanar case as $(z - \zeta) \to 0$.

Chordwise Integration

The form of the integral equation for parallel non-planar surfaces in steady supersonic flow is

$$\frac{\bar{w}_p(\tilde{x},\tilde{y})}{U} = -\frac{1}{4\pi\rho U^2} \oint_{\tilde{\eta}_a}^{\tilde{\eta}_b} \oint_{\tilde{\xi}_{LE}}^{\tilde{\xi}_{mc}} \Delta\bar{C}_p(\xi,\eta)\, \frac{2x_o}{r^2 R}\left[1 - \frac{2z_o^2}{r^2} - \frac{z_o^2\beta^2}{R^2}\right] d\tilde{\xi}\, d\tilde{\eta} \qquad (C1)$$

where $\tilde{\eta}_a$ and $\tilde{\eta}_b$ are the left and right hand limits of integration defined by wing geometry and the Mach hyperbola. If the chordwise integration is carried out to the Mach hyperbola, a 3/2 singularity is encountered of the form

$$\lim_{\tilde{\xi}\to\tilde{\xi}_{mc}} \left[(x-\xi)^2 - \beta^2 r^2\right]^{-3/2}$$

Hence, the finite value of the improper integral must be taken.

In order to determine the finite value of the integral, the differentiation of the potential equation for the downwash must be considered. Let the downwash be expressed as the following simplified form:

$$w(x,y) = \frac{\partial}{\partial z} \int_{\eta_a}^{\eta_b} \int_{\xi_{LE}}^{\xi_{mc}} \Delta C_p(\xi,\eta)\,\phi(x,\xi,y,\eta,z,o)\, d\xi\, d\eta$$

where $\phi(\ )$ is the potential at point (x,y,z) due to a point load at $(\xi, \eta, 0)$. Since the differential operator is outside the integral sign, Leibnitz's rule must be used to perform the operation

$$\frac{d}{dt}\int_{a(t)}^{b(t)} g(x,t)dx = g\left|b(t),t\right| \frac{\partial b(t)}{\partial t}$$

$$-g\left|a(t),t\right| \frac{\partial a(t)}{\partial t} + \int_{a(t)}^{b(t)} \frac{\partial}{\partial t}\left|g(x,t)\right| dx \qquad \text{(C2)}$$

The limits a(t) and b(t) are constant in subsonic and coplanar supersonic flow; thus, their derivatives are zero. For the supersonic non-coplanar case, however, the derivatives are not zero. Since the chordwise term is of much greater importance for interference effects, only the derivatives resulting from the variation of ξ_{mc} with z will be accounted for.

For the chordwise integral, $H(y,\eta)$, a constant pressure distribution, $\Delta\bar{C}_p$, will be assumed for simplicity. The integral may then be expressed as

$$H(y,\eta) = \Delta C_p \frac{\partial}{\partial z}\int_{\xi_{LE}}^{\xi_{mc}} \phi(x,\xi,y,\eta,z,o)d\xi$$

which, with the application of equation (C2), becomes

$$H(y,\eta) = \Delta C_p\left|\phi(x,\xi_{mc},y,\eta,z,o) \frac{\partial \xi_{mc}}{\partial z}\right.$$

$$\left. + \int_{\xi_{LE}}^{\xi_{mc}} \frac{\partial}{\partial z}\left|\phi(x,\xi,y,\eta,z,o)\right| d\xi \right| \qquad \text{(C3)}$$

For

$$\phi(x,\xi,y,\eta,z,o) = -\frac{2U}{4\pi\rho}\frac{z_o x_o}{r^2 R}, \quad x_o \geq \beta r$$

it can be shown (after some algebraic manipulations given in reference 6) that the following is true

$$\phi(x,\xi_{mc},y,\eta,z,o)\ \frac{\partial \xi_{mc}}{\partial z} = -\frac{2U}{4\pi\rho}\frac{z_o^2\beta^2}{r^2}\left[\underset{\xi\to\xi_{mc}}{\text{LIM}}\left(\frac{1}{R}\right)\right] \tag{C4}$$

The differentiation inside the integral in equation (C3) is the kernel function

$$\frac{\partial}{\partial z}\phi(x,\xi,y,\eta,z,o) = -\frac{2U}{4\pi\rho}\frac{x_o}{r^2 R}\left[1 - \frac{2z_o^2}{r^2} - \frac{z_o^2\beta^2}{R^2}\right]$$

$$= \frac{U}{4\pi\rho}K(x,\xi,y,\eta,z,o) \tag{C5}$$

Combining equations (C3), (C4) and (C5) and removing the singularity yields

$$H(y,\eta) = \frac{\Delta C_p U}{4\pi\rho}\left\{\frac{2z_o^2\beta^2}{r^2}\left[\underset{\xi\to\xi_{mc}}{\text{LIM}}\left(\frac{1}{R}\right)\right] + \fint_{\xi_{LE}}^{\xi_{mc}}\frac{2x_o z_o^2\beta^2}{r^2 R^3}\,d\xi\right.$$

$$\left. + \int_{\xi_{LE}}^{\xi_{mc}}\left[K(x,\xi,y,\eta,z,o) - \frac{2x_o z_o^2\beta^2}{r^2 R^3}\right]d\xi\right\} \tag{C6}$$

But

$$\fint_{\xi_{LE}}^{\xi_{mc}}\frac{2x_o z_o^2\beta^2}{r^2 R^3}\,d\xi = \frac{2z_o^2\beta^2}{r^2}\left[\underset{\xi\to\xi_{mc}}{\text{LIM}}\left(\frac{1}{R}\right) - \frac{1}{R_{LE}}\right]$$

Thus, equation (C6) becomes

$$H(y,\eta) = \frac{\Delta C_p U}{4\pi\rho}\left\{ - \frac{2z_o{}^2\beta^2}{r^2 R_{LE}} + \int_{\xi_{LE}}^{\xi_{mc}} \left[K(x,\xi,y,\eta,z,o) - \frac{2x_o z_o{}^2\beta^2}{r^2 R^3} \right] d\xi \right\}$$

which is the final form for the chordwise integral with a constant pressure distribution. For a variable $\Delta\bar{C}_p(\xi,\eta)$, the singularity is treated at the Mach hyperbola, hence,

$$H(y,\eta) = \frac{U}{4\pi\rho}\left\{ - \frac{2z_o{}^2\beta^2}{r^2 R_{LE}} \Delta C_p(\xi_{mc},\underline{\eta}) + \int_{\xi_{LE}}^{\xi_{mc}} \left[\Delta C_p(\underline{\xi},\underline{\eta}) K(x,\xi,y,\eta,z,o) - \frac{2x_o z_o{}^2\beta^2}{r^2 R^3} \Delta C_p(\xi_{mc},\underline{\eta}) \right] d\xi \right\}$$

Thus, for steady or unsteady interference of non-planar surfaces the quadrature integration of the chordwise integral becomes

$$H_q(\underline{y},\underline{\eta}) = \frac{b(\underline{\eta})}{S_o} \frac{(1+\underline{\xi}_{mc})}{2} \frac{\pi}{J} \sum_{j=1}^{J} (1-\delta_j^2)^{\frac{1}{2}} \Delta\bar{C}_{p_q}(\underline{\xi}_j,\underline{\eta}) K(x-\xi_j, y-\eta, z-\zeta, k, M)$$

$$- T_2 \Delta\bar{C}_{p_q}(\xi_{mc},\eta) \frac{2\beta^2}{r^2}\left\{ \frac{1}{R_{LE}} + b(\eta) \frac{(1+\underline{\xi}_{mc})}{2} \frac{\pi}{J} \sum_{j=1}^{J} \frac{x_o (1-\delta_j^2)^{\frac{1}{2}}}{R_j{}^3} \right\}, \quad \underline{\xi}_{mc} < 1$$

where T_2 is defined for equation (A1) and

$$R_j^2 = (x-\xi_j)^2 - \beta^2 r^2$$

$$\delta_j = - \cos\left(\frac{2j-1}{2J}\pi\right), \quad j=1,2,\ldots J$$

$$\underline{\xi}_j = \tfrac{1}{2}\left| (1+\underline{\xi}_{mc})\,\delta_j + (\underline{\xi}_{mc}-1) \right|$$

$$\xi_j = \left| \underline{\xi}_j b(\underline{\eta}) + \xi_m(\underline{\eta}) \right|$$

For the case of the Mach hyperbola falling aft of the trailing edge, the 3/2 singularity need not be considered. Hence, the chordwise integral takes on the form given in Appendix B

$$H_q(y,\eta) = \frac{b(\eta)}{s_o}\frac{\pi}{J}\sum_{j=1}^{J}(1-\xi_j^2)^{\frac{1}{2}}\Delta\bar{C}_{pq}(\xi_j,\eta)\cdot$$

$$K(x-\xi_j,y-\eta,z-\zeta,k,M)\ ,\ \xi_{mc}\geq 1 \qquad \text{(C7)}$$

where

$$\xi_j = -\cos\left(\frac{2j-1}{2J}\pi\right)\ ,\ j=1,2,\ldots J$$

For subsonic flow, the chordwise integral is similar to equations (B6) and (C7)

$$H_q(y,\eta) = \frac{b(\eta)}{s_o}\frac{2\pi}{2J+1}\sum_{j=1}^{J}(1-\xi_j^2)^{\frac{1}{2}}\Delta\bar{C}_{pq}(\xi_j,\eta)\cdot$$

$$K(x-\xi_j,y-\eta,z-\zeta,k,M) \qquad \text{(C8)}$$

where $J = \bar{m}q$ and

$$\xi_j = -\cos\left(\frac{2j-1}{2J+1}\pi\right)\ ,\ j=1,2,\ldots J$$

For $\eta = y$,

$$J = 3\bar{m}_q+1$$

as discussed in Appendix B.

Spanwise Integration

The spanwise integral for non-planar interfering surfaces may be written as

$$I_q(\underline{y}) = \oint_{\underline{\eta}a}^{\underline{\eta}b} G_q(\underline{y},\underline{\eta}) \left[\frac{T_1}{r^2} - \frac{2T_2}{r^4} \right] d\underline{\eta}$$

where the sign $\oint$ denotes a "Pseudo Mangler" evaluation of the integral as discussed in reference 6. The $Gq(\underline{y}, \underline{\eta})$ function is the modified chordwise integral

$$G_q(\underline{y},\underline{\eta}) = \frac{H_q(\underline{y},\underline{\eta})}{\left[\frac{T_1}{r^2} - \frac{2T_2}{r^4} \right]}$$

which will be expanded as

$$G_q(\underline{y},\underline{\eta}) = G_q(\underline{y},\underline{y}) + (\underline{\eta}-\underline{y})G'_q(\underline{y},\underline{y}) + \ldots$$

Following the developments of Appendix B, the spanwise integral is evaluated as

$$I_q(\underline{y}_r) = \frac{\pi}{S} \sum_{s=1}^{S} h(\underline{\eta}_s) G_q(\underline{y}_r,\underline{\eta}_s) + Q_q^S(\underline{y}_r)$$

where $h(\underline{\eta}_s)$ and $\underline{\eta}_s$ are defined in Appendix B

$$\begin{aligned} Q_q^S(\underline{y}_r) = {} & G_q(\underline{y}_r,\underline{y}_r) \left| F_1(\underline{y}_r) \cos(\theta_p-\theta_q) \right. \\ & \left. + F_3(\underline{y}_r) \sin(\theta_p-\theta_q) \right| \\ & + G'_q(\underline{y}_r,\underline{y}_r) \left| F_2(\underline{y}_r) \cos(\theta_p-\theta_q) \right| \end{aligned}$$

and

$$F_1(y_r) = \left[\frac{y_r-\eta_b}{r_{rb}^2} - \frac{y_r-\eta_a}{r_{ra}^2} \right] - \frac{\pi}{S} \sum_{s=1}^{S} h(\eta_s) \left[\frac{1}{r_{rs}^2} - \frac{2z^2}{r_{rs}^2} \right] d(\eta_s)$$

$$F_2(y_r) = \frac{1}{2} \ln \left| \frac{r_{rb}^2}{r_{ra}^2} \right| + z^2 \left[\frac{1}{r_{rb}^2} - \frac{1}{r_{ra}^2} \right] - \frac{\pi}{S} \sum_{s=1}^{S} h(\eta_s)(\eta_s-y_r) \left[\frac{1}{r_{rs}^2} - \frac{2z^2}{r_{rs}^4} \right] d(\eta_s)$$

$$F_3(y_r) = z \left[\frac{1}{r_{rb}^2} - \frac{1}{r_{ra}^2} \right] - \frac{\pi}{S} \sum_{s=1}^{S} h(\eta_s) \frac{z(y_r-\eta_s)}{r_{rs}^4} d(\eta_s)$$

where

$$d(\eta_s) = 1 , \quad \eta_a \le \eta_s \le \eta_b$$

$$d(\eta_s) = 0 , \quad \eta_s < \eta_a , \ \eta_s < \eta_b$$

The variables ($\underline{y}, \underline{\eta}, \underline{z}$) are all measured relative to the surface over which the integration is being performed as shown in figure 3. The perpendicular distance from the surface to the downwash point is $\underline{z}$ and it is measured at span station $\underline{y}$. The terms r_{ra}, r_{rb}, r_{rs} are

$$r_{ra}^2 = (\underline{y}_r - \underline{\eta}_a)^2 + \underline{z}^2$$

$$r_{rb}^2 = (\underline{y}_r - \underline{\eta}_b)^2 + \underline{z}^2$$

$$r_{rs}^2 = (\underline{y}_r - \underline{\eta}_s)^2 + \underline{z}^2$$

For subsonic flow,

$$\underline{\eta}_a = -1$$

$$\underline{\eta}_b = +1$$

This completes the equations necessary to perform the spanwise integration for interference effects due to a streamwise planar surface of arbitrary orientation in steady flow.

For unsteady flow, it is necessary to include additional terms which account for the logarithmic singularity in the spanwise integrand, $k^2 \ln|r|$. This singularity is relatively weak for most problems, i.e., $k<1$. The correction terms developed in subsonic flow (ref. 7) are applicable in this case. The spanwise integration function, $h(\underline{\eta}_s)$, is given in Appendix B, equation (B12). The form for the unsteady correction terms becomes

$$Q_q^u(\underline{y}_r) = Q_q^s(\underline{y}_r) + \frac{k^2}{2}\cos(\theta_p - \theta_q)\left\{ G_q(\underline{y}_r, \underline{y}_r)\left[J_1(\underline{y}_r) - \frac{\pi}{S}\sum_{s=1}^{S} d(\underline{\eta}_s) h(\underline{\eta}_s) \ln r_{rs}^2 \right] + G_q'(\underline{y}_r, \underline{y}_r)\left[J_2(\underline{y}_r) - \frac{\pi}{S}\sum_{s=1}^{S} d(\underline{\eta}_s) h(\underline{\eta}_s)(\underline{\eta}_s - \underline{y}_r) \ln r_{rs}^2 \right] \right\}$$

where

$$J_1(\underline{y}_r) = (\underline{y}_r - \underline{\eta}_a) \ln r_{ra}^2 - (\underline{y}_r - \underline{\eta}_b) \ln r_{rb}^2$$

$$+ 2|\underline{z}_o| \left[\tan^{-1}\left(\frac{\underline{y}_r - \underline{\eta}_a}{|\underline{z}_o|}\right) + \tan^{-1}\left(\frac{\underline{\eta}_b - \underline{y}_r}{|\underline{z}_o|}\right) \right] - 4$$

$$J_2(y_r) = -\frac{1}{2}\left[r_{ra}^2 \ln r_{ra}^2 - r_{rb}^2 \ln r_{rb}^2 \right] + \underline{\eta}_a + \underline{\eta}_b - 2\underline{y}_r$$

which completes the equations for unsteady flow.

APPENDIX D

THE NORMAL SHOCK BOUNDARY CONDITIONS ON SMALL FLOW PERTURBATIONS

For a mean flow in which strong shocks are imbedded, special boundary conditions must be satisfied across the shocks on small perturbations to the mean flow. This Appendix presents the derivation of the shock boundary conditions first for steady and then for unsteady flow perturbations. These boundary conditions satisfy the Rankine-Hugoniot condition and continuity of potential across the shock.

Normal Shock Boundary Conditions for Steady Flow

Referring to figure D1, the upstream conditions are M^-, ϕ^- and U^- (referring to Mach, total potential, and velocity normal to the shock) and the downstream conditions are M^+, ϕ^+ and U^+.

Beginning with the Rankine-Hugoniot relation as given by Pai (ref. 19):

$$\frac{U^+}{U^-} = \frac{\gamma-1}{\gamma+1} + \frac{2}{(M^-)^2(\gamma+1)} \tag{D1}$$

or

$$U^+ = U^-\left[1 - \frac{2}{\gamma+1} + \frac{2}{(M^-)^2(\gamma+1)}\right]$$

The velocity change is obtained

$$\Delta U = U^- - U^+ = \frac{2U^-}{\gamma+1}\left[1 - \frac{1}{(M^-)^2}\right] = \frac{2U^-}{\gamma+1}\left[1 - \left(\frac{c^-}{U^-}\right)^2\right] \tag{D2}$$

Now, let

$$U^- = 1 + \phi_x^-$$

From which

$$\left(\frac{1}{U^-}\right)^2 = 1 - 2\,\phi_x^- + \ldots \tag{D3}$$

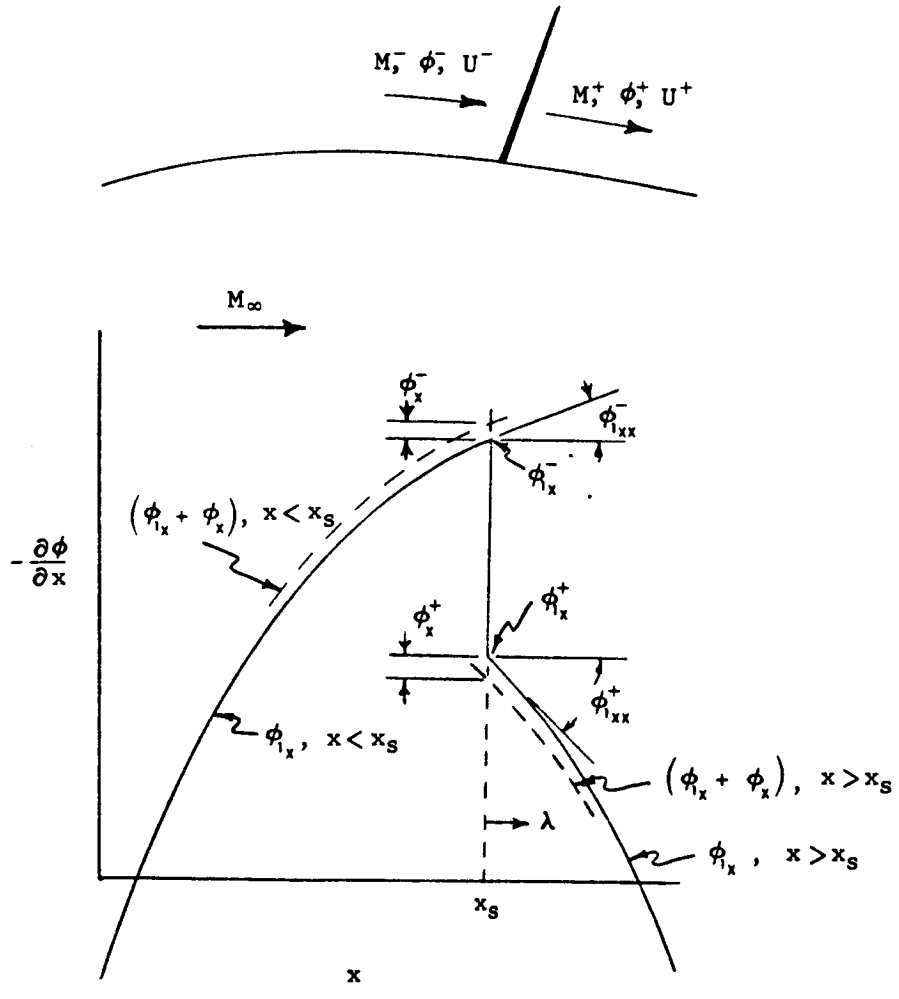

Figure D1.- Flow Variables in the Vicinity of an Idealized Normal Shock

From Landahl (ref. 12, equation (1.4)), c^2 can be expressed as

$$c^2 = \frac{1}{M_\infty^2} - (\gamma-1)\phi_x$$

for first order effects. Thus,

$$\left(\frac{c^-}{U^-}\right)^2 = \left[\frac{1}{M_\infty^2} - (\gamma-1)\phi_x^-\right]\left[1 - 2\phi_x^- + \ldots\right]$$

from which the first order terms are

$$\left(\frac{c^-}{U^-}\right)^2 \approx \frac{1}{M_\infty^2}\left\{1-\left[2 + M_\infty^2\,(\gamma-1)\right]\phi_x^-\right\} \tag{D4}$$

For

$$U^+ = 1+\phi_x^+$$

the velocity change is

$$\Delta U = (1+\phi_x^-) - (1+\phi_x^+) = \phi_x^- - \phi_x^+ \tag{D5}$$

Substituting equations (D3), (D4) and (D5) into (D2) yields

$$\phi_x^- - \phi_x^+ = \frac{2}{\gamma+1}\left(1+\phi_x^-\right)\left\{1 - \frac{1}{M_\infty^2}\left[1 - \left(2+M_\infty^2(\gamma-1)\right)\phi_x^-\right]\right\}$$

from which the first order terms are

$$\phi_x^- - \phi_x^+ \approx \frac{2}{\gamma+1}\left[\left(1 - \frac{1}{M_\infty^2}\right) + \left(\frac{1}{M_\infty^2} +\gamma\right)\phi_x^-\right] \tag{D6}$$

Letting

$$\mu = \frac{\gamma-1}{\gamma+1} + \frac{2}{(\gamma+1)M_\infty^2} \tag{D7}$$

equation (D6) becomes

$$\phi_x^+ + \mu\phi_x^- = \frac{2}{\gamma+1}\left(\frac{1}{M_\infty^2} - 1\right) \tag{D8}$$

which differs from the derivation of Landahl by the presence of μ. For $M_\infty=1$, $\mu=1$, then equation (D8) would correspond to Landahl's equation (equation (10.9), ref. 12).

The total potentials, $\boldsymbol{\phi}^-$ and $\boldsymbol{\phi}^+$, are the sum of the mean potential, ϕ_1, plus the perturbed potentials, ϕ,

$$\boldsymbol{\phi}^- = \phi_1^- + \lambda\phi_{1x}^- + \phi^- \tag{D9a}$$

$$\boldsymbol{\phi}^+ = \phi_1^+ + \lambda\phi_{1x}^+ + \phi^+ \tag{D9b}$$

where λ is the shock displacement as shown in figure D1. From the condition of equality of potential across the shock,

$$\boldsymbol{\phi}^- = \boldsymbol{\phi}^+ \tag{D10}$$

The following relation between λ and ϕ

$$\lambda = -\frac{\phi^+ - \phi^-}{\phi_{1x}^+ - \phi_{1x}^-} \tag{D11}$$

since

$$\phi_1^- = \phi_1^+$$

The fundamental assumption which underlies equation (D9) is that the potential ϕ_1 is analytically continuous on both sides of the shock, and that it can be expanded in a Taylor series forward and aft of the shock. Equations (D9) contain only first order variation of $\boldsymbol{\phi}$ due to a perturbation ϕ, therefore, equation (D11) is the first order movement of the shock due to ϕ that is necessary to maintain equality of potential.

Another relationship can be obtained between λ and ϕ by differentiating equations (D9)

$$\boldsymbol{\phi}_x^- = \phi_{1x}^- + \lambda\phi_{1xx}^- + \phi_x^-$$

$$\boldsymbol{\phi}_x^+ = \phi_{1x}^+ + \lambda\phi_{1xx}^+ + \phi_x^+$$

and substituting into equation (D8). Thus,

$$(\phi_{1x}^+ + \lambda\phi_{1xx}^+ + \phi_x^+) + \mu(\phi_{1x}^- + \lambda\phi_{1xx}^- + \phi_x^-) = \frac{2}{\gamma-1}\left(\frac{1}{M_\infty^2} - 1\right)$$

which separates into the following for the zero order terms

$$\phi_{1x}^{+} + \lambda\phi_{1x}^{-} = \frac{2}{\gamma+1}\left(\frac{1}{M_{\infty}^{2}} - 1\right) \tag{D12}$$

and the perturbation terms

$$\lambda = - \frac{\phi_{x}^{+} + \mu\phi^{-}}{\phi_{1xy}^{+} + \mu\phi_{1xx}^{-}} \tag{D13}$$

Equation (D13) is the first order shock movement due to ϕ that is necessary to satisfy the Rankine-Hugoniot relation.

With equations (D11) and (D13), can be eliminated to obtain

$$\frac{\phi^{+} - \phi^{-}}{\phi_{1x}^{+} - \phi_{1x}^{-}} = \frac{\phi_{x}^{+} + \mu\phi_{x}^{-}}{\phi_{1xx}^{+} + \mu\phi_{1xx}^{-}}$$

which may be simplified to

$$\phi_{x}^{+} - K\phi^{+} = - \mu\phi_{x}^{-} - K\phi^{-} \tag{D14}$$

where

$$K = \frac{\phi_{1xx}^{+} + \mu\phi_{1xx}^{-}}{\phi_{1x}^{+} - \phi_{1x}^{-}} \tag{D15}$$

Since the constant K is a function of the mean flow potential and ϕ^{-} is unaffected by conditions downstream of the shock, equation (D14) represents a constraint on the downstream perturbation ϕ^{+}.

Normal Shock Boundary Conditions for Unsteady Flow

The Rankine-Hugoniot relation as given in equation (D2) is also used for unsteady flow. The velocities, U^- and U^+, are expressed as

$$U^- = 1 + \phi_x^- - ik\lambda e^{ikt} \tag{D16a}$$

$$U^+ = 1 + \phi_x^+ - ik\lambda e^{ikt} \tag{D16b}$$

which includes the shock velocity in the exponential terms. Landahl has given an expression for the speed of sound in unsteady flow (equation 1.4, ref. 12) as

$$c^2 = \frac{1}{M_\infty^2} - (\gamma-1)(\phi_x + \phi_t) \tag{D17}$$

With equations (D16) and (D17), the expression for $(1/M^-)^2$ becomes

$$\left(\frac{c^-}{U^-}\right)^2 = \left[\frac{1}{M_\infty^2} - (\gamma-1)(\phi_x^- + \phi_t^-)\right]\left[1 - 2(\phi_x^- - ik\lambda e^{ikt}) + \ldots\right]$$

from which the first order terms are

$$\left(\frac{c^-}{U^-}\right)^2 \approx \frac{1}{M_\infty^2}\left[1 - (2 + M_\infty^2(\gamma-1))\,\phi_x^- + M_\infty^2(\gamma-1)\phi_t^- + 2ik\lambda e^{ikt}\right] \tag{D18}$$

Substituting equation (D18) into (D2) yields

$$(\phi_x^- - \phi_x^+) = \frac{2}{\gamma+1}\left[1 + \phi_x^- - ik\lambda e^{ikt}\right]\left\{1 - \frac{1}{M_\infty^2}\left[1 - (2 + M_\infty^2(\gamma-1))\,\phi_x^- - M_\infty^2(\gamma-1)\,\phi_t^- + 2ik\lambda e^{ikt}\right]\right\}$$

from which the first order terms are

$$\phi_x^+ + \mu\phi_x^- + \Gamma\phi_t^- - \frac{4ik\lambda}{\gamma+1} e^{ikt} = \frac{2}{\gamma+1}\left(\frac{1}{M^2} - 1\right) \tag{D19}$$

where

$$\Gamma = \frac{2\ (\gamma - 1)}{\gamma+1}$$

Except for the exponential and ϕ_t terms, equation (D19) is identical to (D8).

Following the development for steady flow, the total potentials due to an unsteady perturbation are

$$\phi^- = \phi_1^- + \lambda e^{ikt}\ \phi_{1x}^- + \phi^-\ e^{ikt} \tag{D20a}$$

$$\phi^+ = \phi_1^+ + \lambda e^{ikt}\ \phi_{1x}^+ + \phi\ e^{ikt} \tag{D20b}$$

The equality of potential condition for unsteady flow yields equation (D11) for the shock movement necessary to maintain this condition.

Next, the derivative terms for equation (D19) are obtained from equation (D20)

$$\phi_x^- = \phi_{1x}^- + \lambda e^{ikt}\ \phi_{1xx}^- + \phi_x^-\ e^{ikt} \tag{D21a}$$

$$\phi_x^+ = \phi_{1x}^+ + \lambda e^{ikt}\ \phi_{1xx}^+ + \phi_x^+\ e^{ikt} \tag{D21b}$$

$$\phi_t^- = ike^{ikt}\ (\lambda\ \phi_{1x}^- + \phi^-) \tag{D21c}$$

Substitution of equations (D21) into (D19) yields

$$(\phi^+_{1x} + \lambda e^{ikt}\phi^+_{1xx} + \phi^+_x e^{ikt}) + \mu(\phi^-_{1x} + \lambda e^{ikt}\phi^-_{1xx} + \phi^-_x e^{ikt})$$

$$+\Gamma ike^{ikt}(\lambda\phi^-_{1x} + \phi^-) - \frac{4ik}{\gamma+1} e^{ikt} = \frac{2}{\gamma+1}\left(\frac{1}{M^2} - 1\right)$$

from which the first order terms obtained are

$$\phi^-_{1x} + \mu\phi^+_{1x} = \frac{2}{\gamma+1}\left(\frac{1}{M^2} - 1\right)$$

and

$$\lambda = -\frac{\phi^+_x + \mu\phi^-_x + i\nu\phi^-}{\phi^+_{1xx} + \mu\phi^-_{1xx} + i\nu\phi^-_{1x} - \frac{4ik}{\gamma+1}} \qquad \text{(D22)}$$

where

$$\nu = \Gamma k = \frac{2(\gamma-1)}{\gamma-1} k \qquad \text{(D23)}$$

Equation (D22) differs from its counterpart in steady flow, equation (D13), by the terms containing $i\nu$.

With equations (D11) and (D22), λ can be eliminated to obtain

$$\frac{\phi^+ - \phi^-}{\phi^+_{1x} - \phi^-_{1x}} = \frac{\phi^+_x + \mu\phi^-_x + i\nu\phi^-}{\phi^+_{1xx} + \mu\phi^-_{1xx} + i\nu\phi^-_{1x} - \frac{4ik}{\gamma+1}}$$

which may be simplified to

$$\phi^+_x - K^*\phi^+ = -\mu\phi^-_x - K^*\phi^- - i\nu\phi^- \qquad \text{(D24)}$$

where

$$K^* = \frac{\phi^+_{1xx} + \mu\phi^-_{1xx} + i\nu\phi^-_{1x} - \frac{4ik}{\gamma+1}}{\phi^+_{1x} - \phi^-_{1x}}$$

or

$$K^* = K + i\nu\left[\frac{\phi_{1x}^- - \frac{2}{\gamma-1}}{\phi_{1x}^+ - \phi_{1x}^-}\right] \tag{D25}$$

which completes the normal shock boundary conditions for unsteady flow.

Comparison of equation (D24) with the boundary conditions derived by Landahl (equation 10.11, ref. 12) shows a significant discrepancy. However, with the restrictions

$$k \sim 1$$

and

$$\frac{2}{\gamma-1} \gg \phi_{1x}^- \sim (\phi_{1xx}^+ + \mu\phi_{1xx}^-)$$

equation (D24) reduces to

$$\phi_x^+ + \frac{4ik\phi^+}{(\gamma+1)(\phi_{1x}^+ - \phi_{1x}^-)} = -\mu\phi_x^- + \left[\frac{4ik}{(\gamma+1)(\phi_{1x}^+ - \phi_{1x}^-)} + \frac{2ik(\gamma-1)}{\gamma+1}\right]\phi_x^-$$

or

$$\phi_x^+ - \frac{4ik\phi^+}{(\gamma+1)(\phi_{1x}^+ - \phi_{1x}^-)} = \mu\phi_x^- + \frac{4ik\phi^-}{(\gamma+1)(\phi_{1x}^- - \phi_{1x}^+)}\left[1 - \frac{\gamma-1}{2}(\phi_{1x}^- - \phi_{1x}^+)\right]$$

which is identical to Landahl's equation. Thus, Landahl's boundary conditions are valid only for high frequency oscillations and weak shocks as is implied by the restrictions. Equation (D24) is therefore more general and is necessary for use with a method which will be used in flutter and dynamic response analysis.

APPENDIX E

CALCULATION OF POTENTIALS FOR THE SHOCK BOUNDARY CONDITIONS

The potentials needed for the shock boundary conditions are the supersonic potential just forward of the shock, ϕ^-, due to the upstream surface and the subsonic potential aft of the shock, ϕ^+, due to the doublet. Also needed are the potential derivatives, ϕ_x^- and ϕ_x^+.

The supersonic potential at point x,y,z due to a doublet sheet lying in the $\xi-\eta$ plane is the integral over the sheet:

$$\frac{\phi}{U_{b_r}} = -\frac{2}{4\pi\rho U^2}\int_{\eta_a}^{\eta_b}\int_{\xi_{LE}}^{\xi_{mc}} \frac{z}{r^2}\left[\frac{x-\xi}{\sqrt{(x-\xi)^2+\beta^2 r^2}}\right]\Delta p(\xi,\eta)\, d\xi d\eta \tag{E1}$$

The nature of the term

$$\frac{z}{r^2} = \frac{z}{(y-\eta)^2+z^2}$$

in the integrand is such that

$$\lim_{\substack{z\to o \\ y\neq\eta}} \left(\frac{z}{r^2}\right) = 0$$

and

$$\lim_{\substack{z\to o \\ y=\eta}} \left(\frac{z}{r^2}\right) = \lim_{z\to o}\left(\frac{1}{z}\right) = \infty$$

Let

$$G(y,\eta) = -\frac{4}{\rho U^2}\int_{\xi_{LE}}^{\xi_{mc}} \frac{x-\xi}{\sqrt{(x-\xi)^2+\beta^2 r^2}}\,\Delta p(\xi,\eta)\, d\xi \tag{E2}$$

Thus,

$$\frac{\phi}{Ub_r} = -\frac{1}{8\pi}\int_{\eta_a}^{\eta_b} \frac{z}{r^2}\, G\,(y, \eta)\, d\eta \tag{E3}$$

where $G(y, \eta)$ has the same definition as given in Appendix B. In order to treat the singularity in equation (E3), the integrand is modified as follows:

$$\frac{\phi}{Ub_r} = -\frac{1}{8\pi}\int_{\eta_a}^{\eta_b} \frac{z}{r^2}\left[\, G\,(y,\eta) - G\,(y, y)\right] d\eta - \frac{1}{8\pi}\, G\,(y, y)\int_{\eta_a}^{\eta_b} \frac{z\, d\eta}{r^2}$$

The first integral can be evaluated numerically and the second analytically as

$$\int_{\eta_a}^{\eta_b} \frac{z\, d\eta}{(y-\eta)^2 + z^2} = \tan^{-1}\left(\frac{y - \eta_a}{z}\right) - \tan^{-1}\left(\frac{y - \eta_b}{z}\right)$$

Taking the limit $z \to 0$ for both integrals leaves

$$\frac{\phi}{Ub_r} = -\frac{1}{8}\, G\,(y, y), \quad \eta_a < y < \eta_b \tag{E4}$$

The same equation is applicable for the doublet line.

The potential derivatives are directly related to the pressure coefficient forward and aft of the shock. For ϕ_x, the derivative is taken with respect to the aft limit of integration, hence

$$\frac{\phi_x}{U} = -\frac{1}{4}\, C_p\,(x_s, y) \tag{E5}$$

where x_s is the shock location. Equation (E5) is applicable to either the supersonic or subsonic regions. Since the shock boundary conditions are satisfied aft of the shock, the value of C_p for the shock doublet is zero.

The normal shock boundary conditions are satisfied with the following terms in steady flow:

$\phi_x^- = -\frac{1}{4} C_p^- (x_s, y)$ — pressure coefficient at the trailing edge of the supersonic region at y.

$\phi^- = -\frac{1}{8} G^- (y, y)$ — chordwise integral directly upstream of the shock boundary condition point, (x_s, y).

$\phi_x^+ = -\frac{1}{4} C_p^+ (x_s, y)$ — pressure coefficient at the leading edge of the subsonic region at y.

$\phi^+ = -\frac{1}{8} \left| G^-(y, y) + G_D(y, y) \right|$ — total potential just aft of the shock due to the supersonic region and the shock doublet.

Substituting these quantities into equation (18) or (D14) yields

$$-\frac{1}{4} C_p^+ (x_s, y) + \frac{K}{8} \left| G^-(y, y) + G_D (y, y) \right| = \frac{\mu}{4} C_p^- (x_s, y) + \frac{K}{8} G^- (y, y)$$

or

$$C_p^+ (x_s, y) - \frac{K}{2} G_D (y, y) + \mu C_p^- (x_s, y) = 0 \qquad \text{(E6)}$$

It should be noted that in steady flow, the $G^-(y,y)$ term is cancelled.

For unsteady flow, all of the above terms are the same except they are complex. Substitution into equation (19) or (D24) yields

$$-\frac{1}{4} C_p^+ (x_s, y) + \frac{K^*}{8} \left| G^-(y, y) + G_D (y, y) \right| = \frac{\mu}{4} C_p^- (x_s, y) + \frac{1}{8} (K^* + i\nu) G^- (y, y)$$

or

$$C_p^+ (x_s, y) - \frac{K}{2} G_D (y, y) + \mu C_p^- (x_s, y) + \frac{i\nu}{2} G^- (y, y) = 0 \qquad \text{(E7)}$$

For unsteady flow, the $G^-(y,y)$ term is retained.

APPENDIX F

CALCULATION OF LOCAL MACH NUMBER

The local Mach number, M_L, is used extensively in the transonic algorithm. As a result, it must be inexpensive and simple to calculate. The input data from which the local Mach number is obtained must be simple and flexible in format. These requirements are satisfied through a two-step procedure which starts with input values of M_L given at even spaced points over the planform and ends up with a function for M_L in the form of Tschebychev polynomials.

The input data is given at even spaced chordwise intervals, $\Delta\xi$, starting at the leading edge and ending at the trailing edge. The chordwise distributions are given also at even spaced spanwise intervals, $\Delta\xi$, starting at the inboard tip and ending at the outboard tip. The intervals are tied to the total number of chordwise, $\bar{m}$, and spanwise, $\bar{n}$, downwash points as follows:

$$\Delta\xi = \frac{1}{\bar{m}} \qquad \text{(chord fraction)}$$

$$\Delta\eta = \frac{1}{\bar{n}} \qquad \text{(semi-span fraction)}$$

There are

$\bar{m} + 1$ values of M_L input chordwise at
$\bar{n} + 1$ spanwise stations.

The locations are the sets

$$\xi_i = (0, \frac{1}{\bar{m}}, \frac{2}{\bar{m}}, \ldots 1) \qquad \text{(F1a)}$$

$$\eta_j = (0, \frac{1}{\bar{n}}, \frac{2}{\bar{n}}, \ldots 1) \qquad \text{(F1b)}$$

It is possible to input a single chordwise distribution into the program which is used at all span stations if desired.

Next, the input M_L are fit with the surface spline procedure described in Appendix G that is used for structural mode interpolation. The surface spline is used to calculate M_{L2} values at the optimum fitting points for Tschebychev polynomials of the first kind, Tn.

The Tn polynomials are defined as

$$T_0(x) = 1$$
$$T_1(x) = x$$
$$T_2(x) = 2x^2-1$$
$$\vdots$$
$$T_n(x) = 2x\ T_{n-1}(x) - T_{n-2}(x)$$

over the interval

$$-1 \leq x \leq 1$$

From reference 20, an arbitrary function of x can be expressed as an N term expansion of $T_n(x)$ as follows:

$$f(x) = \frac{Co}{2} + \sum_{n=1}^{N-1} C_n\ T_n\ (x) \qquad \text{(F2)}$$

The coefficients, C_n, can be obtained by a simple vector multiplication

$$C_n = \frac{2}{N} \sum_{i=1}^{N} f\ (x_i)\ T_n\ (x_i) \qquad \text{(F3)}$$

where the x_i are roots of the $T_{N+1}(x)$ polynomial,

$$x_i = \cos\left(\frac{2i-1}{2N}\pi\right),\ i = 1,\ 2,\ \ldots\ N \qquad \text{(F4)}$$

Thus, the new values of M_L are calculated at

$$x_i = (x_1, x_2, \ldots x_{\bar{m}+1}) \tag{F5a}$$

$$y_j = (y_1, y_2, \ldots y_{\bar{n}+1}) \tag{F5b}$$

where the x_i and y_j are calculated with equation (F4) for $N = (\bar{m}+1)$ and $(\bar{n}+1)$, respectively. The relationships between the (ξ, η) in equation (F1) and (x,y) in equation (F5) are

$$\xi = \frac{x+1}{2}$$

$$\eta = \frac{y+1}{2}$$

Since $0 \leq \xi \leq 1$ and $0 \leq \eta \leq 1$.

Once the C_n are calculated from equation (F4) with the new values of M_{L2}, the value of M_L at any point on the planform can be obtained with equation (F2).

APPENDIX G

STRUCTURAL MODE INTERPOLATION

The structural modes are interpolated in the program with a surface spline fit (ref. 21) which simulates the deflected shape of an infinite plate pinned at the points which are being interpolated from. The scheme is one of the more dependable methods that is currently available. It has some disadvantages, however, in that it does not extrapolate well under certain conditions and it tends to "sag" in cases where there are large spaces between fitting point groups.

The spline equation is

$$w_j = a_1 + a_2 x_j + a_3 y_j + \sum_{n=1}^{N} b_n (r_{nj})^2 \ln \left| (r_{nj})^2 \right| \qquad \text{(G1)}$$

For n=1,2,...N where w_j is the function value at point (x_j,y_j) and

$$r_{nj}^2 = (x_n - x_j)^2 + (y_n - y_j)^2$$

The points (x_n,y_n) are the fitting points. The coefficients $[a_1,a_2,a_3,b_1,\ldots b_N]$ are determined by equating the w_j to the known deflections at points $(x_j,y_j) = (x_n,y_n)$ for n=1,2,...N. Three other equations are also satisfied,

$$\sum_{n=1}^{N} b_n = \sum_{n=1}^{N} x_n b_n = \sum_{n=1}^{N} y_n b_n = 0$$

to give the necessary N+3 equations to solve for the N+3 unknown coefficients. With the coefficients known, deflections can then be calculated at any point desired within the planform.

A scaling and coordinate transformation is performed such that the (x,y) values never exceed 1.0. A structural surface is defined in different ways as shown in figure D1. For the corner points, x_{I_1}, x_{I_2}, y_I and x_{o_1}, x_{o_2}, y_o, a point (x,y)

within the structural surface is transformed to (ξ , η) as

$$\xi = \frac{x-x_m}{b(y)}$$

$$\eta = \frac{y-y_m}{S}$$

where

$$x_m = \frac{x_{I_1} + x_{I_2}}{2} + \frac{y - y_I}{2S}\left(\frac{x_{o_1} + x_{o_2} - x_{I_1} - x_{I_2}}{2}\right)$$

$$b(y) = \frac{x_{I_2} - x_{I_1}}{2} + \frac{y - y_1}{2S}\left(\frac{x_{o_2} - x_{o_1} - x_{I_2} + x_{I_1}}{2}\right)$$

$$y_m = \frac{y_I + y_o}{2}$$

$$S = \frac{y_o + y_I}{2}$$

As can be seen in the figure, use of a square structural surface simply scales the (x,y) to (ξ , η) which are geometrically similar but less than unity in magnitude. The trapezoidal structural surface skews the structural points into a square plane which is sometimes desired. Skewing is not recommended for delta or other pointed tip planforms.

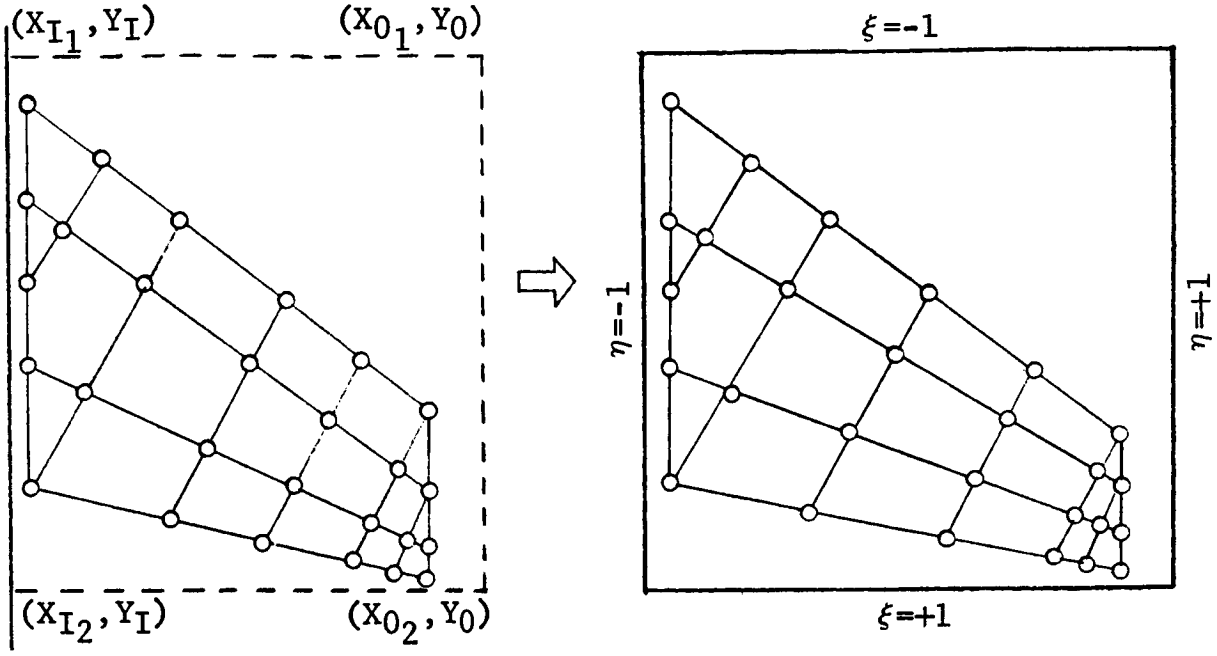

(a) Rectangular Structural Surface

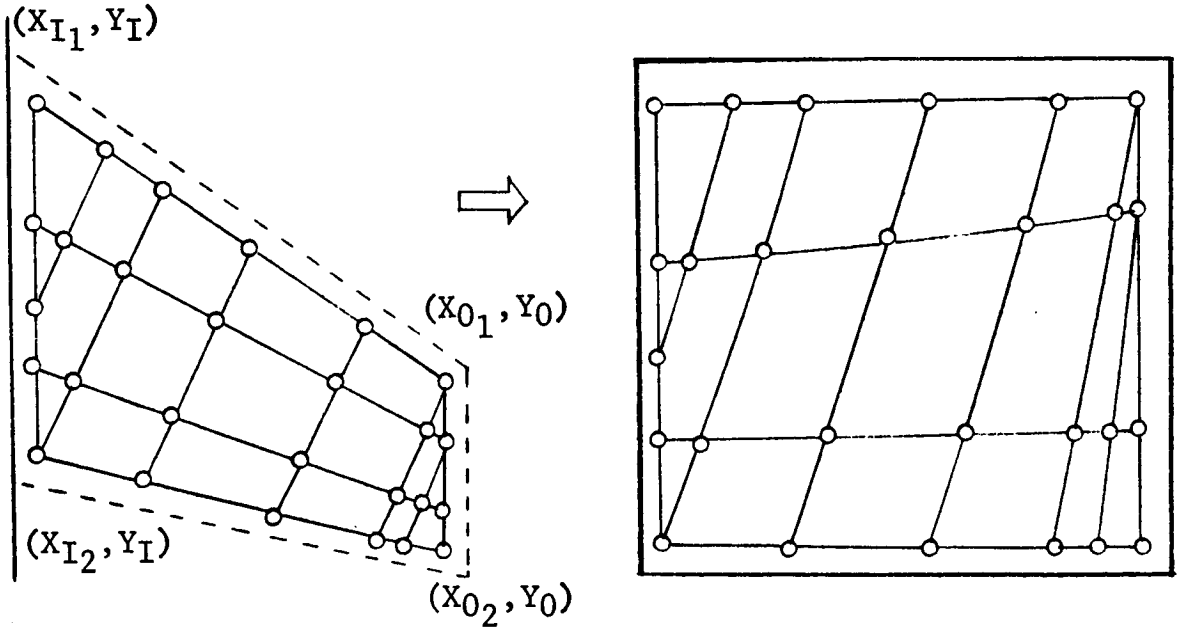

(b) Trapezoidal Structural Surface

Figure G1.- Coordinate Transformation For Structural Surfaces

APPENDIX H

PROGRAM UTILIZATION AND INPUT DATA ORGANIZATION

The program is applicable to steady and unsteady flow in all Mach number ranges, subsonic, transonic and supersonic. It can be used to obtain uniform flow solutions in both subsonic and supersonic flow. Non-uniform flow solutions can be obtained for all Mach ranges including mixed transonic flow with imbedded shocks. In order to use the non-uniform flow capability, the Mach number distributions and shock locations are input and must be obtained from an outside source such as experiment or a finite difference solution.

Interference effects can be calculated for coplanar, non-coplanar, and intersecting planar surfaces. The aerodynamic geometry data format permits the input of arbitrarily arrayed surfaces which are constrained only to being streamwise. Each surface may or may not have an image surface, hence, asymmetric configurations may be constructed.

The program can be used to calculate generalized forces in unsteady flow and pressure distributions in either steady or unsteady flow. The solutions obtained are essentially independent in computer cost of the number of modes or downwash vectors input. Once computed, inverted, and saved on a magnetic tape, the aerodynamic matrices can be used on subsequent problems for very little cost as long as Mach number, reduced frequencies, and aerodynamic geometry remain unchanged. Thus, the method is tailored for design applications where the structural mode shapes change continually for structure changes and payload variations while aerodynamic parameters remain constant.

Presented in the following sections are the detailed instructions for providing input data to the program. The first section describes the general arrangement of the data and the second describes the specific items in the data.

Deck Arrangement

The major input data classifications are: (1) the library data which contains structural geometry data and the mode shapes and (2) the problem data which includes all aerodynamic geometry and option data. The program can be used to calculate generalized forces or pressure distributions. The generalized forces can be obtained only for unsteady flow whereas the pressure distributions can be obtained for steady or unsteady flow.

Library data organization.- The library data organization presented below is in the form of card sets, L-N, where L refers to library data and N is a sequence number corresponding to a specific function as described. The cards sets may be composed of one or more cards and their contents are described in the following section. All card sets are required if library data is used with exception of L-6 and L-7 which are optional as noted.

Card Set	Function
L-1	"LIBR" card
L-2	option data
L-3	constants
L-4	structural point locations
L-5(1) ... L-5(NSUR)	structural surface data for "NSUR" total surfaces
L-6	zero deflextion points - supplied if option L3≠0 on card L-2
L-7	mass data - supplied if L2≠0 on card L-2
L-8	mode deflection data

Problem data organization.- The problem data organization is presented below in a format similar to that of the library data. The sets denoted as P-N are mandatory for all problem decks regardless of whether or not library decks are used. Those denoted as P(L)-N are used only when the library is used and P(P)-N are used only when no library is used. Specific contents of each card set are described in the section following that for the library data.

Card Set	Function	
P-1	title data	
P-2	major options	
P-3	general aerodynamic data, integer	
P-4	general aerodynamic data, real	
P-5(1)	integer control data	Data for aerodynamic surface no. 1
P-6(1)	geometric data	
P-7(1)		
P(L)-8(1)	structural surface used if "LIBR" data is input	
P-9(1)	Mach distribution data if ITRANS≠0 on card P-5(1)	
.		
.		
.		
P-5(NSURF)		Data for aerodynamic surface no. NSURF
P-6(NSURF)		
P-7(NSURF)		
P(L)-8(NSURF)		
P-9(NSURF)		

P(P)-10(1)
.
.
.
P(P)-10(NSURF)

} downwash vector data for all surfaces if "LIBR" data is not supplied

"END" card

Input Format Description for
Structural and Mode Shape Data Library

In order to have an input library which contains the structural and mode data for all the following aerodynamic problems, the first card, L-1, must have the four characters "LIBR" in cols. 1-4 on the first card. Anything else may follow on that card, for example:

Cols.

1-4	5-80
LIBR	ARY FOR F-111 MODES, SWEEP=26 DEG

Card L-1

It is recommended that the cards be sequenced, however, it is not mandatory.

The second card set, L-2, is two cards in a 6I10 format which contain the following:

Cols. (right adjust all data) 6I10 format

1-10	11-20	21-30	31-40	41-50	51-60
NF	NSUR	NMODES	N1=0	N2=0	L1
L2	L3	L4			

Card L-2

where

NF = total number of structural points at which mode deflections are given, NF $\leq$ 200.

NSUR = total number of structural surface spline fits to be used for mode interpolation, NSUR $\leq$ 10.

NMODES = total number of mode shapes supplied, NMODES $\leq$ 20.

N1=N2=0 = unused constants which must be zero.

L1 = 0, a comment card of any format will be expected at the beginning of each mode shape deck.

$\neq$ 0, no comment card is expected.

L2 = 0, no mass data will be input for computing the generalized masses.

$\neq$ 0, mass data will be input (see Card L-7).

L3 = 0, no structural points will be modified to have zero deflection in each mode.

$\neq$ 0, "L3" total structural points will be modified (see Card L-6), L3 $\leq$ NF.

L4 = 0, pitch and roll modes will not be added.

$\neq$ 0, (a) the pitch mode will be added as mode "NMODES" + 1 with deflections (XF(I), I=1, NF). (see Card L-4)

(b) the roll mode will be added as mode "NMODES" + 2 with deflections (YF(I), I=1, NF). (see Card L-4)

The third card set, L-3, is also two cards in a 6F10.0 format which contains the following:

Cols. (use decimal or right adjust all data) 6F10.0 format

1-10	11-20	21-30	31-40	41-50	51-60
XMODE	XMASS	DH	DW1	DW2	BREF
RHO					

Card L-3

where

XMODE = uniform mode deflection multiplier. All mode deflections are multiplied by this quantity which is normally
XMODE=1.0

XMASS = uniform mass multiplier, normally
XMASS=1.0

DH = uniform multiplier for all deflections calculated with the spline interpolation. (These are usually the deflections used to calculate generalized forces and masses.) Normally, DH=1.0

DW1 = uniform multiplier for all slopes calculated with the spline interpolation. (These are "α" values in steady flow or the real part of the downwash in unsteady flow.) Normally,
DW1=1.0

DW2 = uniform multiplier for all deflections calculated with the spline interpolation as the imaginary term in the unsteady downwash. Normally,
DW2=1.0

BREF = reference length in same dimensions as other geometric data. This value must be the same as that used in the problem data.

RHO = density, slugs/ft^3. If RHO=0, the default value at sea level is used.
RHO=0.0023769 slugs/ft^3

[NOTE: for geometric data input in units other than inches, a conversion factor must be input through either RHO or XMASS.]

The next card set, L-4, is composed of as many cards as are necessary to contain the NF structural point locations in the following form:

read FORMAT 8A10 format					
(input according to FORMAT)					
XF(1)	YF(1)	XF(2)	YF(2)	XF(3)	YF(3)
...					
XF(NF-1)	YF(NF-1)	XF(NF)	YF(NF)		

where

XF(I),YF(I) = X,Y coordinates of the I^{th} structural point.

The XF(I) are used to compute the pitch mode for L4≠0 and YF(I) are used for the roll mode.

The next card set, L-5, is composed of NSUR subsets, each of which contains the following descriptive information for each structural surface:

Cols. (right adjust all data) 6I10 and 6F10.0 formats

1-10	11-20	21-30	31-40	41-50	51-60
NFS(N)	IF(1,N)	IF(2,N)	...		
		...	IF(NFS(N),N)		
XIS(1,N)	XIS(2,N)	YCS(1,N)	XOS(1,N)	XOS(2,N)	YCS(2,N)

Card L-5N, N=1, NSUR

where

NFS(N) = total number of structural points out of the NF set that correspond to the N^{th} structural surface, NFS(N) ≤ 100.

IF(I,N) = the structural point number assigned to the I^{th} point in the N^{th} surface.

XIS(1,N) = x coordinate of the inboard leading edge of the N^{th} structural surface area.

XIS(2,N) = x coordinate of the inboard trailing edge.

XOS(I,N) = x coordinate of the leading and trailing edges at the outboard tip.

YCS(I,N) = y coordinates of the inboard and outboard stations.

Referring to figure H1, the spline interpolation scheme can be used to fit discontinuous structures. The structural points assigned to each surface may be used in one or more surfaces. Also, it is not necessary to use all of the NF points. The structural surface boundary coordinates XIS, XOS and YCS are used to bound the structural point sets. Normally, they are at the corners of a square as shown in the figure. Since the corners are transformed to the corners of a square, the boundary coordinates can also be used to skew or distort the physical coordinate system as shown in figure H2. The transformed plane is the plane in which the spline fit is made, hence, the decision to distort the physical coordinate system should be carefully considered since the result may be to introduce errors into the interpolation. As an example, if the corner points of a delta wing are used, then a simple pitch mode will appear in the transformed plane as a twisted mode with the pitch angle slope at the root and no pitch at the wing tip. Spline interpolation will not usually yield a uniform slope distribution in the physical coordinate system for such cases.

If option L3≠0 in card set L-2, the following data is now input. Card set L-6 contains the data for modifying several structural points such that they have zero deflections for all modes with exception of the pitch and roll modes calculated for option L4 not zero. The data is input as follows:

Cols. (right adjust all data) 6I10 format

1-10	11-20	21-30	31-40	41-50	51-60
NF2	IF2(1)	IF2(2)	...		
		...	IF2(L3)		

Card L-6

where

NF2 = number of structural point deflections to be given in the mass and mode data following this card set. (NOTE: for L3=0, NF2=NF)

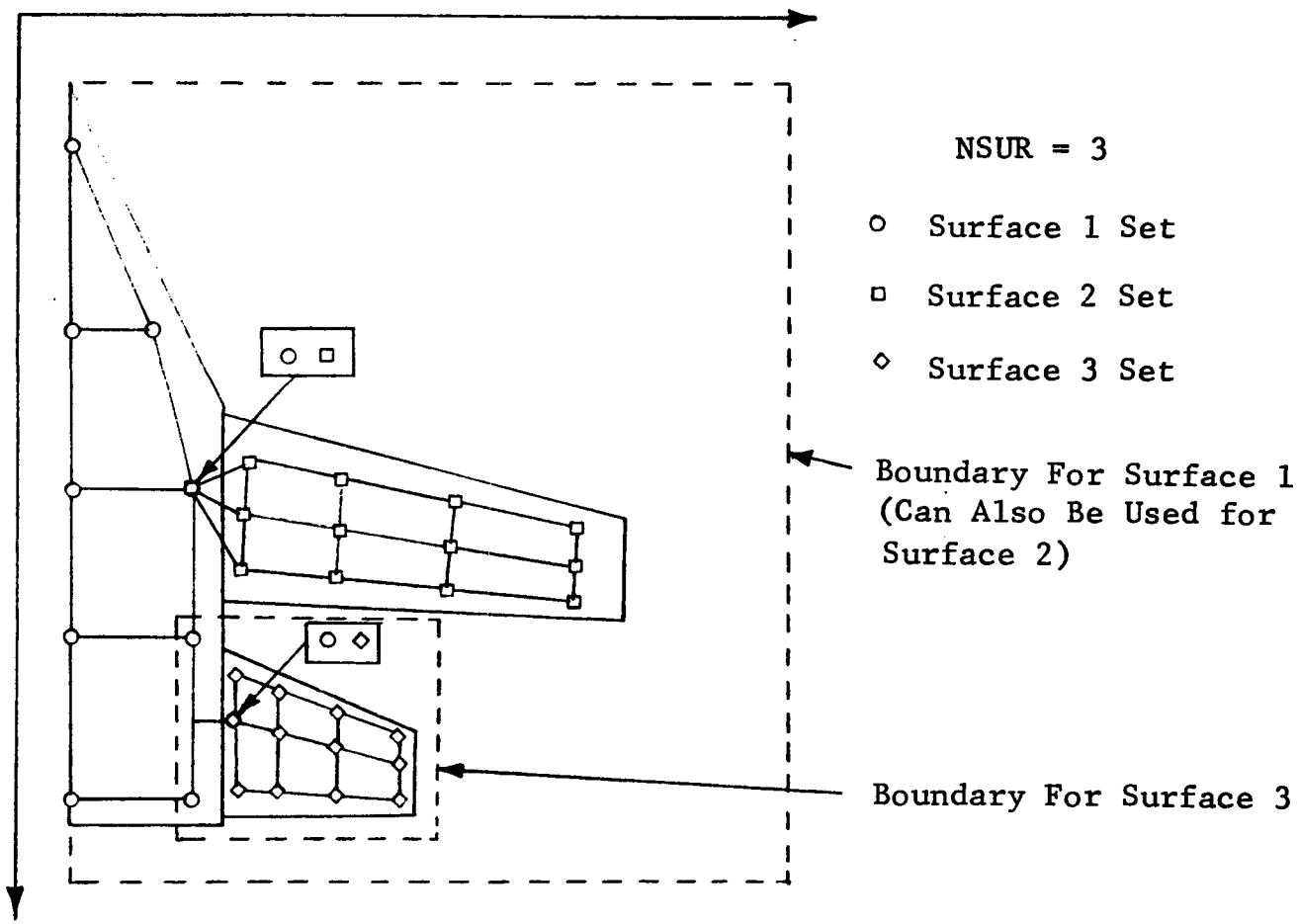

Figure H1.- Structural Surface Subsets

IF2(I) = structural point which will have zero deflection for all modes input.

This deck permits setting zero deflections at points in addition to those input with the mode shapes. As a result, NF2 will usually be smaller than NF and the (XF(I),YF(I)) data given in card set L-4 will include the locations of the additional L3 points as well as the NF2 points. If desired, NF2 can be the same as NF and the modal deflections will be zeroed at the IF2(I) points in place of the values read as input.

If option L2≠0, the mass data is read next in card set L-7:

read FORMAT 8A10 format			
(input according to FORMAT)			
AMASS(1)	AMASS(2)	...	Card L-7
...	AMASS(NF2)		

where

AMASS(I) = mass, m_i, assigned to the I^{th} structural point.

The generalized masses, M_{rs}, are computed as

$$M_{rs} = \frac{XMASS*XMODE*XMODE*232.0}{32.2*RHO*(BREF**3)} * \sum_{i=1}^{NF2} m_i h_{ir} h_{is}$$

where h_{ir}, h_{is} = modal deflections at the i^{th} point for modes r and s, respectively,

and XMASS and XMODE are input in card set L-3.

The deflections are those to be input in the following set.

Card set L-8 completes the structural library by supplying the mode shapes. The form is as follows:

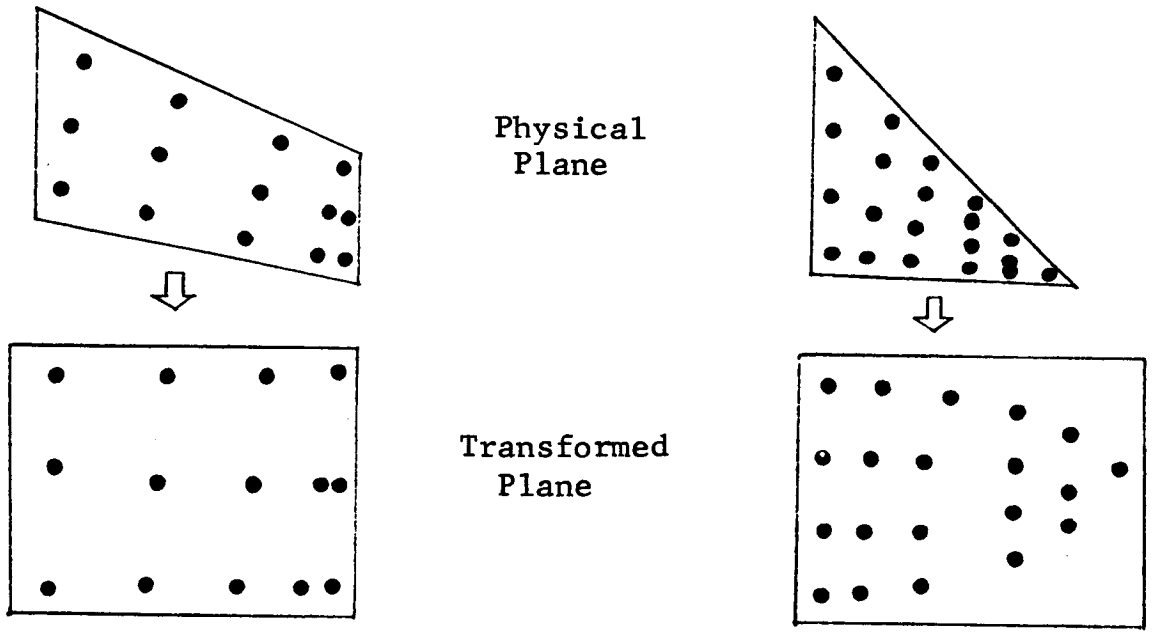

Figure H2. - Distortion of the Physical Coordinate System With Structural Surface Boundaries

(input according to FORMAT on CARD L-7)

Comment Card for L1=0		
H(1,1)	H(2,1)	...
	...	H(NF2,1)
. . .		
Comment Card for L1=0		
H(1,NMODES)	H(2,NMODES)	...
	...	H(NF2,NMODES)

Card L-8

where

H(I,J) = modal deflection at the I^{th} point for the J^{th} mode.

Input Format Description for Aerodynamic Option and Geometric Data Problem Decks

The problem decks contain all aerodynamic data and the structural surfaces used by each aerodynamic surface if the library is used. If no library is supplied, the downwash is input in the problem decks. In order to distinguish cards that are input only when a library is used, these will be denoted as P(L)-N where N is the problem card set number. For cards used only when no library is used, the designation will be P(P)-N. Regardless of how many problem decks are used in a single computer run, the format which follows will always be used. If a library is used, all problems following must be set up for use with a library.

The first card set, P-1, is a two card title set which is printed at the beginning of each problem in the output. The format is

Cols.

1-64
TITLE 1
TITLE 2

Card P-1

Like the library data, it is recommended that the problem decks also be sequenced.

The next card set, P-2, contains the major aerodynamic option data as follows:

Cols. (right adjust all data) 6I10 format

1-10	11-20	21-30	31-40	41-50	51-60
IOP1	IOP2	IOP3	IOP4	IQT	IOPLU

Card P-2

where, referring to figure H3,

IOP1 ≤ 0, the aerodynamic matrices will be computed for all frequencies.

< 0, the matrices will also be written on tape unit "|IOP1|".

> 0, the matrices will be read from tape unit "IOP1".

IOP2 0, aerodynamic results will be obtained in the form of pressure distributions, C_{L_α}, X_{cp}, Y_{cp} and spanwise distributions of lift and chordwise center of pressure.

=0, generalized forces will be computed for "NMODES" total pressure distributions and "NMODES" total integration modes.

IOP3=IOP4=0, dummy options not used.

IQT =0, generalized forces will not be written on output tape.

> 0, generalized forces will be written on tape "IQT" if IOP2=0.

IOPLU=0, aerodynamic matrices written or read from tape "|IOP1|" are in the inverted form.

$\neq 0$, aerodynamic matrices on tape "|IOP1|" are in the uninverted form.

The next card set, P-3, contains integer data which are common to all aerodynamic surfaces. The format is

Cols. (right adjust all data) 6I10 format

1-10	11-20	21-30	31-40	41-50	51-60
NSURF	LS	NALP	NK	NW	IDUMP
IDNWSH	JSUROP				

Card P-3

where

NSURF = number of aerodynamic surfaces
NSURF $\leq$ 10.

LS = symmetry option.

= 0, symmetric flow.

$\neq$ 0, antisymmetric flow.

NALP = number of alpha or downwash vectors to be input. If "LIBR" data is input, NALP=NMODES $\leq$ 20.

NK = number of reduced frequencies. NK 50.

NW = total number of aerodynamic control points and shock load functions for all surfaces (see card P-5)
NW $\leq$ 100, steady flow: NW $\leq$ 70, unsteady flow.

IDUMP $\neq$ 0, various intermediate printout is provided such as the downwash and integration point locations, the uninverted aerodynamic matrices, and the pressure series coefficients.

IDNWSH = 0, downwash vectors are read if "LIBR" data is not used.

$\neq$ 0, angle of attack in all downwash vectors is set uniformly to ALPO(IS) (given in set P-6N) for the ISth surface if "LIBR" data is not used.

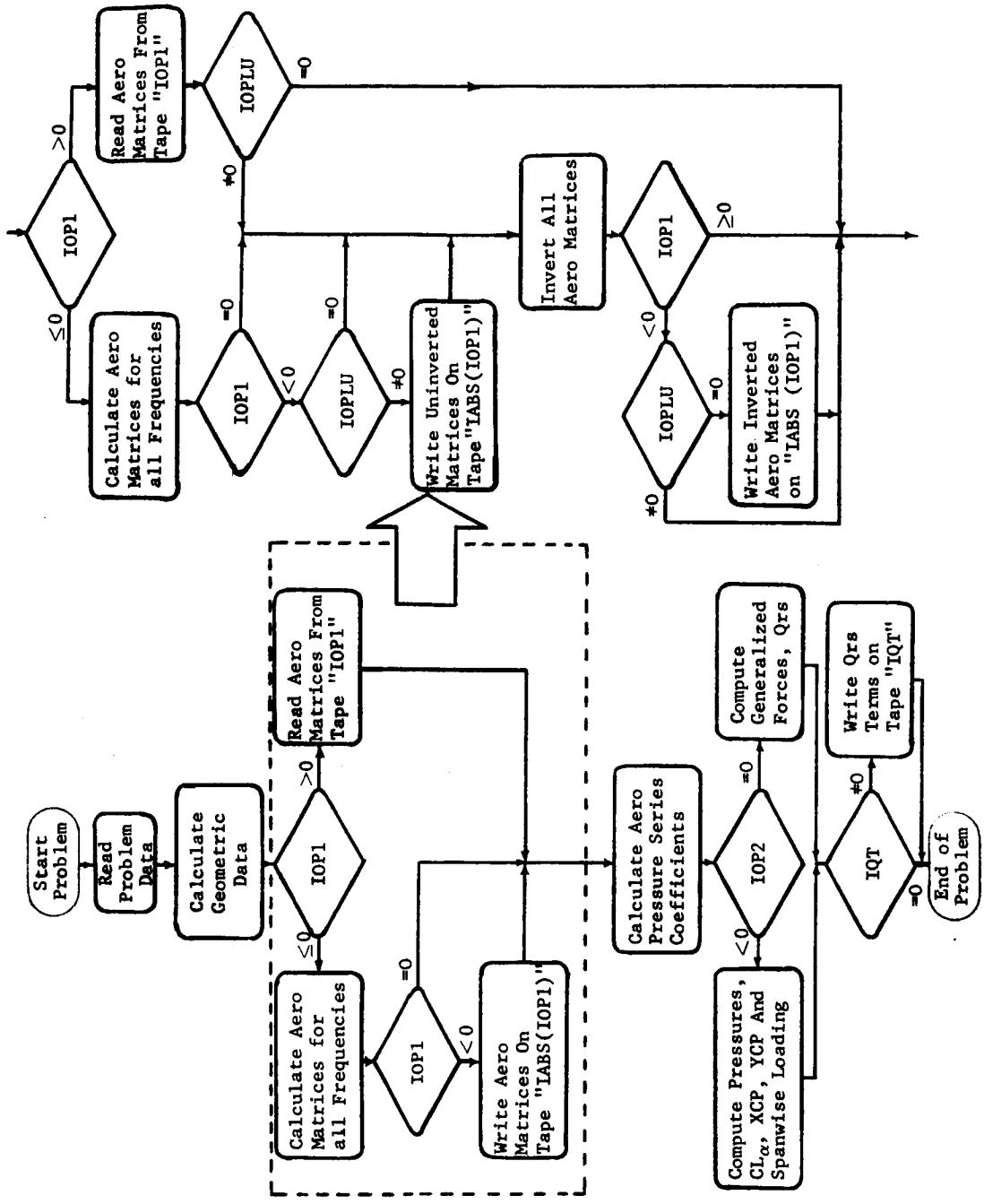

Figure H3.- Flow Diagram For the Aerodynamic Options

JSUROP = 0, regular pressure functions are used on all surfaces.

≠ 0, supersonic weighting function is used for totally supersonic flow problems. This cannot be used for transonic or subsonic problems, however, the Mach number distribution may be non-uniform as long as no subsonic regions are present.

The next card set contains the real data which are common to all aerodynamic surfaces. The format is

Cols. (right adjust all data or use decimal) 6F10.0 format

1-10	11-20	21-30	31-40	41-50	51-60
XMACH	BREF	RK(1)	...		
		...	RK(NK)		

Card P-4

where

XMACH = M_∞, free stream Mach number.

BREF = b_{ref}, reference length in same dimensions as all geometric data.

RK(I) = $k_\infty = \frac{\omega b_{ref}}{U_\infty}$, reduced frequency.

which completes the data common to all aerodynamic surfaces.

The following sets are repeated "NSURF" times and they begin with card set P-5N given as follows:

Cols. (right adjust all data) 6I10 format

1-10	11-20	21-30	31-40	41-50	51-60
NC(IS)	NS(IS)	NJ(IS)	NSI(IS)	ITRANS(IS)	NLE(IS)
NTE(IS)	ICHORD(IS)	IXI(IS)	LSPAN(IS)	LSYM(IS)	ISTYPE(IS)
KSURF(IS,1)	...				
...	KSURF(IS,NSURF)				

where, for the ISth surface,

NC(IS) = number of chordwise pressure functions or downwash points, $NC(IS) \leq 10$

NS(IS) = number of spanwise pressure functions or downwash chords, and shock load functions if $KSURF(IS,IS) < 0$, $NS(IS) \leq 15$

** For steady flow,

$$\sum_{JS=1}^{NTR} NS(JS) + \sum_{IS=1}^{NSURF} NC(IS)*NS(IS) = NW \leq 100$$

For unsteady flow,

$$\sum_{JS=1}^{NTR} NS(JS) + \sum_{IS=1}^{NSURF} NC(IS)*NS(IS) = NW \leq 70$$

JS = surface for which $KSURF(IS,IS) < 0$ (transonic solution)
NTR = total number of JS surfaces

NJ(IS) = number of chordwise integration points:
NJ(IS) = 0, standard points are used
NJ(IS) > 0, the input number is used as described below for the option IXI(IS).
$NJ(IS) \leq 15$

NJ(IS) = 0 is recommended for all cases

NSI(IS)= number of integration chords on both the ISth surface and its image.
NSI(IS) = 0, standard chords are used
NSI(IS) > 0, the input number is used as described in table H1 below for the option ISTYPE(IS).
$NSI(IS) \leq 31$

ITRANS(IS) = 0, the Mach number distribution over the ISth surface is uniform and equal to XMACH (card P-4).

> 0, the chordwise Mach number distribution is read from card P-9N and is used at all span stations.

< 0, the chordwise and spanwise Mach number distribution is read from card P-9N.

NLE(IS) = number of x,y coordinate pairs to be read for defining the leading edge.

$$NLE(IS) \leq 10$$

NTE(IS) = number of points for defining the trailing edge.

$$NTE(IS) \leq 10$$

ICHORD(IS) = 1,2,3,4, the type of chordwise pressure distribution to be used for the ISth surface as shown in figure H4.

IXI(IS) = 1,2,3,4, the type of chordwise downwash point distribution used and since the chordwise integration points are interdigitated, this option also determines their distribution as well. Table H2 summarizes the distributions.

IXI(IS)=1 is recommended for almost all cases

LSPAN(IS) = 1,2,3,4, the type of spanwise loading to be used for the ISth surface as shown in figure H4.

LSYM(IS) = 0, symmetric flow.

≠ 0, antisymmetric flow.

ISTYPE(IS) = 1,2,3, the type of surface and image to be used. Type 1 has continuous functions across the centerline whereas types 2 and 3 are independent. The type 2 spanwise loading can be used with all three surface types.

TABLE H2. CHORDWISE DOWNWASH AND INTEGRATION POINTS ($\bar{m}$=NC(IS))

IXI	$\underline{x}_i$	ξ_j*	DEFAULT FOR NJ=0	INPUT FOR NJ=J
1	$\underline{x}_i = -\cos(\frac{2i}{2m+1}\pi)$ $i = 1,2,\ldots\bar{m}$	$\xi_j = -\cos(\frac{2j-1}{2J+1}\pi)$ $j = 1,2,\ldots J$	$J = \bar{m}$ $NJ = J$	$J = INT[n(\bar{m}+\frac{1}{2})]$ $n = 1,3,5,\ldots$
2	$\underline{x}_i = -\cos(\frac{2i}{2\bar{m}+2}\pi)$ $i = 1,2,\ldots\bar{m}$	$\xi_j = -\cos(\frac{2j-1}{2J}\pi)$ $j = 1,2,\ldots J$	$J = \bar{m}+1$ $NJ = J$	$J = n(\bar{m})$ $n = 1,3,5,\ldots$
3	$\underline{x}_i = -1$(leading edge) $\underline{x}_i = -\cos(\frac{2i-2}{2\bar{m}-1}\pi)$ $i = 2,3,\ldots\bar{m}$	$\xi_j = -\cos(\frac{2j-1}{2J+1}\pi)$ $j = 1,2,\ldots J$	$J = \bar{m}-1$ $NJ = J$	$J = INT[n(\bar{m}-\frac{1}{2})]$ $n = 1,3,5,\ldots$
4	read $\underline{x}_i$	read ξ_j	$J = \bar{m}$ $NJ = J$	J = arbitrary

* For supersonic flow the ξ_j are not constant and are a function of the downwash point location. For interference, the ξ_j are constant as determined by IXI and NJ default is NJ=2*NC(IS). If NJ is input, then none of the restrictions given in the table for NJ=J apply.

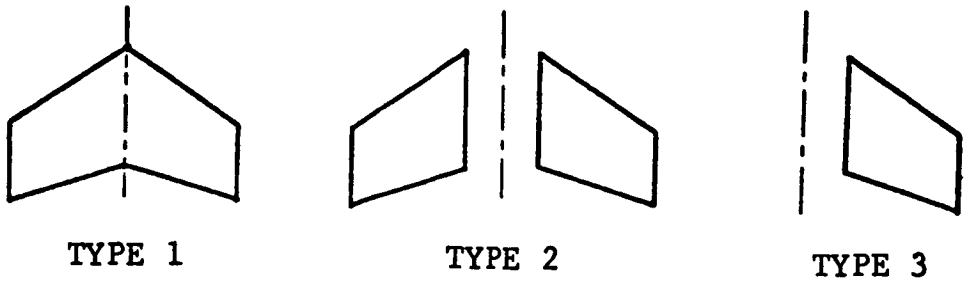

SURFACE TYPES
ISTYPE (IS)

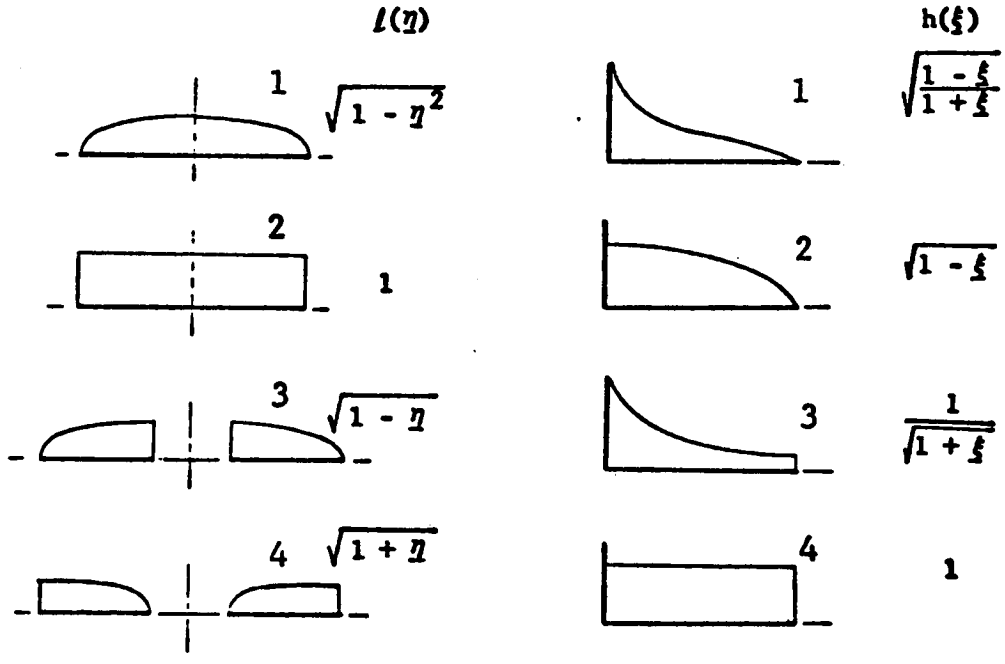

SPANWISE LOADINGS
LSPAN (IS)

CHORDWISE LOADINGS
ICHORD (IS)

Figure H4. - Surface and Loading Types in the Aerodynamic Program

TABLE H1. DOWNWASH AND INTEGRATION CHORDS (R=NS(I))

ISTYPE	DOWNWASH CHORD, $\underline{y}_r$	INTEGRATION CHORD, η_s	DEFAULT FOR NSI=0	INPUT FOR NSI=S
1	$\underline{y}_r = \cos(\frac{r\pi}{2R+1})$ $r = 1,2,...R$	$\eta_s = -\cos(\frac{2s+1}{2S}\pi)$ $s = 1,2,...S$	$S = 2R+1$ $NSI = S$	$S = (2R+1)$ $n = 1,3,5,...$
2	$\underline{y}_r = \cos(\frac{r\pi}{R+1})$ $r = 1,2,...R$	$\eta_s = -\cos(\frac{2s+1}{2S}\pi)$ $s = 1,2,...S'$ repeat for both the surface and its image	$S = R+1$ $NSI = 2S'$	$S = 2n(R+1)$ $n = 1,2,3,...$
3	Same as 2	Same as 2	$S = R+1$ $NSI = S$	$S = n(R+1)$ $n = 1,2,3,...$

KSURF(IS,KS) = interference calculation option as described below and illustrated in figure H5.

For IS = KS:

KSURF(IS,IS) = 0, surface IS is not a transonic surface.

KSURF(IS,IS) > 0, surface IS is the upstream surface in a transonic pair with a shock along its trailing edge. The other surface in the pair is the value of KSURF(IS,IS). (see figure H5)

KSURF(IS,IS) < 0, surface IS is the downstream surface in a transonic pair with a shock at its leading edge. The other surface is the absolute value of KSURF(IS,IS). (see figure H5)

For IS $\neq$ KS,

KSURF(IS,KS) = 0, interference of surface KS on IS will be calculated but spanwise integration correction terms will not be calculated. This option is usually taken if KS is downstream of or parallel to IS.

< 0, no interference is calculated for KS on IS.

> 0, interference is calculated with the spanwise integral correction terms.

The next card set in the NSURF decks is P-6N which contains the following real data:

Cols. (right adjust all data or use decimal) 6F10.0 format

1-10	11-20	21-30	31-40	41-50	51-60
ALPO(IS)	XV(IS)	YV(IS)	ZV(IS)	THETA(IS)	

Card P-6N

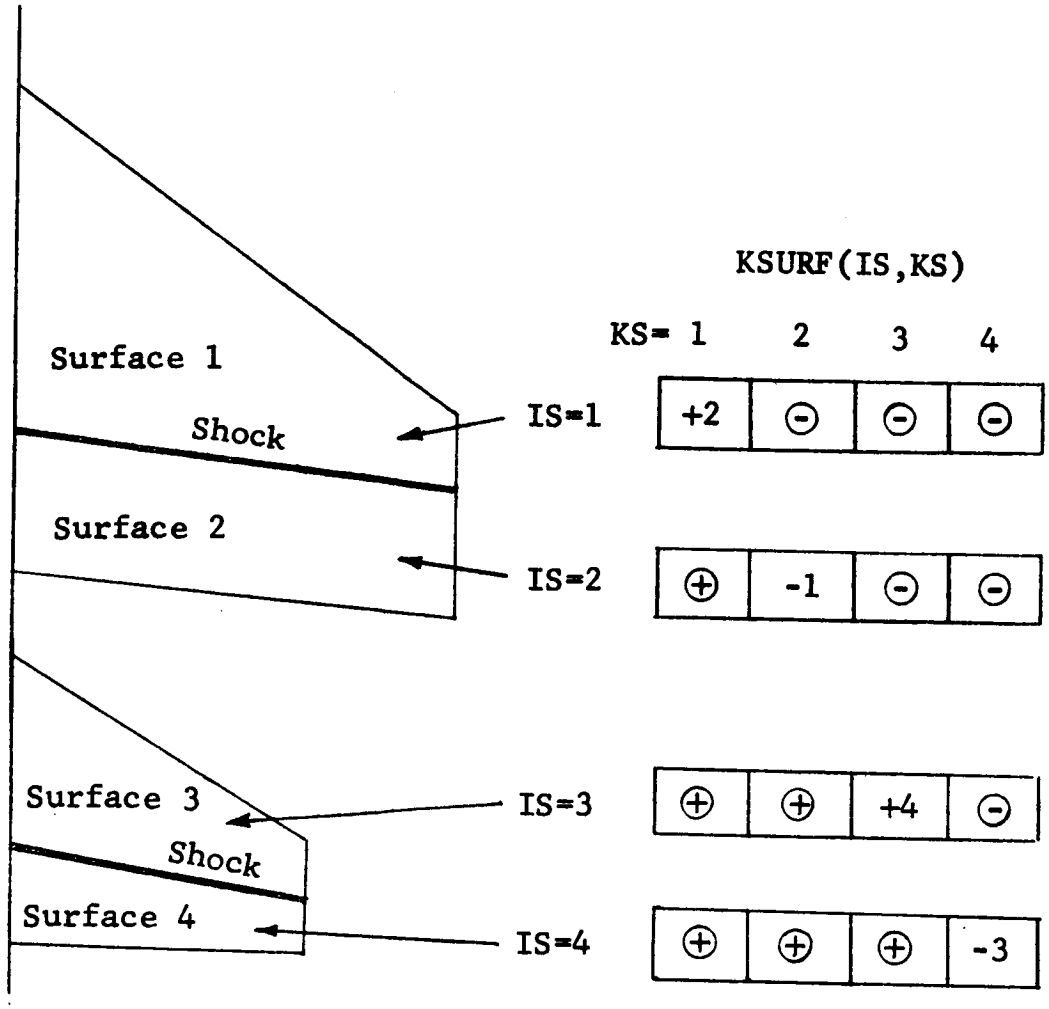

Figure H5. KSURF(IS,KS) For Transonic Flow Over Interfering Surfaces

where

ALPO(IS) = uniform angle of attack, in radians, which is always added to all downwash vectors for all control points that fall on the ISth surface.

XV(IS), YV(IS), ZV(IS) = x,y,z coordinates of the leading edge inboard tip of the surface (see figure H6).

THETA(IS) = inclination of the surface relative to the y-axis (see figure H6).

The planform geometry data is given next in card set P-7N as follows:

Cols. (right adjust all data or use decimal) 6F10.0 format

1-10	11-20	21-30	31-40	41-50 51-60
XLE(1)	YLE(1)	XLE(2)	YLE(2).	...
	...	XLE(NLE)	YLE(NLE)	
XTE(1)	YTE(1)	XTE(2)	YTE(2)	...
	...	XTE(NTE)	YTE(NTE)	

Card P-7N

where

XLE(I),YLE(I) = x,y coordinates of the Ith leading edge break point. It is not necessary for XLE(1)=XV(IS) and YLE(1)=YV(IS).

XTE(I),YTE(I) = x,y coordinates of the Ith trailing edge break point.

The dimensions of XLE, YLE, XTE, YTE are the same as all other input geometric data.

If the structural and mode shape library is used, the following card must be supplied:

Cols. (right adjust) I10 format

1-10	
NST(IS)	

Card P(L)-8N

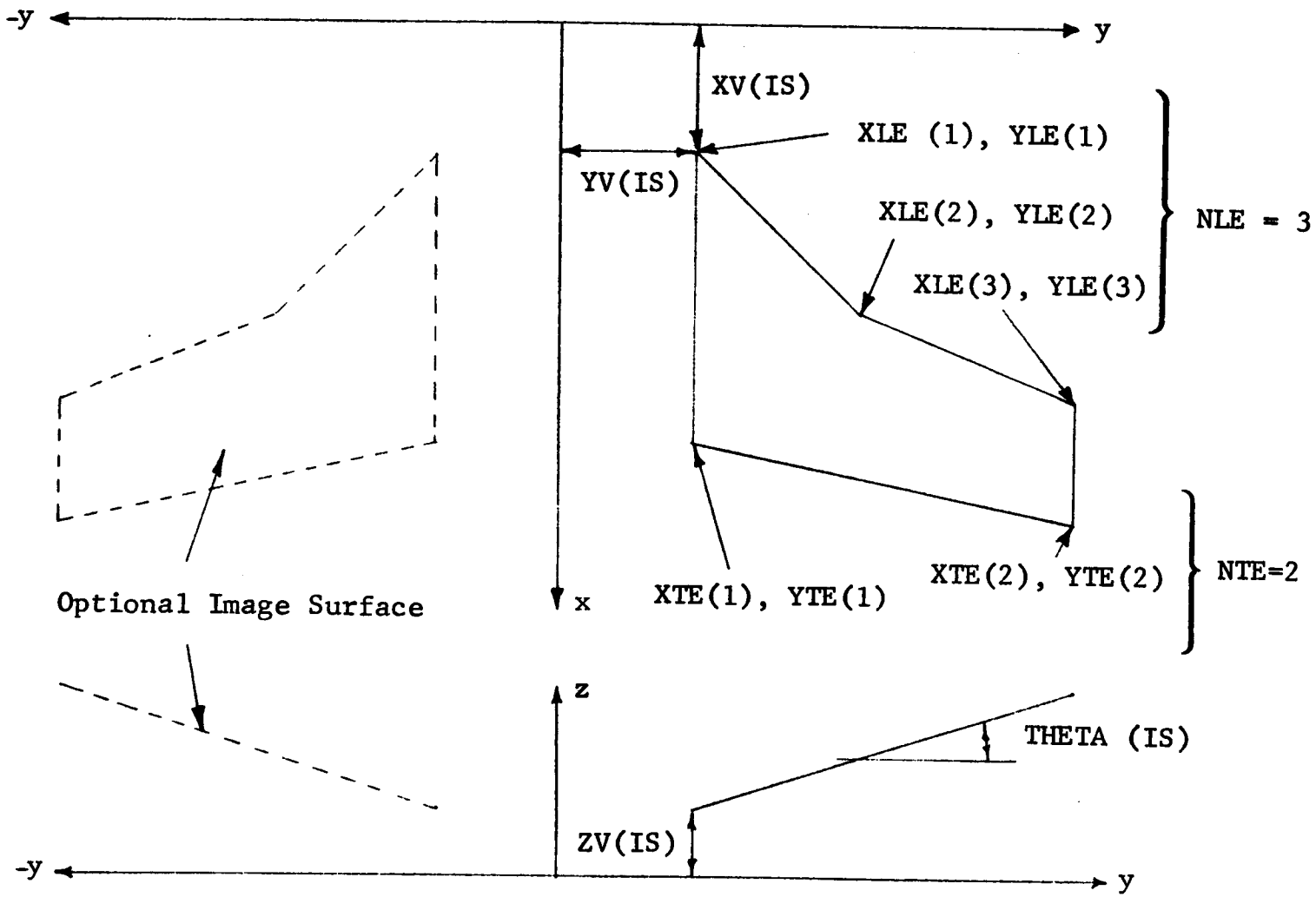

Figure H6. - Aerodynamic Geometry Input Data For Arbitrary Surfaces

where

NST(IS) = the structural surface given in the library from which deflections and downwash are calculated for the mode shapes.

If library data is not supplied then this card must be omitted.

If ITRANS(IS)≠0, then the Mach number distribution data is supplied in card set P-9N. For ITRANS(IS) > 0, the chordwise distribution is assumed constant along the span and the data is given as

Cols. (right adjust or use decimal) 6F10.0 format

1-10	11-20	21-30	31-40	41-50	51-60
GMACH(1,1)	GMACH(2,1)	...			
	...	GMACH(Mc,1)			

Card P-9N
(ITRANS > 0)

where

GMACH(I,1) = input Mach number at constant percent chord line $(\frac{I-1}{Mc-1})$

Mc = NC(IS) + 1

Note that the data is input at constant chord fraction increments from the leading to the trailing edge. For ITRANS(IS) < 0, the distribution is input at (NS(IS)+1) span stations as follows:

Cols. (right adjust or use decimal) 6F10.0 format

1-10	11-20	21-30	31-40	41-50	51-60
GMACH(1,1)	GMACH(2,1)	...	...	GMACH(Mc,1)	
...					
GMACH(1,MS)	GMACH(2,MS)	...	...	GMACH(Mc,MS)	

Card P-9N
(ITRANS < 0)

where

GMACH(I,J) = input Mach number at the $(\frac{I-1}{Mc-1})$ chordwise and $(\frac{J-1}{MS-1})$ spanwise locations.

MS = NS(IS) + 1

Again, the spanwise distribution is uniformly spaced starting from the inboardmost station to and including the tip at $(\frac{1}{MS-1})$ increments.

This completes the input aerodynamic geometry and option data and the problem data if the structural library is used. If the library is not used then the downwash must be input after all aerodynamic data for all surfaces, if the IDNWSH option in card P-3 is not used. For steady flow, the data are input as follows:

Cols. (right adjust or use decimal) 6F10.0 format

1-10	11-20	21-30	31-40	41-50	51-60
ALP(1,1,IS)	ALP(2,1,IS)	...	...	ALP(NI,1,IS)	
...					
ALP(1,NALP,IS)	ALP(2,NALP,IS)	...	...	ALP(NI,NALP,IS)	

Card P(P)-10NN
k=0

where

ALP(I,K,IS) = slope (radians) at the Ith downwash point in the Kth downwash vector on the ISth surface, from LE to TE, outbd to inbd.

NALP = total number of downwash vectors as input on card P-3, NALP $\leq$ 20.

NI = NC(IS)*NS(IS), total number of downwash points on the ISth surface.

For unsteady flow, the only change is the addition of deflections:

Cols. (right adjust or use decimal) 6F10.0 format

1-10	11-20	21-30	31-40	41-50	51-60
ALP(1,1,IS)	ALP(2,1,IS)	...	...	ALP(NI,1,IS)	
H(1,1,IS)	H(2,1,IS)	...	...	H(NI,1,IS)	
...					
ALP(1,NALP,IS)	ALP(2,NALP,IS)	...	...	ALP(NI,NALP,IS)	
H(1,NALP,IS)	H(2,NALP,IS)	...	...	H(NI,NALP,IS)	

Card P(P)-10NN
k≠0

where

H(I,K,IS) = deflection (same dimensions as the geometric data) at the Ith downwash point in the Kth downwash vector on the ISth surface.

In both cases, the downwash data are given only after all of the aerodynamic geometry and option data are completed for all surfaces. Then, as the format shows, all modal data is input for each surface together.

The last card in a problem deck signals the program to continue to the next problem or terminate the job. This is the "END" card which terminates the job.

Cols.

1-4	5-60
ENDb	(JOB WILL BE TERMINATED)

Card "END"

where b is a blank space. For continuation, the characters in Cols. 1-4 may be anything but ENDb, for example

Cols.

1-4	5-60
PROB	LEM 1 END (CONT. ON TO NEXT PROBLEM)

Card "END"

which will continue the job.

REFERENCES

1. Stenton, T. E.; and Andrew, L. V.: Transonic Unsteady Aerodynamics for Planar Wings with Trailing Edge Control Surfaces. AFFDL-TR-57-180, U.S. Air Force, Aug. 1968.

2. Magnus, R.; and Yoshihara, H.: Inviscid Transonic Flow Over Airfoils. AIAA Journal, vol. 8, no. 12, Dec. 1970, pp. 2157-2162.

3. Murman, E.; and Cole, J.: Calculation of Transonic Flows. AIAA Journal, vol. 9, no. 1, Jan. 1971, pp. 121-141.

4. Bailey, F. R.; and Steger, J. L.: Relaxation Techniques for Three-Dimensional Transonic Flow About Wings. AIAA Paper No. 72-189, Jan. 1972.

5. Magnus, R.; and Yoshihara, H.: Finite Difference Calculations of the NACA 64A-410 Airfoil Oscillating Sinusoidally in Pitch at $M_\infty = 0.72$. CASD-NSC-74-004, Office of Naval Research, Aug. 1974.

6. Cunningham, A. M., Jr.: The Application of General Aerodynamic Lifting Surface Elements to Problems in Unsteady Transonic Flow. NASA CR-112264, Feb. 1973.

7. Cunningham, A. M., Jr.: A Collocation Method for Predicting Oscillatory Subsonic Pressure Distributions on Interfering Parallel Lifting Surfaces. AIAA Paper No. 71-329, Apr. 1971.

8. Cohen, D.: Formulas for the Supersonic Loading, Lift and Drag of Flat Swept-Back Wings with Leading Edges Behind the Mach Lines. NACA Report 1050, 1951.

9. Ii, J. M.; Borland, C. J.; and Hogley, J. R.: Prediction of Unsteady Aerodynamic Loadings of Non-Planar Wings and Wing-Tail Configurations in Supersonic Flow, Part 1 - Theoretical Development, Program Usage and Application. AFFDL-TDR-71-108, U.S. Air Force, Mar. 1972.

10. Woodward, F. A.; and Hague, D. S.: A Computer Program for the Aerodynamic Analysis and Design of Wing-Body-Tail Combinations at Subsonic and Supersonic Speeds, Volume I: Theory and Program Utilization. ERR-FW-867, Fort Worth Division of General Dynamics, Feb. 1969.

11. Landrum, E. J.: A Tabulation of Wind-Tunnel Pressure Data and Section Aerodynamic Characteristics at Mach Numbers 1.61 and 2.01 for Two Trapezoidal Wings and Three Delta Wings Having Different Surface Shapes. NASA TN D-1344, Sept. 1962.

12. Landahl, M. T.: Unsteady Transonic Flow. Pergamon Press, New York, Oxford, London, Paris, 1961.

13. Lessing, H. C.; Troutman, J. L.; and Meness, G. P.: Experimental Determination of the Pressure Distribution on a Rectangular Wing Oscillating in the First Bending Mode for Mach Numbers from 0.24 to 1.30. NASA TN D-344, Dec. 1960.

14. Becker, J.: Vergleich gemessener und berechneter instationärer Druckverteilungen für den hohen Unterschall an einem elastischen gepfeilten Flugel. EWR-Report Nr. 403-69, Messerschmitt-Bölkow-Blohm, Sept. 1969.

15. Tijdeman, H.: Correspondence to S. R. Bland on Corrections to Experimental Data published by NLR, (Amsterdam). Sept. 1973.

16. Bergh, H.; Tidjeman, H.; and Zwaan, R. J.: High Subsonic and Transonic Effects on Pressure Distributions Measured for a Swept Wing with Oscillating Control Surfaces. Z. Flugwiss., 18 (1970), Heft 9/10, pp. 339-347 (in English).

17. Laschka, B.; and Schmid, H.: Unsteady Aerodynamic Forces on Coplanar Lifting Surfaces in Subsonic Flow (Wing-Horizontal Tail Interference). Jahrbuch 1967 der WGLR, pp. 211-222 (in English).

18. Multhopp, H.: Methods for Calculating the Lift Distribution of Wings, (Appendix I, Contributed by W. Mangler). Report No. Aero-2353, Royal Aircraft Establishment, Farnborough, Hants, Jan. 1950.

19. Pai, S.: Introduction to the Theory of Compressible Flow. D. Van Nostrand Company, Inc., Princeton, Toronto, New York, London, 1959.

20. Anon.: Tables of Chebyshev Polynomials $S_n(x)$ and $C_n(x)$, (Introduction by Cornelius Lanczos). Applied Mathematics Series, 9, National Bureau of Standards, 1952.

21. Harder, R. L.; and Desmarias, R. N.: Interpolation Using Surface Splines. J. Aircraft, Vol. 9, No. 2, Feb. 1972, pp. 189-191.

NASA CR-144895

DISTRIBUTION LIST
NAS1-12399

	No. Copies
NASA Langley Research Center Hampton, VA 23665	
Attn: Report & Manuscript Control Office, Mail Stop 180A	1
Technology Utilization Office, Mail Stop 139A	1
Dr. Samuel R. Bland, Mail Stop 340	58
NASA Ames Research Center Moffett Field, CA 94035	
Attn: Library, Mail Stop 202-3	1
NASA Flight Research Center P. O. Box 273 Edwards, CA 93523	
Attn: Library	1
NASA Goddard Space Flight Center Greenbelt, MD 20771	
Attn: Library	1
NASA Lyndon B. Johnson Space Center 2101 Webster Seabrook Road Houston, TX 77058	
Attn: Library, Code JM6	1
NASA Marshall Space Flight Center Huntsville, AL 35812	
Attn: Library	1
Jet Propulsion Laboratory 4800 Oak Grove Drive Pasadena, CA 91103	
Attn: Library, Mail Stop 111-113	1
NASA Lewis Research Center 21000 Brookpark Road Cleveland, OH 44135	
Attn: Library, Mail Stop 60-3	1
NASA John F. Kennedy Space Center Kennedy Space Center, FL 32899	
Attn: Library, IS-DOC-1L	1
National Aeronautics and Space Administration Washington, DC 20546	
Attn: KSA-10/Library	1
RW/NASA Headquarters	1

	No. Copies
NASA Scientific & Technical Information Facility 6571 Elkridge Landing Road Linthicum Heights, MD 21090	30 plus reproducible